Library

Evaluation of Mucosal Damage and Recovery in the Gastrointestinal Tract of Rats by Penetration Enhancers

by

Yogeeta Narkar

A dissertation submitted in partial fulfillment

Of the requirements for the degree of

DOCTOR OF PHILOSOPHY

(Pharmaceutical Sciences)

at the

UNIVERSITY OF WISCONSIN-MADISON

2006

AWPP
N231e
2006

Evaluation of Mucosal Damage and Recovery in the Gastrointestinal Tract of Rats by Penetration Enhancers

Yogeeta Narkar

Under the guidance of Professor Joseph R. Robinson

At the University of Wisconsin-Madison

Improving oral absorption of poorly absorbed drugs has always been a major focus in drug delivery research. When poor intestinal epithelial permeability is associated with high polarity or low water solubility, absorption promoters could be used to overcome epithelial absorption barrier. Penetration enhancers have been studied for almost five decades to improve oral drug absorption. Two important aspects of studies involving penetration enhancers are evaluation of efficacy and safety. Many studies have established the efficacy of penetration enhancers in causing drug absorption enhancement. But, safety has always been a concern with penetration enhancers. The possibility of increasing absorption of toxic substances especially the endogenous endotoxins due to the local action of penetration enhancers has deterred the regulatory bodies from approving them for human use.

In this study, we have attempted to address this issue by evaluating kinetics of mucosal recovery by measuring absorption of poorly absorbed markers and morphological changes. We developed a pharmacokinetic tool to evaluate functional recovery of gastrointestinal mucosa dynamically, after administration of a penetration enhancer. We found that it is possible to achieve absorption enhancement with temporary and reversible

alteration of mucosal barrier properties. The changes noted in absorption of marker molecules as a result of treatment with a penetration enhancer and the subsequent recovery were in accordance with morphological changes observed using microscopy techniques. After treatment with a penetration enhancer for 14 days, no permanent changes in absorption kinetics and morphology were observed. These results hopefully will help to improve the design of future studies involving the use of penetration enhancers and in a better understanding of their effects on the mucosal membrane.

Approved _____

Professor Joseph R. Robinson

Date _____

ACHNOWLEDGEMENTS

I would like to thank Professor Joseph Robinson for his guidance, support, constructive criticism and patience throughout the graduate studies, which has been a very fulfilling experience for me. I learnt a lot from his unique perspective on the scientific matters and practical approach.

I would also like to thank my committee members Dr. Ralph Albrecht, Dr. Ronald Burnette, Dr. Glen Kwon and Dr. Lian Yu for their helpful suggestions. This work would not have been possible without generous help from Dr. Albrecht and Dr. Burnette. I sincerely thank Dr. Albrecht for letting me use his lab resources for microscopy work. I am greatly indebted to Dr. Burnette for taking time out of his busy schedule to write software for pharmacokinetic modeling.

I would like to acknowledge help from Dr. Thorson's group in letting me use the HPLC and co-operation of Sharon Hilderbrandt during the in-vivo work. I am thankful to Beth Schiffman and Scott, RARC, UW for training me in in-vivo techniques and lending the anesthesia machine from time to time.

I thank Dr. Reiner Blehr for preparing and evaluating the microscopy specimens and Irawati Kandela for her help in the microscopy work.

I thank Paul Hutson for his help and discussions during the early stages of pharmacokinetic modeling.

I would like to express my heartfelt thanks to my present and former labmates, Adam Alani, Deepa Rao, Lan Xiao and Dr. Jaehan Park for all their help and support during

difficult times. I also acknowledge friends and colleagues in the school of pharmacy, Ling Xiao, Joe Su, Hak Auth and Dr. Oana Martin.

I am grateful to the School of Pharmacy, UW for giving me the chance of fulfilling my dreams of graduate studies and the financial support throughout the study.

I would not be where I am today without the unconditional love and endless support of my mother and sisters. They taught me the value of hard work and having faith in myself. I also want to thank my brothers-in-law who have become a part of our family. I want to thank my parents-in-law for their constant support and encouragement.

Finally, I want to thank my husband for his understanding, patience, help and unwavering love.

Table of Contents

Figure/Table legends

Chapter 4-B

Chapter 4-C

Chapter 4-E

Chapter1: Introduction

I. The Gastrointestinal Tract- Overview

The oral route is the most common and convenient route for drug administration with 84% of the top 50 drugs sold in the US and Europe in 2001 being orally administered [1]. In order to design an effective oral drug delivery system, it is crucial to understand the functional anatomy and physiology of the gastrointestinal tract (GIT). In the gastrointestinal tract, the small intestine is the major site for digestion and absorption of nutrients, water and electrolytes and drugs. It is divided along its length, into three portions: duodenum, jejunum and ileum. In man, the entire length is approximately 6 meters, with the duodenum comprising about 5%, the jejunum 45% and the ileum 50%. Most absorption occurs in the duodenum and the proximal half of the jejunum. The absorption of water and electrolytes also occurs in the lower part of the small intestine and the large intestine [2].

A. Structure of the digestive tract

The wall of the gastrointestinal tract is composed of four basic layers or tunics, the mucosa, submucosa, muscularis externa and the serosa [3] (Figure 1-1).

Tunica serosa is the outermost protective covering of the digestive tube. It consists of a thin layer of loose connective tissue and houses vascular and nerve supplies to the digestive tract. It also helps to protect the intestine from trauma.

Tunica muscularis consists of an inner layer of circularly aligned and an outer layer of longitudinally oriented muscle fibers. It is the sequential contraction of these muscle layers that is responsible for generating the peristaltic waves that propel the food along the GIT.

Tunica submucosa, immediately beneath the mucosa, is a layer of loose to dense

connective tissue containing blood and lymphatic vessels. It contains fibroblasts, adipocytes, macrophages, lymphocytes, basophils, neutrophils, eosinophils, monocytes, plasma and mast cells, which play an important role in the barrier function of mucosa.

Tunica mucosa is the innermost layer of the digestive tube and lines the lumen. It functions to secrete mucus, digestive enzymes and hormones, and absorb soluble digestion products from the lumen into the blood stream. The mucosa is composed of three sublayers: epithelium, lamina propria, and muscularis mucosae.

The epithelial cells cover the mucosa in a monolayer and are thus in direct contact with the lumen. Beneath the epithelium is the lamina propria – a layer of loose connective tissue through which course blood vessels and lymphatics that supply the epithelium. Beneath the lamina propria is a thin layer of smooth muscle (muscularis mucosae), which permits the mucosa to dynamically move and fold [4, 5].

The mucosa of the small intestine has various structural features. Since this is the site of interest for drug absorption, it is crucial to understand its anatomical and functional organization.

B. Structure of the small intestinal mucosa

The absorptive surface of the small intestine is greatly increased by its complex folding as illustrated in Figure 1-2. In general, due to the presence of plicae circulares, villi and microvilli, the total surface area of the small intestine in humans is approximately 200 m^2, which represents an increase in surface area by 50,000-fold [6, 7].

The crypts of Lieberkühn are located between the intestinal villi. Undifferentiated cells close to the bottom of the crypts regenerate the epithelium with a turnover time of 4-5

days. The surface layer of the intestinal mucosa is a continuous sheet of columnar epithelium, which contains enterocytes, goblet cells and a few endocrine cells. Enterocytes are the most common and are involved in drug and nutrient transport. These cells are polarized, i.e. they have distinguishable apical and basolateral membranes separated by a tight junctional complex. The tight junction constitutes a selective but variably efficient ionic barrier, sealing the intercellular space from the outside environment.

The goblet cells are present throughout the intestinal surface. The mucin secreted by the goblet cells form a gel coat exterior to the microvilli, often referred to as the glycocalyx. It extends 200 μm from the tips of the microvilli and is composed of complex glycoproteins. The function of the mucin coat appears to be to protect the underlying mucosa from injury and to lubricate, thereby aiding in passage of food.

The lamina propria contains the lymphocytes, eosinophils, mast cells, macrophages and plasma cells associated with the lymphoid tissue. Lymphocytes form 20% of the total cell population of the intestinal mucosa and are associated with defense mechanisms of the gastrointestinal barrier [2, 8].

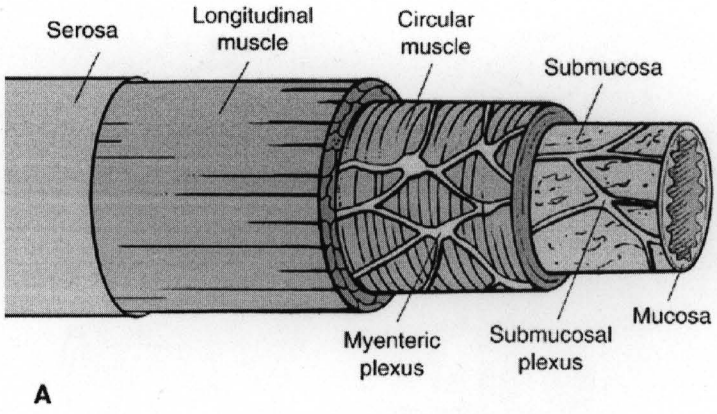

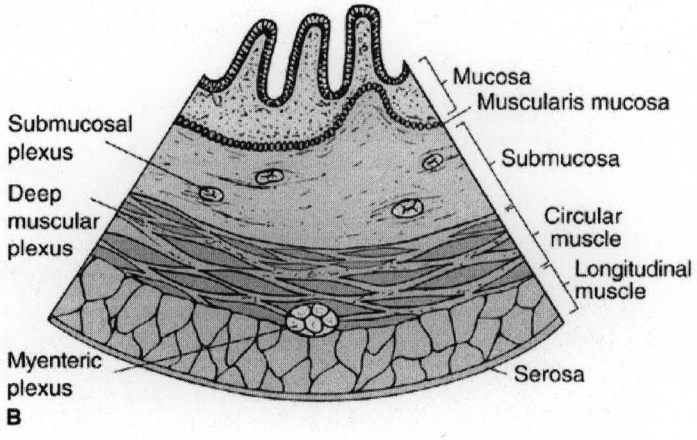

Figure 1-1: Structural anatomy of the small intestine (Reproduced from reference 3)

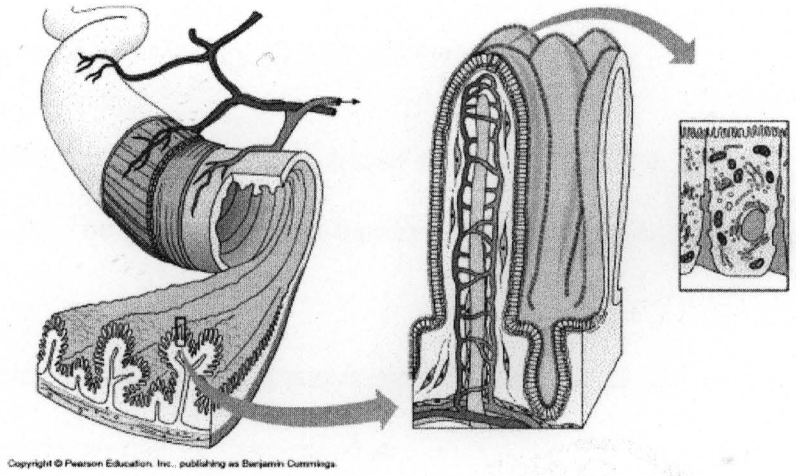

Plicae circulares (folds) **Villi** **Microvilli**

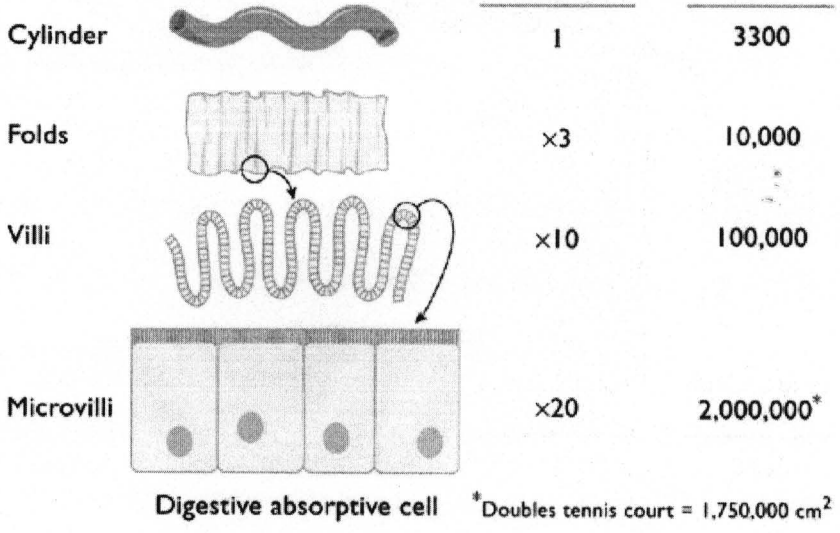

Figure 1-2: Amplification of surface area in the small intestine (Reproduced from reference 5)

II. The Absorption Barrier in the Gastrointestinal Tract

A. Anatomy and physiology of the absorption barrier

The gastrointestinal mucosa forms a barrier between the body and the luminal environment [9]. The gastrointestinal barrier is often discussed as having two components (Figure 1-3):

- The **intrinsic barrier**, which is composed of the epithelial cells lining the digestive tube and the tight junctions that tie them together
- The **extrinsic barrier** consists of secretions and other influences that are not physically part of the epithelium, but which affect the epithelial cells and maintain their barrier function

The Intrinsic Gastrointestinal Barrier

The mucosal lining of the gastrointestinal tract is composed of a relatively rapidly proliferating and continually renewing sheet of epithelial cells that serve a variety of specialized physiological functions including selective absorption of nutrients, immune surveillance and the formation of a permeability barrier between the luminal environment and the body interior. The epithelial cells are derived from a population of rapidly proliferating stem cells located in the crypts. Over the course of a 4- to 6-day lifespan, undifferentiated crypt cells migrate out of the proliferative crypt zone along the so-called crypt-villus axis, where they mature and acquire phenotypic characteristics before undergoing apoptotic cell death and extrusion at the villus tip [10-16]. The epithelial cells in the stomach and intestines are circumferentially tied to one another by tight junctions, which seal the paracellular spaces and thereby establish the basic gastrointestinal barrier.

Throughout the digestive tube, maintenance of an intact epithelium is thus critical to the integrity of the barrier.

As discussed later in this chapter, a foreign molecule can pass from the gut lumen into the systemic circulation, by crossing the mucosal epithelial lining either across the epithelial cells (transcellular route) or around the epithelial cells (paracellular route). Since the materials of concern i.e. toxins and allergens are water-soluble macromolecules, they are most likely to take the paracellular route for passive diffusion. The paracellular route is normally guarded by the tight junctions [17-22]. Microscopically they appear as a series of discrete membrane contacts of adjacent cells which consist of a cluster of protein species such as zonula occludens 1, 2 and 3, cingulin, 7H6 and transmembrane proteins such as occludin and claudin (Figure 1-4). Occludins and claudins are the major sealing proteins. Tightness of the tight junctions is physiologically controlled by their degree of phosphorylation. In the small intestine of humans the width of the paracellular pathway at the tight junctions is estimated to be 4-8 A^0, sealing the gap effectively for molecules larger than 500 D [23]. When injured, they can be repaired within 30 minutes *in vitro* [24].

Another important cell type that forms the intrinsic barrier is T-cells. T-cells are located in the loose connective tissue of the lamina propria (lamina propria lymphocytes) and are interspersed among the epithelial layer (intraepithelial lymphocytes). The surveillance system formed by the T-cells along with M-cells of Payer's patches is responsible for recognition and eradication of pathogens and antigens [25, 26].

The Extrinsic Gastrointestinal Barrier

Mucus and Bicarbonate

The entire gastrointestinal epithelium is coated with mucus, which is synthesized by goblet cells that form part of the epithelium. The 200 μm mucus layer is the primary barrier limiting the passage of hydrophobic substances [27]. Mucus serves an important role in mitigating shear stresses on the epithelium. A thick layer of mucus on the gastric epithelium protects them by retarding back-diffusion of protons [28, 29]. It also serves as a physical trap for bacteria, preventing them from reaching the epithelial surface [30, 31].

Hormones and Cytokines

Normal proliferation of gastric and intestinal epithelial cells, as well as proliferation in response to injuries such as ulceration and resection, is known to be affected by a large number of endocrine and paracrine factors. Prostaglandins, particularly prostaglandin E2 and prostacyclin, have been known to have "cytoprotective" effects on the gastrointestinal epithelium [32, 33]. Their cytoprotective effect appears to result from a complex ability to stimulate mucus and bicarbonate secretion, to increase mucosal blood flow and, particularly in the stomach, to limit back diffusion of acid into the epithelium.

Two peptides that have received attention for their potential role in barrier maintenance are epidermal growth factor (EGF) and transforming growth factor-alpha (TGF-alpha) [34-37]. EGF is secreted in saliva and from duodenal glands, while TGF-alpha is produced by gastric epithelial cells. Both peptides bind to a common receptor and stimulate epithelial cell proliferation. In the stomach, they also enhance mucus secretion. Other cytokines such as fibroblast growth factor and hepatocyte growth factor have been shown to

enhance healing of gastrointestinal injuries in rats and mice [38, 39].

Trefoil proteins are a family of small peptides that are secreted abundantly by goblet cells in the gastric and intestinal mucosa, and coat the apical face of the epithelial cells. A number of studies have demonstrated that trefoil peptides play an important role in mucosal integrity and repair of lesions. They cause redistribution of E-cadherin in the cytosol, a process that must take place before restitution [30, 40, 41, 42]. Mice with targeted deletions in trefoil genes showed exaggerated responses to radiation and chemical injury and delayed mucosal healing [43].

Antibiotic Peptides and Antibodies

An important part of barrier function is to prevent transit of bacteria from the lumen through the epithelium. Paneth cells are epithelial granulocytes located in small intestinal crypts. When exposed to bacteria, bacterial antigens and endotoxins, they synthesize and secrete several antimicrobial peptides, chief among them are isoforms of alpha-defensins known also as cryptidins ("crypt defensin") and type II phospholipase A_2. These peptides have antimicrobial activity against number of potential pathogens, including several genera of bacteria, some yeasts and Giardia trophozoites. Their mechanism of action is similar to neutrophilic alpha-defensins, which permeabilize target cell membranes causing eventual death [44, 45].

In addition to non-specific antimicrobial molecules, barrier function is supported by the gastrointestinal immune system. One facet of this defense system is that much of the epithelium is bathed in secretory immunoglobulin A. This class of antibody is secreted from subepithelial plasma cells and transcytosed across the epithelium into the lumen. Luminal

IgA and IgM provide an antigenic barrier by binding bacteria and other antigens. This barrier function is specific for particular antigens and requires previous exposure for development of the response [46, 47].

B. Disruption of the barrier function

Despite its robust and multi-faceted nature, the gastrointestinal barrier can be breached. Breaks in epithelial continuity are daily events caused by mechanical strain due to intestinal motility and physiologic digestive trauma, pathological conditions as well as chemical factors associated with food and drugs.

Infectious and inflammatory conditions

Diverse insults to the intestinal mucosa, including infectious processes, ischemia and damaging chemicals, promote infiltration of neutrophils [48]. This common endpoint results because many types of injuries lead to local production of neutrophil chemoattractants such as leukotrienes, interleukins and activated complement components. In response to chemoattractants, neutrophils migrate out of capillaries, infiltrate the subepithelial mucosa and often transmigrate through the gastric or intestinal epithelium. In crossing the epithelium, neutrophils must break junctional complexes between epithelial cells. This "impalement" through tight junctions necessarily causes a transient increase in permeability. When the insult is minor, the junctions reseal quickly, but transmigration of large numbers of neutrophils induces significant damage to the barrier function [49].

In inflammatory bowel disease (IBD), cell death can directly compromise barrier function of the intestinal epithelium [50, 51]. Alcoholic cirrhosis is another inflammatory

condition in which barrier integrity has been implicated as a disease mechanism [52]. It was suggested that exposure to ethanol causes iNOS activation, nitric oxide overproduction, nitration and oxidation of tubulin, decreased levels of stable polymerized tubulin and increased levels of disassembled tubulin which leads to disruption of the tight junctions.

Effects of Stress

Stress comes in a myriad of forms and is an integral part of all illness and trauma. The stress response involves modulation of various hormones and cytokines, as well as significant effects on neurotransmission. The foremost effect of stress on the gastrointestinal tract is decreased mucosal blood flow and thereby compromised integrity of the mucosal barrier [53, 54]. Among other things, reduced mucosal blood flow suppresses production of mucus and limits the ability to prevent back diffusion of protons. As a consequence, significant stress is almost always associated with mucosal erosions, particularly in the stomach.

Wear and tear of the gut by food and drugs

Wear and tear in the gastrointestinal tract by normal food materials and drugs is a common phenomenon. Myers et al showed that red and black pepper caused mucosal inflammation in the stomach of healthy human volunteers [55]. Paprika and cayenne pepper were found to significantly decrease TEER in a human intestinal epithelial cell line, HCT-8 and increase permeability of 10, 20 and 40-kDa dextrans [56]. Raw garlic powder is known to cause ulcer-like erosions in the gastric mucosa. In a study by Hoshino et al, boiled garlic powder was shown to cause reddening/inflammation of the stomach in dogs. In the same study, the authors further showed effects of an enteric-coated dietary supplement

formulation, which contained garlic powder. 3 hours after administration of the formulation, the small intestine of the dog was isolated and observed under a scanning electron microscope. The micrographs showed ruptured villi, indicating loss of epithelial cells [57]. Similar effects were shown by Amagase et al in rats. Garlic extract as well as commercially available formulations containing garlic powder caused loss of epithelial cells in the ileum of rats [58]. Kvietys et al studied effect of hydrolytic products of food digestion on jejunal mucosa in rats. Upon ingestion of fatty food, it is broken down into mono- and di-glycerides and fatty acids. These hydrolytic food products are subsequently solubilized in the mixed micelles of bile salts and acids. When the rat jejunum was perfused with emulsified lipids i.e. 20 mM sodium taurocholate and 10-40 mM oleic acid, concentrations being similar to those in the postprandial chyme, it was found to cause exfoliation at the villus tip. Restitution occurred within 50 minutes after perfusion with saline at 1 ml/min rate [59]. Bird et al found that when mice were given a gavage of 0.1 to 0.4 ml beef tallow or corn oil, the damaging effect of the orally administered fat boluses could be visualized under a light microscope 2-4 hours after administration of fat boluses [60]. The epithelium appeared normal only after 12 hours.

Alcohol is a popular beverage. When 4.8 oz of 20% ethanol was administered to healthy human volunteers, ruptured duodenal and jejunal villi were observed with fractures extending through both the epithelium and the lamina propria within 15 minutes [68]. The percentage of damaged villi as observed under a light microscope, returned to the control value in about 2 hours. In yet another study, 25 ml of 50% ethanol caused extensive apical rupture with shedding of epithelium and release of mucus in the stomach in healthy human volunteers [69]. After the extensive damage observed, restitution appeared to occur by lateral

movement of basal processes of the epithelial cells in 15 minutes. After 30 minutes, there was evidence of extensive repair.

Certain drugs are also used commonly on a recurring basis and have demonstrated reversible damage in the gastrointestinal mucosa, examples include NSAIDs [172, 173] and common laxatives. Ricinoleic acid is a component of the cathartic castor oil. Bretagne et al tested three laxatives, ricinoleic acid, dioctyl sodium sulfosuccinate and magnesium sulfate on seven healthy human subjects [61]. All the three laxatives were found to induce water and electrolyte secretion, a rise in intraluminal DNA and enzyme activity, indicative of mucosal damage. Similar studies have been reported by Moriarty et al [62] and Saunders et al [63] using human and rat models respectively. Chenodeoxycholic acid, a demonstrated penetration enhancer [64-66], has been used therapeutically since the early 1970's for dissolution of gallstones prescribed in doses up to 20 mg/kg for up to 2 years [67].

In summary, it has been shown in several studies that normal food materials as well as certain drugs cause damage to the gastrointestinal mucosa; and damage and subsequent recovery are normal processes that take place regularly in the gastrointestinal tract. Due to the occasional breaks in the gastrointestinal barrier, endotoxins and bacteria translocate from the gut into the blood [165]. As a result, the portal vein blood generally shows a higher level of endotoxins as compared to the systemic circulation. The toxins in the portal vein are cleared by the reticuloendothelial system in the liver in normal humans [166-169].

C. Restitution and healing after injury

The critical first task following disruption of the gastrointestinal epithelium is to cover the denuded area and rapidly re-establish the intrinsic barrier. This is accomplished by a process called restitution, in which, epithelial cells adjacent to the defect flatten and migrate over the exposed basement membrane. Restitution provides a rapid mechanism for covering a defect in the barrier and does not involve proliferation of epithelial cells [71-74]. Numerous factors are involved in this process, which are summarized in Figure 1-5.

Restitution *in vivo* has been reported to begin as quickly as 15 minutes after injury [70]. The time reported for completion of this process depends upon the type of model used in the study and the concentration of the chemical used to inflict wounds. For example, when the rabbit jejunum was treated with 0.5mM chenodeoxycholate for 25 minutes in an *in vitro* system, mucosal permeability to lactulose returned to the normal value after 40 minutes [65]. Similarly, when the guinea pig ileum was exposed to 0.06% Triton-X 100 (0.75 mM) for 5 minutes in an *in vitro* model, it took one hour for the tissue to seal the defect, when observed under a light microscope [170]. Whereas in an *in situ* perfusion model, when the small intestine of rat was perfused with 20 mM deoxycholate for 30 minutes, it took one hour to cover the denuded villus tips with epithelium, when observed under a light microscope [70]. In all the three studies listed above, even though recovery time was about 1 hour, it should be noted that the concentration of surfactant used in the *in situ* perfusion study was much higher compared to those used for the *in vitro* models.

Morphologic characteristics of epithelial repair

It was recognized by Hudspeth in 1975 that physical removal of a single cell from an epithelium was followed by a rapid self-sealing response whereby neighboring cells reestablished cell-cell contact [24]. This process, which was later termed as "restitution" occurs by migration of still viable remaining epithelial cells from areas adjacent to the injured surface to cover the denuded area (Figure 1-5).

Under normal conditions, intestinal epithelial cells are polarized. The apical membrane and the basolateral membrane are delineated by the intercellular junctional complexes, which exist between adjacent cells. During restitution, cells bordering the zone of injury flatten and take on squamoid appearance and then begin to spread by extending pseudopod-like structures called lammelipodia. They lose apical-basolateral polarity and undergo brush border and junctional disassembly and become polarized along a leading-trailing edge axis forming a contractile purse-string of actomyosin cables connected via intercellular adherens junctions. This actin-myosin purse-string serves to draw the flattened migratory epithelial cells forward over their underlying basal lamina [71-74]. Junctional complexes between epithelial cells reform upon cell-cell contact. In severely damaged villi, restitution is further facilitated by villus contraction mediated by neurally regulated myofibroblasts within the injury zone. This process effectively reduces the surface area to be repaired [70, 75]. Following reestablishment of cell-cell contacts, junctional complexes (tight junction and adherens junction) between epithelial cells reform, a process critical to the restoration of epithelial barrier function [76].

Regulation of epithelial restitution by peptide factors

Numerous cytokines and growth factors are involved in epithelial mucosal repair [30, 42, 77, 78]. These mediators are present both in the lumen (as a result of secretion of these factors from the epithelial cells) and in the submucosal location (secreted by mucosal and submucosal cells) (Figure 1-5). Myofibroblasts immediately beneath the defective epithelial cells secrete hepatocyte growth factor (HGF) and keratinocyte growth factor (KGF). Immune and inflammatory cells in the submucosa also produce growth factors and cytokines that affect epithelial repair in a similar way. For instance, macrophages and mononuclear cells secrete proinflammatory cytokines interleukin (IL) 1 and 2 as well as tumor necrosis factor (TNF) and transforming growth factors (TGF). Platelets release several growth modulating factors such as vascular endothelial growth factor (VGEF), epidermal growth factor (EGF), TGF-β, platelet-derived growth factor, HGF and insulin-like growth factor, in regions of tissue injury [79]. These growth factors interact with basolateral membrane receptors on epithelial cells and stimulate both cell migration and cell proliferation. The precise details of the mechanism remain to be elucidated. HGF is also shown to promote epithelial junction disassembly and epithelial migration.

In addition to the action of growth factors, other regulatory peptides are also involved. Intestinal trefoil factor (ITF) is found primarily in the small and large intestine and is secreted by goblet cells. ITF largely remains in the lumen of the intestine, maintaining contact with the apical epithelium via interaction with mucus [30, 80]. In response to injury, local concentrations are elevated by regulated secretion and release from injured goblet cells. ITF causes loss of the adherens junction protein E-cadherin from the membrane and its redistribution into the cytosol, a process that must precede restitution [81].

Interaction of epithelial cells with extracellular matrix during repair

An intact basement membrane is required for cell migration during restitution. A dynamic interaction between migrating epithelial cells and the basement membrane is equally important [82]. The major components of the basement membrane are collagen type I and IV, laminin and fibronectin. The production of these components by epithelial cells and underlying mesenchymal cells is regulated by growth factors and cytokines. Integrins are the epithelial cell receptors that mediate cell-basement membrane interactions and their regulation is critical in mucosal repair. They also play an important role in formation and degradation of the basement membrane. The population of these receptors is dynamically controlled by growth factors [42].

Intracellular mechanisms of epithelial repair

The increased interaction of integrins with the basement membrane initiates signaling events, which affect actin-myosin based cytoskeletal architecture. The actin-myosin cytoskeletal motor activity is mediated by conventional type II myosin, which is composed of two heavy chains, two essentially light chains, and two regulatory light chains. Regulated cyclic phosphorylation of myosin light chain by myosin light chain kinase is required for migration and for extension of lammelipodia. Actomyosin filaments at the leading edge of migration undergo a dynamic and tightly regulated process of sequential assembly and disassembly, a phenomenon known as 'treadmilling', which propels the cell forward. Calcium (Ca^{2+}) is required for cell migration because of its effect on myosin light chain phosphorylation. It is also required for remodeling of the actin cytoskeleton. Villin, an actin cross-linking protein that is a key structural component of enterocyte microvilli, has been

shown to serve as an actin-severing protein under the high intracellular Ca^{2+} conditions associated with cell injury. This actin-severing function is critical for apical membrane remodeling and plasma membrane plasticity required for cell migration [83].

Nonpeptide factors in the regulation of mucosal repair

Polyamines, butyrate and other short-chain fatty acids are known to influence epithelial repair. Polyamines such as spermidine and spermine regulate cellular myosin II level as well as its association with actin stress fibers. The mechanism of action of butyrate and short-chain fatty acids is poorly understood [84, 85].

The factors that regulate the process of restitution are not fully catalogued and their interrelationships are yet to be elucidated [42, 86, 87].

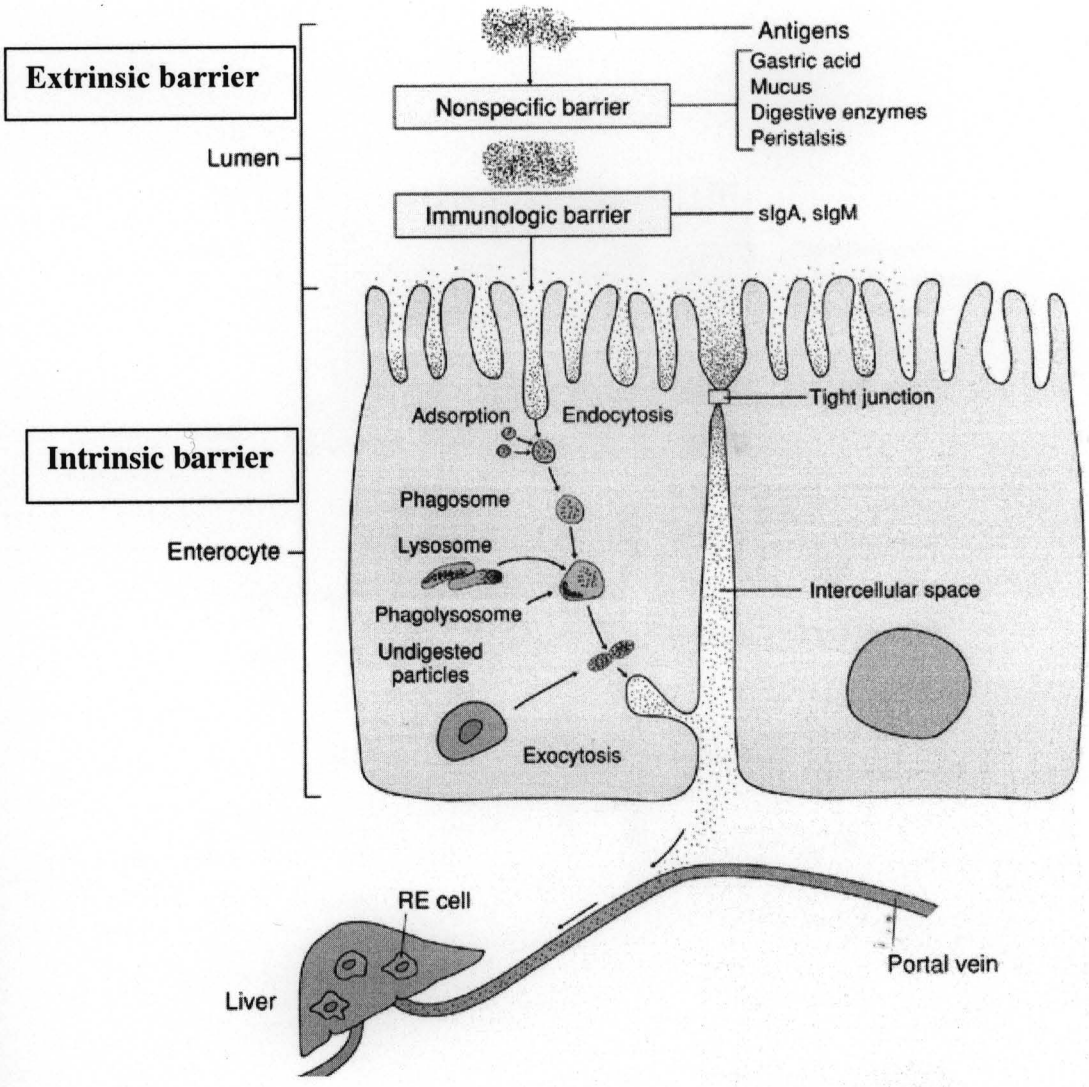

Figure 1-3: Gastrointestinal barriers-Intrinsic and Extrinsic (Reproduced from reference 3)

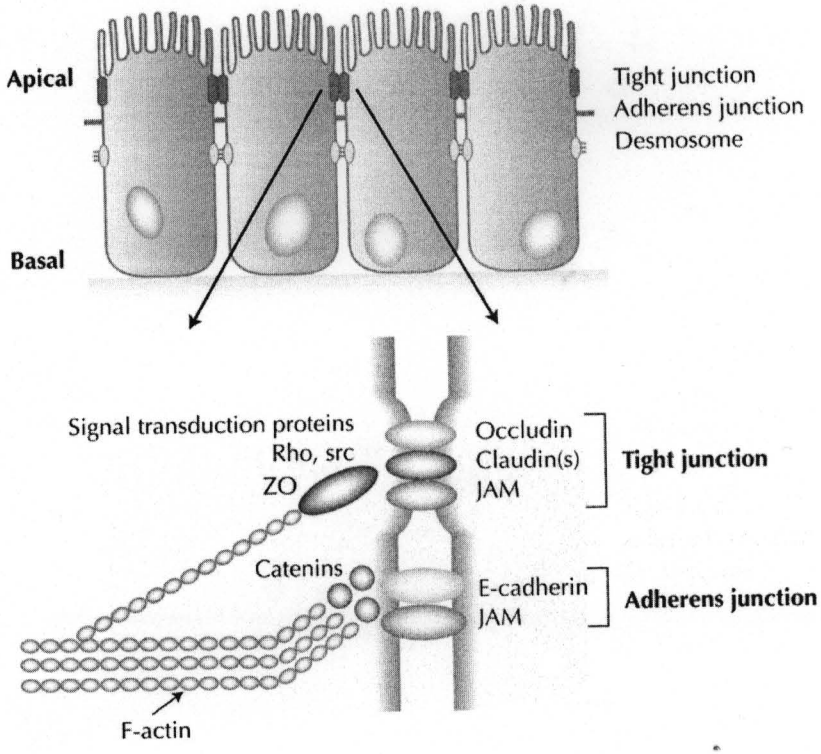

Figure 1-4 Junctional complexes in the small intestinal epithelium (Reproduced from reference 3)

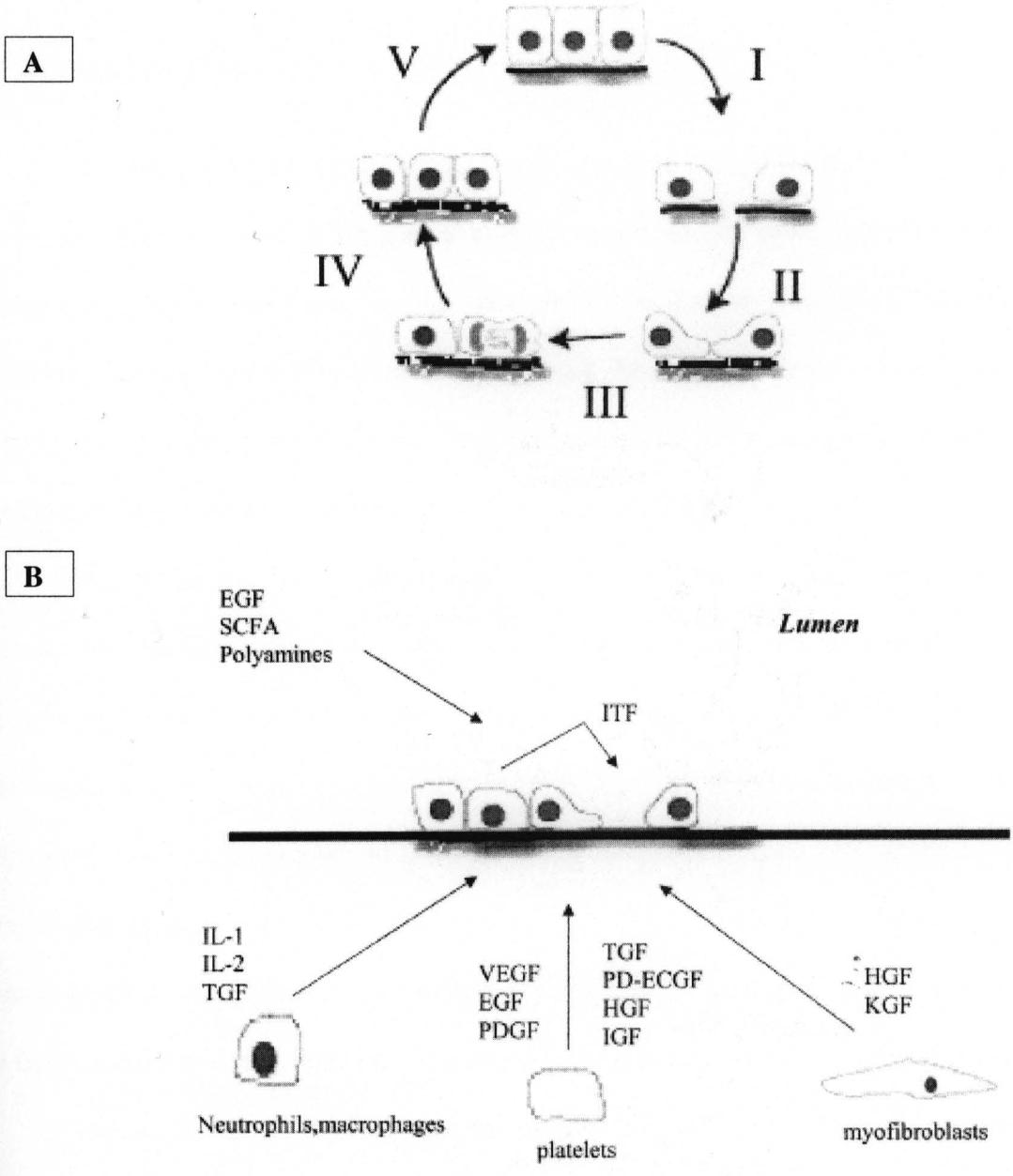

Figure 1-5: A. Restitution I. Damage occurs in the small intestine II. Epithelial cells surrounding the area of damage flatten and migrate III. Tight junctions are reformed IV. Cells divide if additional repair is needed V. Intact epithelial barrier is reinstated

B. Molecular mechanism of restitution (Reproduced from reference 87)

III. Absorption in the Gastrointestinal Tract

A. Absorption pathways

The major barrier to the movement of solutes from the gut lumen into the blood is the mucosal epithelial layer. A drug or a nutrient molecule can cross this barrier passively (transcellular or paracellular) or via transporters (active or facilitated). Alternatively, substances can be internalized by endo/transcytosis. As shown in figure 1-6, a solute can take any of these transport mechanisms, depending upon its physicochemical characteristics, which have been described extensively in literature [88, 89].

In order for drugs to be absorbed by endogenous transport mechanisms, they need to mimic chemical structures of nutrients that utilize these transporters. The uptake mechanism by phagocytosis is limited to particulate matter and macromolecules. Due to these limitations, the most common absorption pathway for drugs is passive diffusion. Passive diffusion refers to movement of a solute along its concentration and electrical gradient. Depending upon the physicochemical properties of a drug, it can take either the transcellular route, which crosses both the lipid bilayer regions and the membrane bound protein regions or the paracellular route, which extends through the water-filled tight junction channels.

Transcellular absorption requires certain characteristics like aqueous and lipid solubility, which can be described by its octanol/water partition coefficient (P). An optimum log P value for a drug is considered to be between 1 and 3. At low P values, drug cannot penetrate the lipid membrane and at high log P values, diffusion through the unstirred water layer of the membrane becomes the rate-limiting step in the absorption process. The water-filled channels at the tight junction offer a diffusion pathway for water-soluble molecules.

The rate-limiting factor for this paracellular absorption pathway is the size, which is 4-8 A^0 in the small intestine, allowing relatively free passage of molecules of molecular weight less than 500 D. Another rate-limiting factor is the limited surface area of this route itself, which is less than 5% of the total surface area of the small intestine.

B. Factors affecting absorption (physicochemical factors for drugs and physiological factors of the GIT)

Oral absorption of drugs is limited by many factors. Physicochemical factors of drugs associated with poor membrane permeability are low partition coefficient, extensive H-bonding with water or high polar surface area, low aqueous solubility and high molecular weight [90]. For some drugs, permeation through the intestinal epithelium is hindered by metabolism by brush border enzymes (Cyt P450) and efflux by P-glycoprotein (P-gp). Physiologic parameters include regional pH, mucosal surface area, metabolism and gastric and intestinal permeability [91, 92].

C. Improvement of drug absorption

Oral absorption of drugs can be improved by modifying the properties of drugs or by incorporating drugs into suitable vehicles or by modifying the absorption properties of the membrane itself.

Drug Modification

The physicochemical properties like solubility, stability, and partition coefficient of a drug can be modified by preparing a suitable analog or prodrug [93, 94]. Prodrugs and

analogs have also been prepared to target specific absorptive transporters like PepT1 (peptide transporter), cobalamine, folate, transferrin and biotin transporters, by incorporating substrate structure features into the molecule for optimum molecular recognition by transporters [95]. This approach is not always feasible. An analog or a prodrug becomes a new drug entity, and safety and efficacy of these molecules need to be established. Since specific transporters are few in number and their transport capacity is limited, targeting these transporters with a prodrug approach is not always practical.

Formulation Modification

Incorporating drugs of interest in a formulation vehicle is the most commonly used method. Polymeric nanoparticles/microspheres have been prepared for enhanced uptake of proteins mainly through M-cells of payer's patches. The particles protect proteins in the harsh intestinal environment and their surface properties (mainly hydrophobicity) can be controlled through polymer chemistry for increased uptake in the gut. Absorption can also be improved by using lipid based drug delivery systems. Formulation modification is the most desirable approach, since it does not involve synthesis of new drug entities. There are a few disadvantages of this approach. Dispersion of the particulate delivery system throughout the gut may prevent particles from accumulating in sufficient amounts onto the absorbing surfaces thus failing to trigger the membrane capping for phagocytosis. Low drug loading capacity of nanoparticles, low transcytosis/phagocytosis efficiency of M-cells, entrapment of nanoparticles in the mucus are additional disadvantages of the delivery system [96, 97]. Physical instability of liposomal/lipid delivery systems in the intestinal lumen and variability in drug absorption profile from these vehicles may also pose problems [98, 99].

Membrane Modification

As an alternative to modifying the drug or its formulation to increase absorption, the barrier function of the intestinal epithelium itself can be altered by using penetration enhancers. Penetration enhancers facilitate movement of administered substances across biological barriers. They may act by one or more of the following mechanisms that have been described at length in various reviews [100-107]. These mechanisms are: 1) improve solubility of drugs through their surface-active action, e.g. surfactants including bile salts and salts of fatty acids; 2) improve diffusivity of the drug through the mucus layer by the mucolytic action, e.g. bile salts; 3) inhibit drug uptake by efflux pumps in the apical intestinal epithelium e.g. glycerides and pluronics, and finally; 4) improve permeability of drugs through the gastrointestinal epithelium, which is achieved through their action on the plasma membrane of the epithelial cells and the tight junctions. The fourth mechanism of action is essentially membrane modification, the details of which are described below.

Transcellular absorption of drugs is enhanced by extraction of membrane components and/or increasing membrane fluidity. Traditionally, nonionic (Brij, Tweens) and anionic (Sodium dodecyl sulfate) surfactants as well as bile salts such as deoxycholate, taurodihydrofusidate and taurodeoxycholate were studied to enhance absorption of drugs. These classical penetration enhancers mainly act by initial insertion into the membrane and subsequent solubilization and extraction of membrane components like phospholipids, cholesterol and proteins, thereby disrupting the lipid bilayer [105, 108-111]. α and β-cyclodextrins have been shown to selectively extract phospholipids and cholesterol respectively, thereby increasing transcellular drug absorption [109, 112]. Fatty acids and their

derivatives act primarily by increasing membrane fluidity [113, 114]. These molecules insert themselves inside the phospholipid bilayer and disrupt lipid packing. Medium-chain glycerides act by a similar mechanism. In addition to the effect on the phospholipid bilayer, fatty acid derivatives also interact with membrane proteins and cause perturbation of the membrane [115]. The most commonly used fatty acid for this purpose is oleic acid. Increasing membrane fluidity can improve absorption of small molecules by improving their diffusion across the lipid bilayer due to reduced viscosity of the membrane. In general, since the transcellular route accounts for more than 95% of the total surface area in the small intestine, it becomes an important route for drug delivery considerations.

Paracellular junctions are water-filled channels and the main route of permeation for highly water-soluble compounds. Paracellular enhancers have been studied in order to improve permeation of hydrophilic macromolecules like proteins and peptides. Paracellular absorption enhancers act by disruption of the tight junctions, which restrict passage of molecules under normal conditions. Ca^{+2} ion chelators like EDTA, EGTA and citrate open tight junctions by sequestering Ca^{+2} ions in the extracellular fluid that leads to disruption of actin filaments and adherens junctions [116, 117]. Sodium salts of fatty acids affect the integrity of the tight junctions through their Ca^{+2} chelating action. Tomita et al showed that sodium caprate and sodium laurate at 0.25% concentration, increased the pore size in the rat colon from 8 A^0 to 14 A^0, whereas sodium taurocholate, sodium caprylate and EDTA increased it to 11-12 A^0 at the same concentration [118]. Recently, a lot of research has been focused on use of chitosans as absorption enhancers. The mechanism of action of these polymers is not clear yet. But it was proposed that absorption-enhancing effects of chitosans on epithelial cells are mediated through their positive charges. The interaction of chitosans

with the cell membrane results in a structural reorganization of tight junction-associated proteins ZO-1 and F-actin, which is followed by enhanced transport through the paracellular pathway [119, 120].

Penetration enhancers increase permeability for a wide variety of drugs nonselectively. They are considered grossly damaging and are not approved for clinical use.

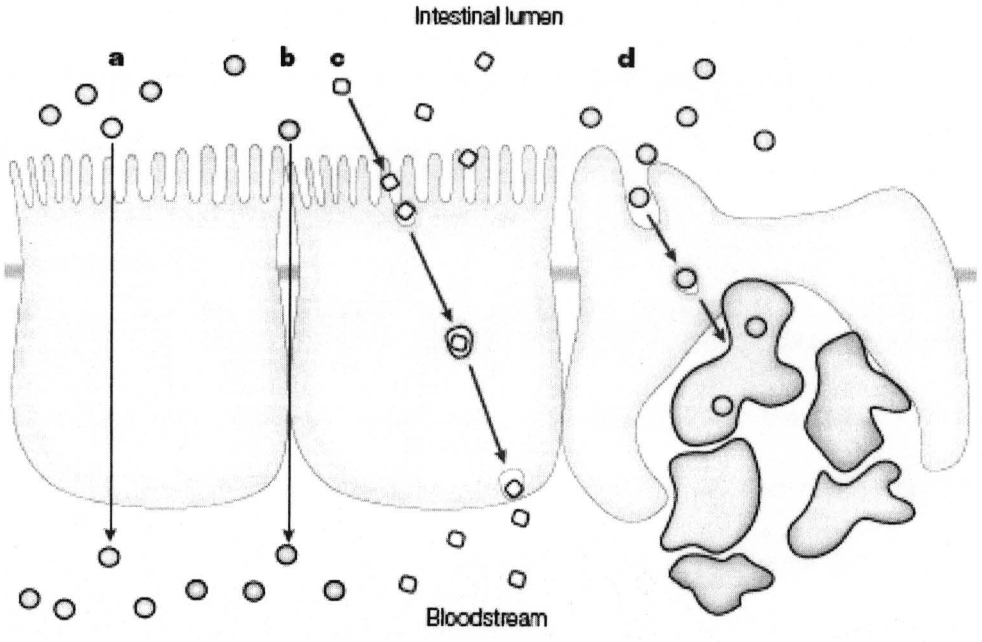

Figure 1-6: Pathways of absorption A. Passive transcellular B. Passive paracellular C. Carrier-mediated D. Endo/phagocytosis (Reproduced from reference 164)

IV. Models and Methods Used in Penetration Enhancer Studies

A. Models

Two important aspects of studies involving penetration enhancers are testing their efficacy (enhancement in absorption) and assessing safety (measurement of damage and recovery). There are three kinds of models used to study different aspects of oral drug absorption. These are *in vitro, in situ* and *in vivo* models.

1. In vitro models

There are numerous *in vitro* models available to study drug absorption. Everted intestine preparations, mucosal sheets and cultured cells are the most common in this category [121]. The everted intestinal methods are simple and rapid but have several shortcomings. Electron microscopy has shown that the integrity of the isolated intestinal tissue is maintained for only short periods of time (5 minutes) [122, 123]. After one hour, there was total disruption of the epithelial tissue. The binding of drug to muscularis and serosal tissues can also alter the diffusion process.

The latter disadvantage of everted intestinal model can be eliminated in the mucosal sheet model, if the mucosal sheets are stripped to remove the serosa and the muscle layers [124, 125]. If the mucosal sheets are mounted on the Ussing type diffusion chambers, measurement of the electrical parameters of the membrane is possible to indicate viability of the tissue, during the course of the experiment. Care should be taken in clamping the tissue into the chamber. Edge damage can occur during the procedure, which will lead to false experimental results [126, 127].

Recently, immortalized tumor cell lines like, Caco-2 and HT-29 have been used to

study drug transport. Caco-2 cells mimic the intestinal absorptive cells in many transport and metabolism properties. HT-29 cells can be induced to form mucin-producing goblet cells and therefore offer a cell culture model for the study of the effect of mucin on drug transport [128, 129]. Cell culture models are easy to work with, once culture conditions have been established. It is easier to manipulate transport media conditions like pH, ion concentrations, metabolic inhibitors and experimental conditions like temperature, unstirred water layer. This allows the mechanisms of transport and metabolism to be more easily probed [127, 130, 131]. Also, relatively clean samples, compared to tissue and blood, can be prepared for analysis. A very important advantage of cell lines is that they allow the isolation of specific cell types e.g. enterocytes, crypt cells and goblet cells. This permits delineation of the importance of different cell populations in the absorption and metabolism of drugs.

In vitro models especially cell culture models are useful in understanding the mechanism of action of penetration enhancers. The obvious disadvantage of these models is slow recovery due to lack of blood supply, especially in case of cell cultures, which lack the basal lamina and other underlying structures.

2. *In situ* models

A significant advantage of the *in situ* technique is that even though the animal is anesthetized, the mesenteric blood flow and the basal lamina are intact [89, 132, 133]. A major disadvantage of this technique is that results of both absorption enhancement and damage/recovery depend upon hydrodynamics in the lumen i.e. perfusion rate of luminal fluid in the open loop method, and variable absorption and secretion of water in the closed loop method which affect the effective concentration of the drug and penetration enhancers

in the lumen [134, 135]. It is still an excellent approach to study the factors that are of importance to drug absorption.

3. *In vivo* models

Use of intact and conscious animals is important in every stage of drug development, before testing in humans. From *in vivo* studies, absolute bioavailability from different drug formulations can be determined after oral and intravenous dosing, formulation factors can be optimized to achieve the desired pharmacokinetic profile and pharmacological effects. The effects of several physiological factors, such as pH, presence of food on drug absorption can be assessed. For the penetration enhancer approach, a more realistic estimate of absorption enhancement, damage and recovery could be obtained in intact animals. However, while choosing an animal model, interspecies differences and limitations should be kept in mind. Small animals such as mice, rats and guinea pigs cannot be used to test solid dosage forms. Larger animals such as dogs, pigs and monkeys permit studies on intact solid dosage forms. Monkeys are closest to humans in terms of evolutionary development and therefore might be expected to respond to treatments as humans would. But lack of availability, high cost of maintenance and specialized handling and housing procedures preclude their use as animal models [136]. Among other models, pigs are closest in anatomy and physiology of the digestive of tract to humans. Again, the size, cost and difficulty in handling limit their use as an animal model [137, 138]. The most commonly used laboratory animal in testing dosage forms is dog. Dogs have a short GI transit time of 6-8 hours as opposed to 24-72 hours in humans [139]. The short transit time may cause a problem in testing penetration enhancers, especially if incorporated in solid dosage forms, since their efficacy, toxicity and reversibility

of action are contact-time dependent. Rats are the second most commonly used laboratory animals in oral absorption studies. The GI transit time in rats is 24-48 hours, which is similar to humans. One important physiological difference is that rats lack the gall bladder and bile is secreted continuously [140, 141]. Since, the bile salts and acids are natural penetration enhancers, they may interfere in action of administered penetration enhancers. This problem can be solved by incorporating appropriate negative control groups in the study.

B. Methods used to evaluate damage and recovery

Methods used to evaluate damage in *in-vitro* and *in-situ* models, include measurement of release of membrane components like proteins, phospholipids, cholesterol, and intracellular components like cytoplasmic lactate dehydrogenase (LDH), which indicates loss of plasma membrane integrity [142]. In cell culture studies in addition to above methods cell viability tests are also used because of the relatively cleaner samples. The MTT assay is a quantitative colorimetric assay that detects living cells, based on the ability of the live cells to cleave a tetrazolium salt by mitochondrial dehydrogenase. This reaction does not take place in dead cells [142]. Tinctatorial studies are also performed on cell culture models to evaluate integrity of membrane of cell or cell organelles. The trypan blue exclusion test is used to indicate plasma membrane integrity. If the plasma membrane remains intact, the cell doesn't stain. The neutral-red assay evaluates lysosomal function and membrane damage. Neutral red dye passively permeates plasma membrane and gets concentrated in the lysosomes of the viable cells [143, 144]. DNA-propidium iodide staining assay detects damage to the nuclear membrane by measuring fluorescence induced by intercalation of propidium iodide with DNA in cells with damaged nuclear membrane [145, 146].

The most commonly employed method for measuring both damage and recovery for *in vitro* models is measuring transepithelial electrical resistance (TEER) to indicate loss and recovery of tight junction integrity [125]. Recovery is also measured by measuring time required to regain control value of permeability coefficient of marker molecules like mannitol, phenol red, inulin, polyethylene glycol and FITC-dextran. Histological evaluation is a valuable tool that has been used traditionally for *in vitro*, *in situ* and *in vivo* models. It can be made semi-quantitative by assigning histological scores depending upon observations under light microscopy or electron microscopy. The factors considered are: the amount of mucus and debris, contraction, swelling or erosion of villi, alignment of epithelial cells, narrowness of the tight junctions, intactness of the microvilli etc.

In recovery experiments, for *in vitro* models, the tissue or cells are treated with a certain concentration of penetration enhancer for a specific period of time, after which it is replaced by the control medium and then the desired parameters are measured in order to determine the time of recovery. For *in situ* models, an intestinal segment is perfused with a certain concentration of penetration enhancer for a specific period of time, after which it is washed off with the control perfusion medium and then the desired parameters are measured in order to determine the time of recovery. The obvious limitation of these two models for use in recovery experiments is that the resulting recovery time would depend upon the contact time between the penetration enhancer solution and the tissue/cell model, which is up to the discretion of the experimenter. For *in situ* models the additional variable factor is rate of perfusion. These variables could be avoided and more realistic estimates of recovery times could be obtained in an *in vivo* model.

Chapter 2: Statement of Research Problem and the Overall Plan of Research

Penetration enhancers increase permeability for a wide variety of drugs nonselectively. A disadvantage of this approach is disruption of the epithelial membrane of the gut by these molecules. Enhancers acting by this mechanism are considered grossly damaging and are not approved for clinical use. The safety considerations are usually associated with ulceration caused in the mucosa by enhancer molecules and immunological concerns arising from enhanced permeation of endotoxins and antigens as a result of disruption of the mucosal barrier.

It has been shown that restitution, a first-line defense mechanism in concert with subsequent proliferation repair injuries sustained after intake of various foodstuffs and after thermal, mechanical or hyperosmolar damage. This raises a question- Is it possible to use penetration enhancers to increase oral absorption of drugs such that after temporary alteration, barrier properties of the mucosa are retained after the normal repair mechanisms? If a penetration enhancer is chosen in such a way that the frequency and extent of erosions/damage caused is similar to food-induced erosions, it is possible that upon clearance of the enhancers from the lumen, rapid repair and resealing of the surface epithelium can reinstate the barrier properties of the brush border. Meanwhile, if endotoxins or antigens are absorbed in the portal circulation, they can be detoxified by the reticuloendothelial systems of healthy humans. However, caution should be taken in subjects with impaired hepatic function or compromised immunity. The main hurdle in putting this approach into practice is the lack of a quantitative method to measure barrier disruption coupled with subsequent recovery. If such a method were available, it would be possible to determine the amount of penetration enhancers that can be used orally to increase drug permeation without causing irrecoverable damage to the gastrointestinal mucosa.

Safety has always been a concern when using penetration enhancers and measurement of damage and recovery is almost an integral part of the study. So far damage has been evaluated by measuring release of cell membrane components or intracellular contents and histology in *in vitro* (excised tissue or cell culture) and *in situ* models. Additional methods used for *in vitro* models are measurement of intracellular enzyme activity and changes in transepithelial electrical resistance (TEER). Recovery is evaluated by measuring time required to regain the control value of permeability coefficient of marker molecules (mannitol, PEG) and morphology for both *in vitro* and *in situ* models and additionally, TEER for *in vitro* models. A disadvantage of using an *in vitro* system is that recovery is slow due to lack of blood supply and basal lamina as in the case of cell culture models. In *in situ* models, rate of recovery would depend upon the experimental conditions, like perfusion rate and the contact time between the mucosa and the penetration enhancer before the intestinal lumen is washed off with a buffer solution. A whole, live animal model would give a better estimate of recovery due to the presence of an intact blood supply and the basal lamina and lack of any external artifacts.

For *in-vivo* models the commonly employed method is histological evaluation. Histological evaluation gives visual evidence of changes in morphology, but it is a semi-quantitative technique. Since absorption enhancers act by altering the barrier properties of the membrane, measuring absorption of marker molecules through damaged and recovered gut will give a more quantitative and dynamic measure of mucosal recovery. To study the recovery of the barrier function, we propose to use low and high molecular weight markers. A low molecular weight marker is presumably more sensitive in reflecting changes in absorption barrier. A high molecular weight water soluble marker is chosen to see how the

absorption barrier would recover against similar high molecular weight, water soluble, toxic molecules like endotoxins, exotoxins and allergens. Recovery of the absorption barrier measured using marker molecules will be complemented with morphological recovery evaluated using microscopy techniques. These techniques will also be used to evaluate recovery of the mucosa after repeated exposure to a penetration enhancer.

Hypothesis: Penetration enhancers that cause temporary and reversible loss of absorption barrier function of the gastrointestinal epithelium can be used to increase drug absorption without local toxicity, provided recovery is complete and recovery time is less than dosing interval.

The following specific aims were pursued for the proposed study:

Specific Aim 1: Measure absorption enhancement of marker molecules by a penetration enhancer.

Specific Aim 2: Measure absorption barrier recovery with marker molecules at different time points after oral administration of a penetration enhancer.

Specific Aim 3: Evaluate morphological recovery with light microscopy and transmission electron microscopy at different time points after administration of a penetration enhancer.

Specific Aim 4: Measure damage/recovery of the gastrointestinal epithelium after repeated exposure to a penetration enhancer.

Chapter 3: Selection of Materials, Animal Model and General Methodology

Selection of marker molecules

The marker molecules chosen are water-soluble, to exclude the possibility of increased oral absorption of otherwise hydrophobic drugs due to increased solubilization in the presence of penetration enhancers. Two different molecular weight markers are selected to see if absorption barrier recovers at the same or at different time points for different molecular weight markers. The low molecular weight marker chosen is phenol red (PR, 354 D) and the high molecular weight marker is fluorescently-labeled dextran, 10 kD (FD10). A low molecular weight marker is presumably more sensitive in reflecting changes in absorption barrier. A high molecular weight water soluble marker is also chosen to see how the absorption barrier would recover against high molecular weight, water soluble, toxic molecules like endotoxins, exotoxins and allergens. Both these markers are commonly used and poorly absorbed when administered orally [110, 147-150].

Selection of penetration enhancer

The criteria for selection of a surfactant were known local toxicity and non-systemic toxicity. Sodium dodecyl sulfate (SDS) is an anionic surfactant. It is a commonly studied penetration enhancer, which has been shown to extract epithelial membrane components like proteins, phospholipids and cholesterol due to its surface-active behavior [108, 110, 142]. Below the critical micellar concentration, it opens up paracellular junctions by chelating Ca^{+2} ions, which are required to maintain the tight junctions [151]. In a 90-day feeding study, when rats were given 1000 ppm of SDS in daily diet (average consumption of 20 mg of SDS per day), it was shown to be systemically nontoxic [152]. In a similar study by Fitzhugh et al, 1% SDS was shown to cause no systemic toxicity when administered via diet to rats for two

years [153]. This was important information since it was crucial to eliminate any interference from systemic toxicity of a penetration enhancer and to ensure that the changes seen upon treatment with SDS would result solely from the local action of SDS on the intestinal mucosa. Based on the reported information, 1% SDS (34 mM) concentration was chosen as the treatment and 1.5% and 2% SDS (51 mM and 68 mM respectively) concentrations were used as positive controls.

Animals

Male wistar albino rats (about 300 gm body weight) were used in all the experiments. The rats were obtained from Harlan, Madison WI. The animals were housed in a temperature and humidity controlled room and were given standard rat food and water which were freely available. All the procedures used in this study were approved by the research animal resources center (RARC), UW. The animals were fasted overnight with free access to water before experiments, to eliminate effect of food on mucosal damage and recovery.

For all the oral absorption experiments and IV experiments, rats were anesthetized using isoflurane (administered via a nose cone) using NARKOVET 2 isoflurane machine, during blood draws. At the end of the experiments rats were euthanized in a carbon dioxide chamber.

For all morphological experiments, rats were anesthetized using isoflurane (administered via a nose cone) during tissue collection and euthanized by excision of the heart afterwards.

Assay of marker molecules

Blood samples were collected in blood collection tubes containing 50mM EDTA and mixed thoroughly. The tubes were stored on ice till they were centrifuged. The blood samples were spun down at 5000 rpm for 7 minutes. The supernatant plasma was pipetted into sterile microcentrifuge tubes and stored at -80^0C till assays were performed.

Marker molecules were assayed by reverse phase HPLC (Varian Prostar, Model 210) coupled with a UV (Varian Prostar, Model 320) and fluorescence detector (Varian Prostar, Model 363). Briefly, plasma proteins were precipitated by adding 20% trichloroacetic acid and acetonitrile sequentially, in a 2:1:1 proportion to plasma samples. The mixture was vortexed after each addition and centrifuged at 8000 rpm for 5 minutes. The supernatant was diluted with mobile phase in 1:1 proportion. The samples were assayed on a C18 column (Econosil C18, Alltech, IL) using pH 4.0 phosphate buffer (50mM) and acetonitrile (77:23) as a mobile phase. Phenol red was detected at 430 nm on a UV detector and FD-10 was detected on a fluorescence detector set at 490 nm for excitation wavelength and 520 nm for emission wavelength. No secondary peaks were seen either for phenol red or FD-10 in plasma after intravenous or oral administration, which is consistent with the reported literature [154, 155]. The recovery of phenol red and FD-10 from plasma were 83% and 99% respectively whereas the limits of detection were 0.1 and 0.2 μg/ml respectively.

Statistical analysis

The statistical program SIGMASTAT (Windows version 3.11, 2004, Systat software, Inc.) was used to analyze the pharmacokinetic data. Parameters obtained for the treatment groups were compared with the respective parameters from the control group using one-way ANOVA at 5% significance level. To determine the number of animals to be included in treatment and control groups, power analysis was performed with β at 80% and α at 5% level. Goodness-of-fit was evaluated for the model fits by using equations described in Appendix M.

Pharmacokinetic analysis

Two-compartment pharmacokinetic analysis was performed on intravenous bolus and control oral absorption data for phenol red using WinNonlin 4.1 software (Pharsight Corporation, 1998-2003). Statistical moment analysis on phenol red data was performed using WinNonlin 4.1 software. Two-compartment analysis on oral absorption of phenol red with SDS and during recovery periods was performed using MATLAB® 5 software. The details of these models are given in the respective Results and Discussion sections in Chapter 4.

Chapter 4: Experiments and Results

Chapter 4-A: Oral and Intravenous Disposition of Phenol Red and FD-10

1. Materials

All chemicals used were ACS grade. Phenol red (PR) and Fluorescently labeled dextran- 10 kD (FD-10) were purchased from Sigma Chemicals, St. Louis, MO. Acetonitrile and trichloroacetic acid were obtained from Fisher Scientific, St. Louis, MO. Isoflurane (IsoFlo®) was ordered from Abbott labs, Chicago, IL. 2 ml EDTA blood collection tubes containing 50 mM of EDTA were obtained from Midwest-Vet Supply, Madison, WI.

Solutions used for intravenous bolus study were prepared in normal saline solution and aseptically passed through 0.2 μ sterile, pyrogen free filters.

2. Methods

I. Disposition of phenol red after intravenous and oral administration

For an IV bolus study, 0.25 mg of phenol red dissolved in 0.1 ml solution was administered into the jugular catheter and blood samples (300 μl) were withdrawn at 0, 5, 10, 15, 20, 30, 60, 90, 120, 180 and 240 minutes, using sterile and pyrogen free 23 GA 3/4' hypodermic needles and 1 ml tuberculin syringes. After administration of dose and after each blood draw, catheters were flushed with heparin solution (10 IU/ ml; dissolved in 50% glycerin) to prevent clogging due to blood clotting. The plasma was separated and assayed as described in the methodology section. Pharmacokinetic analysis was performed using WinNonlin 4.1 software (Pharsight Corporation, 1998-2003).

For oral absorption studies, an oral gavage of phenol red solution (6 mg dissolved in 2 ml) was given to rats using a 3.5" intragastric feeding tube. Blood samples were drawn from the jugular vein using sterile and pyrogen free 23 GA 3/4 hypodermic needles and 1 ml tuberculin syringes at 0, 10, 20, 30, 60, 120, 180 and 300 minutes. The plasma samples were

separated and analyzed as described in the methodology section. Pharmacokinetic analysis was performed using WinNonlin 4.1 software (Pharsight Corporation, 1998-2003).

II. Disposition of FD-10 after intravenous and oral administration

The IV data for FD-10 was taken from Nishida et al (Table 4-A-3) [156]. The dose and method followed for oral absorption studies for FD-10 were same as described for phenol red.

3. Results and Discussion

I. Disposition of phenol red after intravenous and oral administration

The semi-log plot of plasma concentration-time profile of phenol red obtained after an IV bolus administration was a bi-exponential curve showing that phenol red followed a two-compartment model (Figure 4-A-1). When the oral absorption plot of phenol red was overlaid with the IV plot, the terminal elimination phase for the oral absorption curve was different from that for the IV curve, indicating that phenol red followed flip-flop kinetics i.e. the oral absorption rate constant (K_a) for phenol red is smaller than its elimination rate constant (K_e). The bi-exponential behavior is not apparent in the oral absorption plot due to overlap of the distribution phase with the absorption phase.

The schematic diagram of a two-compartment model is shown in Figure 4-A-2. The data was fitted to a two-compartment model using WinNonlin software. The model fits are shown in figure 4-A-3 and the pharmacokinetic parameters determined for phenol red using both IV and oral study data are listed in tables 4-A-1 and 4-A-2. K_{23} and K_{32} are the distribution rate constants between the central compartment and the peripheral compartment. V_2 is the volume of the central compartment. K_e is the elimination rate constant and total

clearance from plasma (CL) is calculated by dividing volume of distribution by elimination rate constant. Since the elimination rate constant (K_e), total clearance (CL) and volume of distribution in elimination phase (V_{ss}) obtained in our IV study were comparable to the reported values (Table 4-A-1), in spite of the higher doses administered in the reported studies, we assume that no saturation kinetics were achieved in the plasma concentration ranges obtained in our study.

The first order absorption rate constant (K_a) obtained for oral absorption was indeed lower than the elimination rate constant, showing that absorption is the rate-limiting step in oral pharmacokinetics of phenol red (Table 4-A-2).

II. Disposition of FD-10 after intravenous and oral administration

Simulated IV plot was generated using WinNonlin for FD-10 (Figure 4-A-4) with the reported pharmacokinetic parameters listed in table 4-A-3. FD-10 was reported to follow a two-compartment model.

After oral administration, FD-10 was not detected in plasma. This observation can be explained on the basis of size. The hydrodynamic radius of FD-10 is 25 ^{0}A whereas the width of the paracellular junction in the small intestine is 6-8 ^{0}A in rats. Hence, FD-10 was excluded from the paracellular pathway on the basis of size.

Results obtained for oral absorption of PR and FD-10 were used as negative controls for the subsequent experiments.

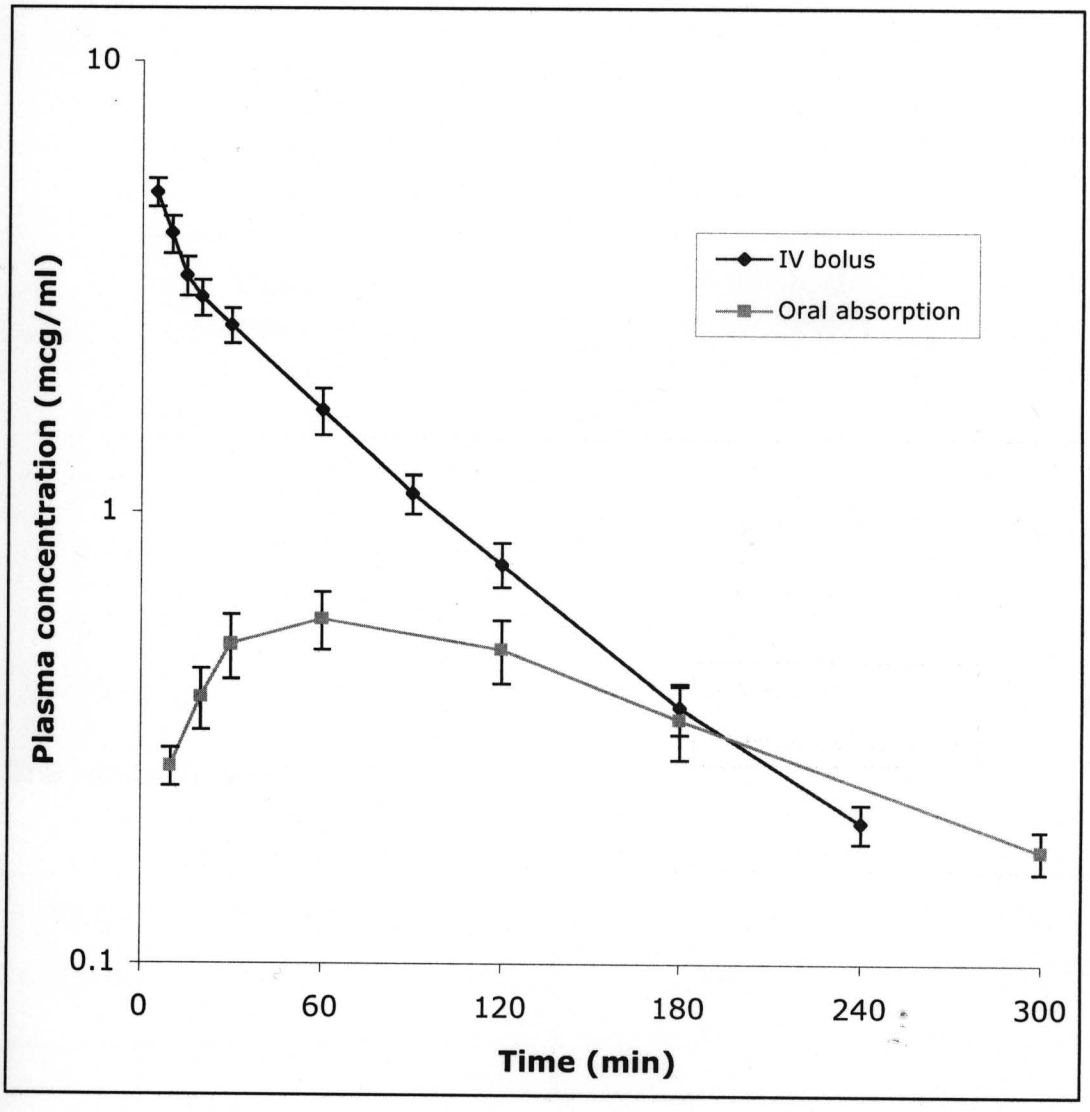

Figure 4-A-1: Plasma concentration-time profiles of phenol red after intravenous bolus and oral administration.

(IV study: N = 3, Oral absorption study: N = 12, Each point represents Mean ± S.E.)

A. Intravenous administration

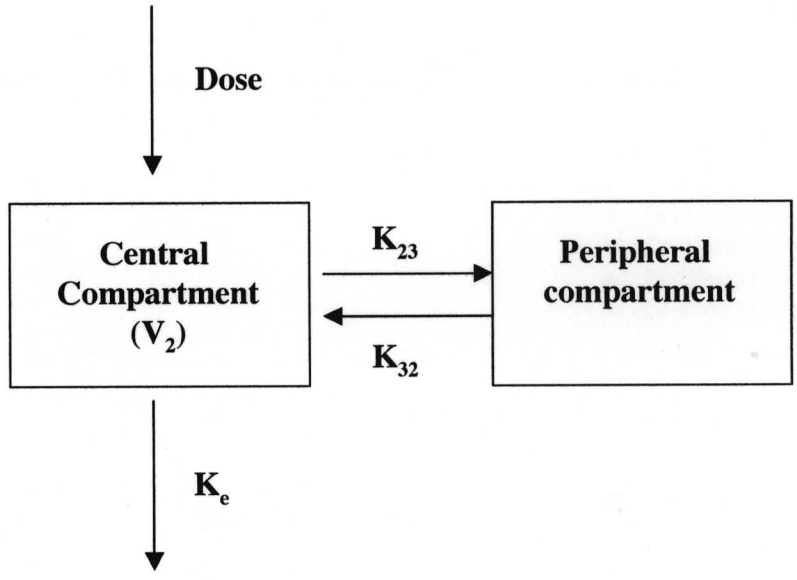

B. Oral administration

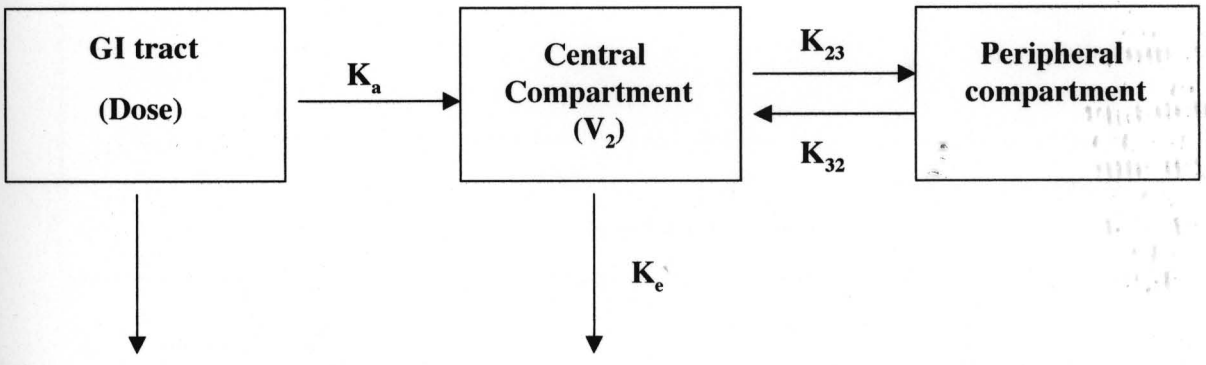

Figure 4-A-2: Two-compartment pharmacokinetic model after intravenous and oral administration

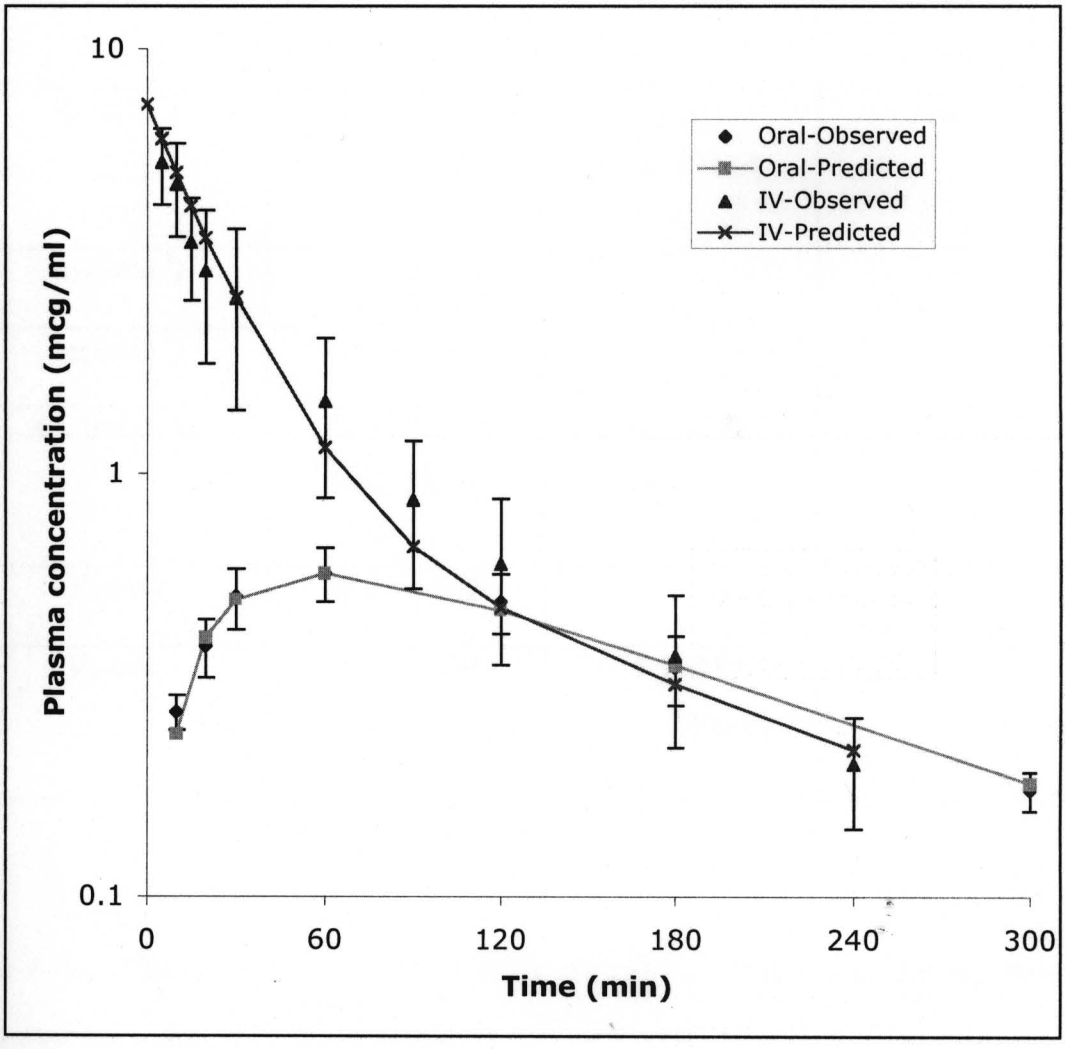

Figure 4-A-3: Observed and predicted plasma concentrations of phenol red obtained by two-compartment model fitting.

(Each point represents Mean ± S.E. for oral and Mean ± S.D. for IV data)

Pharmacokinetic parameters	**Estimated values**	**Reported values**	**References for the reported values**
K_e (min^{-1})	0.024 ± 0.003 Dose: 250 μg	0.0264 Dose: 600 μg	[157]
K_{23} (min^{-1})	0.0138 ± 0.014		
K_{32} (min^{-1})	0.01 ± 0.004		
CL (ml/min)	0.84 ± 0.084 Dose: 250 μg	0.963 ± 0.050 Dose: 3000 μg	[158]
V_2 (ml)	24.27 ± 3.88		
V_{ss} (ml)	59.16 ± 4.089 Dose: 250 μg	50.4 ± 4.2 Dose: 3000 μg	[158]

Table 4-A-1: Pharmacokinetic parameters for phenol red estimated by fitting intravenous bolus data to a two-compartment model.

(N=3, Each value represents Mean ± S.E.)

Pharmacokinetic parameters	Estimated values
K_e (min^{-1})	0.024 ± 0.003
K_{23} (min^{-1})	0.0138 ± 0.014
K_{32} (min^{-1})	0.01 ± 0.004
K_a (min^{-1})	0.009 ± 0.001
F (% Bioavailability)	1.5%± 0.10

Table 4-A-2: Pharmacokinetic parameters estimated for phenol red by fitting oral absorption data to a two-compartment model.

(N=12, Each value represents Mean ± S.E).

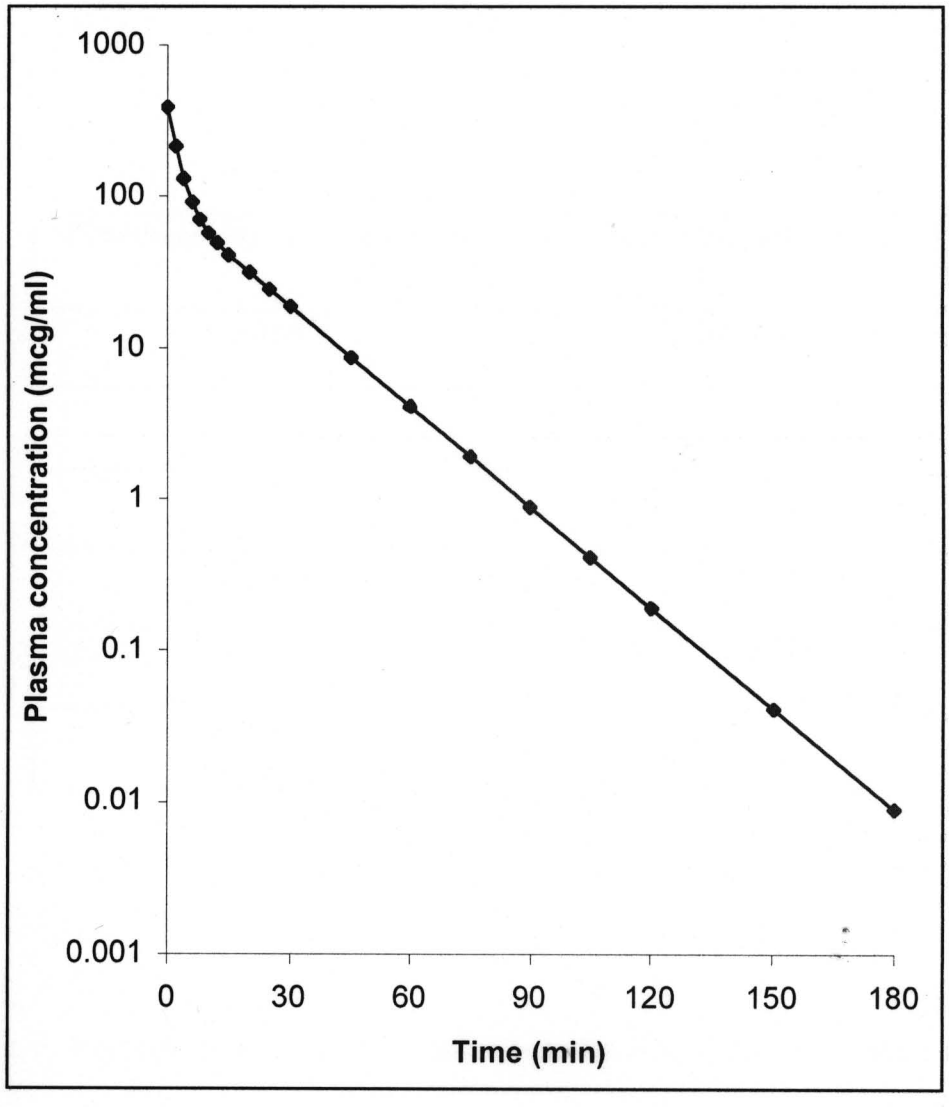

Figure 4-A-4: Simulated plot of plasma concentration versus time generated for FD-10 using WinNonlin (Adapted from reference 156).

Pharmacokinetic parameters	Reported values
K_e (min^{-1})	0.158 ± 0.07
K_{23} (min^{-1})	0.167 ± 0.032
K_{32} (min^{-1})	0.131 ± 0.047
V_1 (ml)	16.57 ± 0.52
V_2 (ml)	29.57 ± 0.58
Dose (mg)	5

Table 4-A-3: Reported pharmacokinetic parameters for FD-10 for an IV bolus experiment (Reference 156).

(N=4, Each value represents Mean ± S.E.)

Chapter 4-B: Oral Absorption Enhancement of Marker Molecules by a Penetration Enhancer

(Objective I)

1. Materials

Besides the materials described in chapter 4-A, the additional material used was sodium dodecyl sulfate (SDS). SDS was obtained from Sigma Chemicals, St. Louis, MO.

2. Methods

The methods used for absorption enhancement experiments were the same as described for oral absorption of marker molecules in chapter 4-A. The only variation made in this section was that the gavage solution contained SDS (1%, 1.5% or 2% w/v) with the marker molecules (PR and FD-10, 6 mg/2ml). Statistical moment (non-compartment) analysis was performed on phenol red data using WinNonlin (Appendix A) to evaluate pharmacokinetic parameters for the control and treatment groups. Two-compartment analysis was further performed on phenol red data using MATLAB® 5 software to estimate changes in absorption rate constant (K_a) with time (programs used are given in detail in Appendices B through E).

3. Results and Discussion

I. Oral absorption enhancement of phenol red upon co-administration with SDS

As explained in Chapter 3, 1% SDS was selected as the treatment and 1.5% and 2% SDS were selected as positive controls. The oral absorption enhancement experiments were performed to ensure that the concentrations of SDS chosen, indeed caused significant increase in plasma concentrations for the marker molecules so that further experiments could be designed to measure absorption barrier recovery. The results of absorption enhancement experiments for phenol red are shown in figure 4-B-1. SDS led to significantly higher plasma

concentrations at all the three concentrations used. The area under the plasma concentration-time curve from time zero to t ($AUC_{0\text{-}300\ min}$) for each treatment was calculated using linear trapezoidal rule. The C_{max}, (maximum drug concentration obtained in plasma), T_{max} (time when maximum plasma concentration is obtained) and AUC (area under the plasma concentration-time curve) values for phenol red are listed in table 4-B-1.

Absorption enhancement of phenol red was SDS dose related. Higher C_{max} was achieved with increasing concentration of SDS. An earlier T_{max} was obtained and it was seen to be about 10 minutes with all the three concentrations of SDS showing that penetration enhancement action of SDS was quick. Since it was difficult to withdraw blood samples earlier than 10 minutes, the accurate T_{max} for the treatment groups could not be estimated. The increase in AUC was found to be linear over the SDS dose range used.

Mean residence time (MRT), mean absorption time (MAT) and bioavailability were determined by performing statistical moment analysis (Appendix A). Mean residence time is the statistically weighted average amount of time that a molecule spends in the body. For an IV bolus experiment, it is the average time that a molecule would spend in the central and the peripheral compartments whereas for oral absorption experiments, it is the average time that a molecule would spend in the gastrointestinal tract during the absorption phase and then in the central and peripheral compartments. Thus, mean absorption time can be calculated by subtracting MRT for IV from MRT of the respective oral absorption groups. MRT and MAT plots are shown in figures 4-B-2 and 4-B-3; and the values are listed in table 4-B-2. MRT values decreased with increasing dose of SDS but never reached the MRT for intravenous bolus group, indicating that phenol red kinetics were probably not affected by SDS. MAT

values decreased with increasing dose of SDS showing that the average time needed for absorption of phenol red decreased when co-administered with increasing amounts of SDS.

Pharmacokinetic evaluation of oral absorption of drugs with penetration enhancers is traditionally done by statistical moment analysis. In our study, it did show results that one would expect from a penetration enhancer and provided a way of comparison among the treatment groups. However, an interesting observation was made when semi-log plots of mean plasma concentration-time profiles obtained for phenol red with SDS were overlaid with the IV plot (Figure 4-B-4). The initial slope (from time 0 to about 60 minutes) for oral absorption curves of phenol red with SDS was similar to that of the IV curve and after 60 minutes, the slopes were similar to that of the negative control plot. It was evident that initially the K_a values were higher than K_e and later became smaller than K_e. This trend could not be captured with non-compartment analysis and we did not find any reported literature that utilized pharmacokinetic modeling to show changes in K_a with time. Since the conventional pharmacokinetic modeling softwares could not be used for this purpose, we used MATLAB to model the oral absorption data by using differential equations, which describe a two-compartment pharmacokinetic model with a first order absorption phase and the ability to change K_a with time.

K_a was allowed to change in a stepwise manner. With microscopy, as described later in chapter 4-D, we saw that damage was caused to the duodenum instantaneously and maximally. In the jejunum damage occurred later and to a lesser extent. We assumed that as the oral gavage solution traveled down the intestinal tract, it experienced different K_a depending upon the damage caused to the mucosal wall with maximum K_a initially. The MATLAB programs used are provided in Appendices B through E. The microconstants (K_{23},

K_{32}, K_e and V_2) and bioavailability used for phenol red in these programs are same as those determined from IV and oral study in Chapter 4-A. The model fits are shown in figure 4-B-5 and residual plots are shown in figure 4-B-6, A through D. Goodness-of-fit statistics was performed according to the equations shown in Appendix M. The R^2 values obtained from the statistical analysis are depicted on the respective graphs. The absorption rate constant values (K_a) used to fit the two-compartment model are depicted in figure 4-B-7 and the results are summarized in table 4-B-3.

The two-compartment analysis showed that with all the concentrations of SDS, the absorption barrier was affected most in the first one hour (in the proximal region of the small intestine) giving large K_a values initially. The SDS effect on the absorption barrier became lesser in later hours (the lower parts of the small intestine), resulting in smaller K_a values. With 1% SDS, K_a came back to the control level in 1 hour. With 1.5% SDS, it did in 2 hours. With 2% SDS it took 4 hours for K_a to come down to the control level.

In the residual plots, the residuals were scattered randomly, showing that there was no bias in the model fitting. The regression coefficients are depicted on the plots to show how tightly the observed values are spread about the predicted values.

The K_a values in the model fitting described above were initially selected manually through use of a series of decreasing step functions of variable duration. Based on the results obtained from the step function analysis a two parameter exponential function was chosen to obtain a best fit continuous time dependent K_a function for the 1% SDS, 1.5% SDS and 2% SDS treatments. The best fit for the two parameter fit of K_a was obtained by doing a grid search for each of the parameters with the goodness-of-fit evaluation accomplished through the minimization of the sum of the squares of the differences between the predicted and

observed concentration values. The MATLAB program used is shown in Appendix N through P. An exponential fitting function was chosen because it, relative to other possible functional dependencies, allowed for the best correct initial, intermediate and final K_a values to be obtained.

The predicted K_a values obtained using a continuous function and a step function are depicted in figures 4-B-9 through 11. The model fits are shown in figure 4-B-12. The predicted K_a was high initially and decreased with time. As seen in figure 4-B-9 through 11, the K_a values predicted by a continuous function were within those selected in a step function. They were within 20% of those estimated from a step function analysis near the recovery times (1 hour for 1% SDS, 2 hours for 1.5% SDS and 4 hours for 2% SDS).

Explaining the changes in K_a mathematically is a difficult challenge due to the complexity of the *in vivo* system coupled with the sparseness of the existing experimental data set (only seven data points per animal were obtained). Nonetheless the experimental data obtained have been able to be adequately fit through the use of a two parameter exponentially time dependent K_a function and validated the K_a values estimated by model fitting with a step function.

II. Oral absorption enhancement of FD-10 upon co-administration with SDS

The results of absorption enhancement experiments for FD-10 are shown in figure 4-B-10. FD-10 was not detected in plasma beyond 3 hours when co-administered with SDS. The area under the plasma concentration-time curve from time zero to t ($AUC_{0\text{-}180\ min}$) for each treatment was calculated using linear trapezoidal rule. The C_{max}, T_{max} and AUC values for FD-10 are listed in table 4-B-4.

In the negative control group, FD-10 was not detected in plasma. When co-administered with SDS, FD-10 was detected in plasma with all the three concentrations of SDS. Higher C_{max} and AUC values and earlier T_{max} were obtained with increasing concentrations of SDS. No further pharmacokinetic analysis was performed on FD-10 because of the limited data obtained.

Once absorption enhancement profiles were obtained for phenol red and FD-10 with SDS, recovery studies were performed after oral administration of SDS at 1, 1.5 and 2% concentrations.

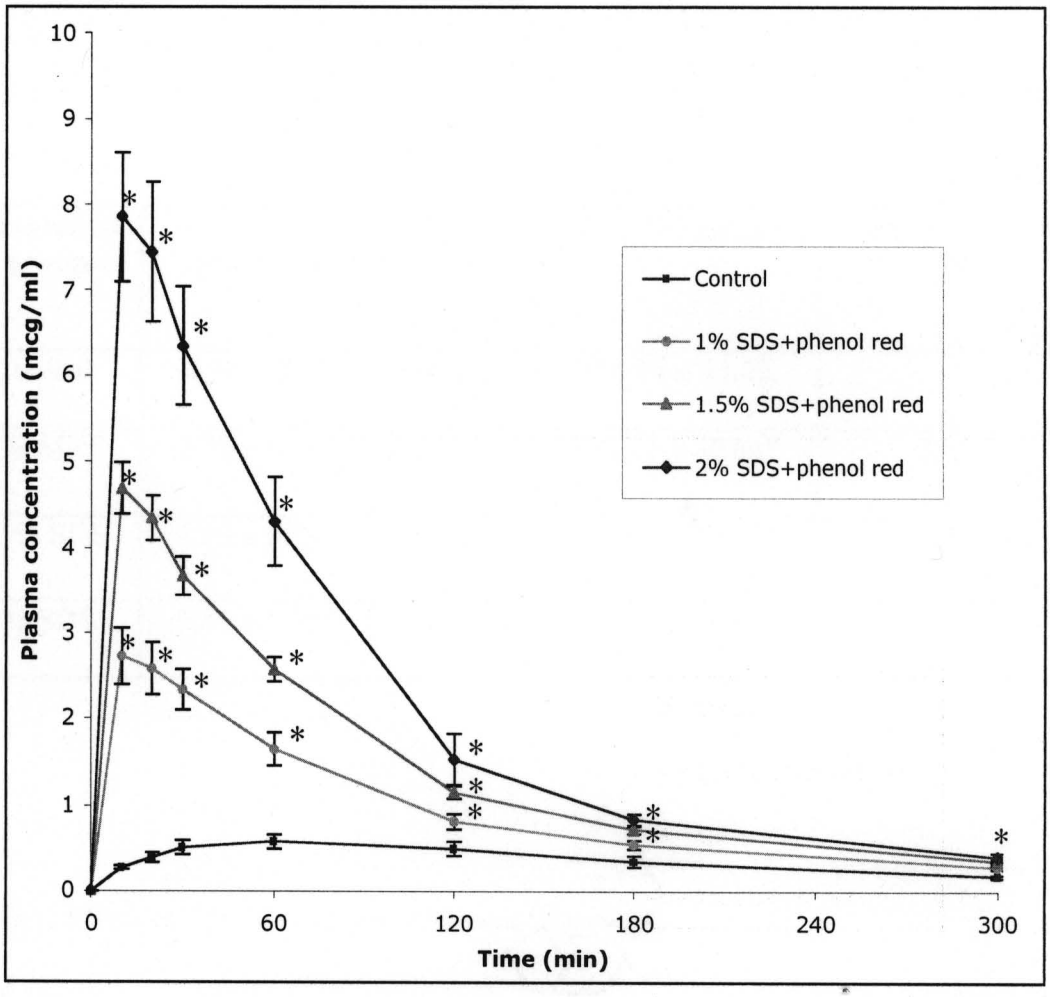

Figure 4-B-1: Plasma concentration-time profile of phenol red when orally administered with and without SDS.

(Control: N = 12, SDS treatment: N = 6, Each point represents Mean ± S.E.

* Statistically significant difference from the control values at $p<0.05$)

Treatment group	C_{max} (mcg/ml)	T_{max} (min)	AUC ($t_{0\text{-}300\ min}$)	Enhancement ratio
Control	0.58 ± 0.08	60 ± 0	108.74 ± 15.72	1
1% SDS	2.73 ± 0.33*	13 ± 2	294.22 ± 30.44*	2.71
1.5% SDS	4.69 ± 0.29*	10 ± U.D.	435.55 ± 23.27*	4.01
2% SDS	7.86 ± 0.75*	10 ± U.D.	665.25 ± 26.03*	6.12

Table 4-B-1: Effect of SDS on oral absorption of phenol red.

(C_{max} and T_{max} are the averages calculated from the observed data. AUC was calculated using the linear trapezoidal rule. Enhancement ratio is the ratio of AUC of the respective treatment group to that of the control group.

Control: N = 12, SDS treatment: N = 6, Values are expressed as Mean ± S.E.

* Statistically significant difference from the control values at $p<0.05$

U.D.- unable to determine)

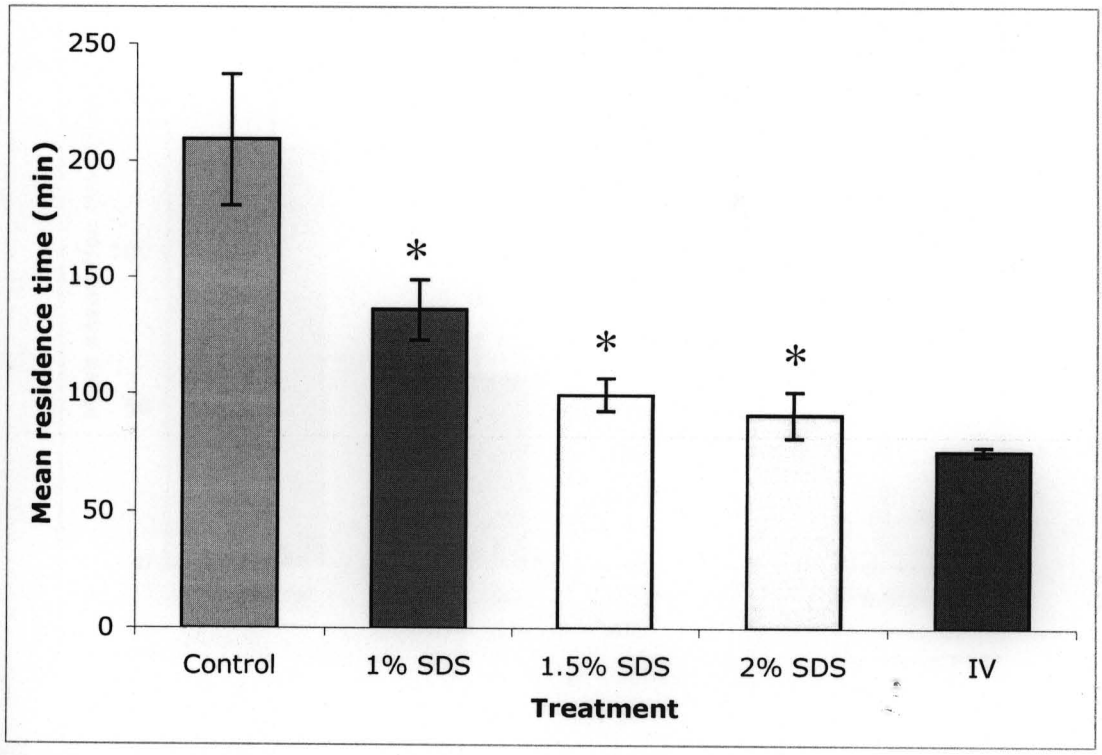

Figure 4-B-2: Statistical moment analysis of oral absorption of phenol red – Mean residence time (MRT) when orally administered with and without SDS.

(MRT was calculated by extrapolating AUC to infinity.

Control: N = 12, SDS treatment: N = 6, Each point represents Mean ± S.D.

* Statistically significant difference from the control values at $p<0.05$)

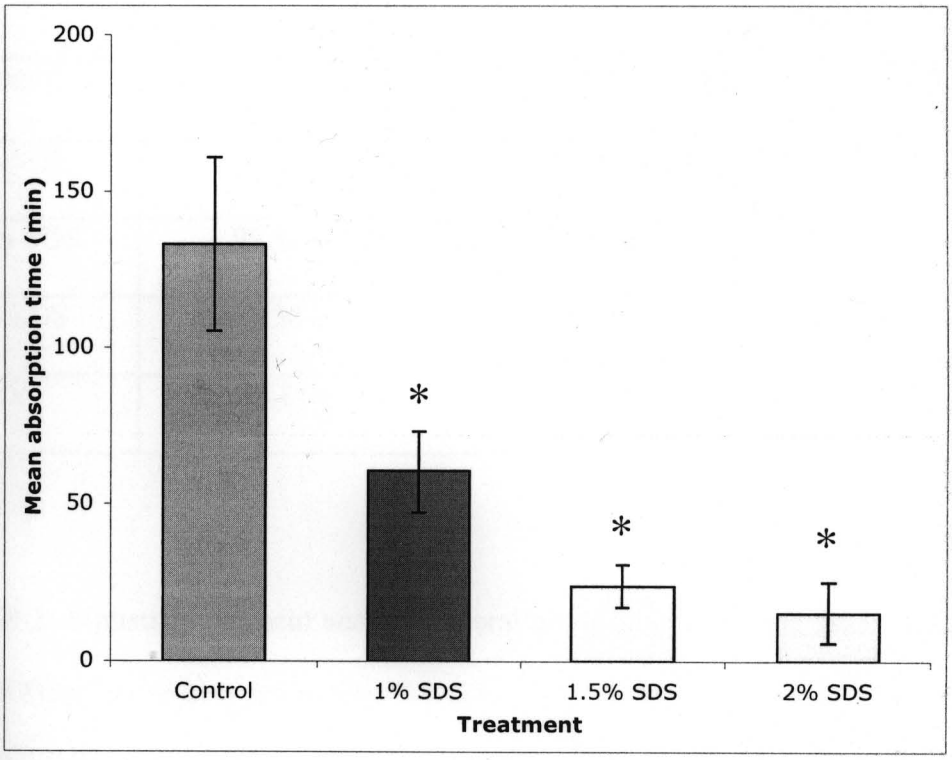

Figure 4-B-3: Statistical moment analysis of oral absorption of phenol red – Mean absorption time (MAT) when orally administered with and without SDS.

(MAT is the difference between MRT of the respective treatment group and that after intravenous administration.

Control: N = 12, SDS treatment: N = 6, Each point represents Mean ± S.D.

* Statistically significant difference from the control values at $p<0.05$)

Treatment group	MRT (min)	MAT (min)	Bioavailability (%)
Control	208.88 ± 8.06	133.07 ± 8.06	1.51 ± 0.10
1% SDS	136.04 ± 5.2*	60.23 ± 5.2*	3.53 ± 0.23*
1.5% SDS	99.80 ± 3.06*	23.99 ± 3.06*	4.83 ± 0.41*
2% SDS	91.30 ± 2.78*	15.49 ± 2.78*	7.26 ± 0.69*
IV	75.81 ± 2.28	-	100

Table 4-B-2: Statistical moment analysis of oral absorption of phenol red – mean residence time (MRT) and mean absorption time (MAT).

MRT was calculated by extrapolating the AUC to infinity. MAT is the difference between MRT of the respective treatment group and that after intravenous administration.

Bioavailability was calculated by extrapolating AUC to infinity.

(Control: N = 12, SDS treatment: N = 6, Each value represents Mean ± S.E.

* Statistically significant difference from the control values at $p<0.05$)

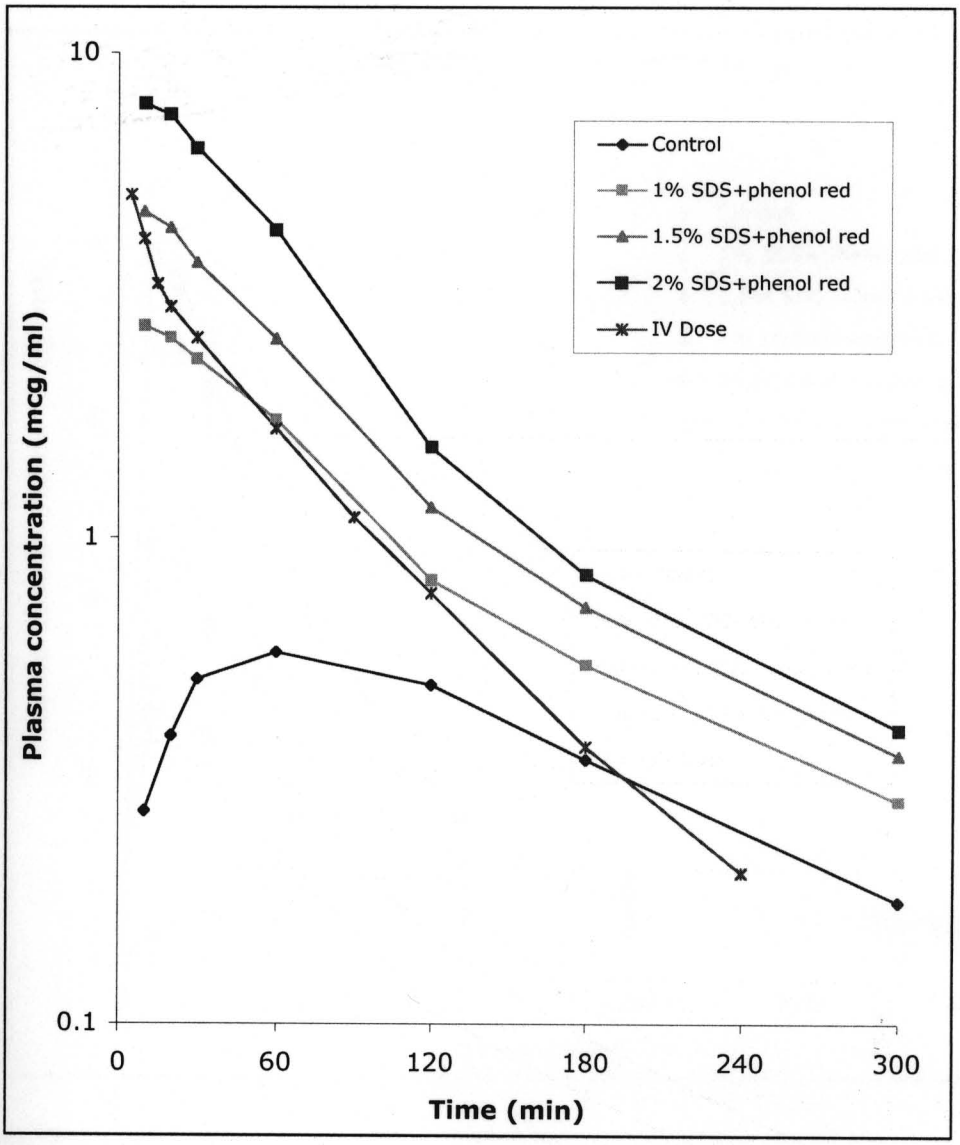

Figure 4-B-4: Overlay of semi-logarithmic plots of plasma concentrations of phenol red after IV bolus administration and oral administration with and without SDS.

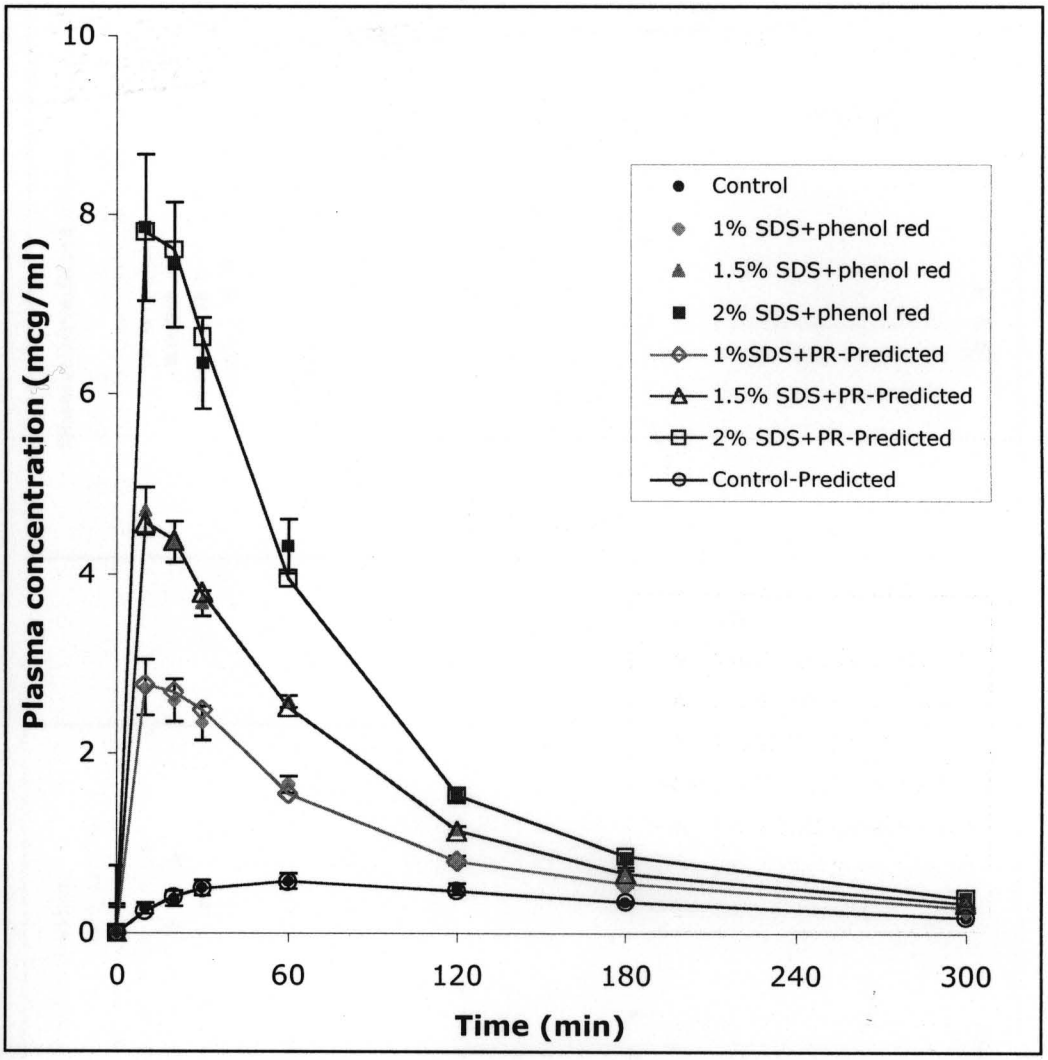

Figure 4-B-5: Observed and predicted plasma concentrations obtained by two-compartment model fitting using a step-function analysis for phenol red when orally administered with and without SDS.

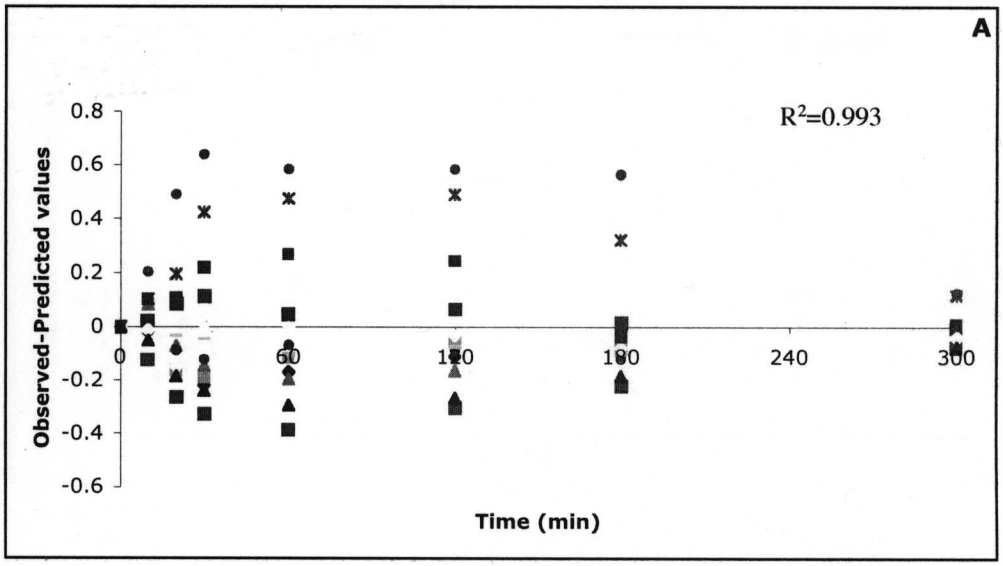

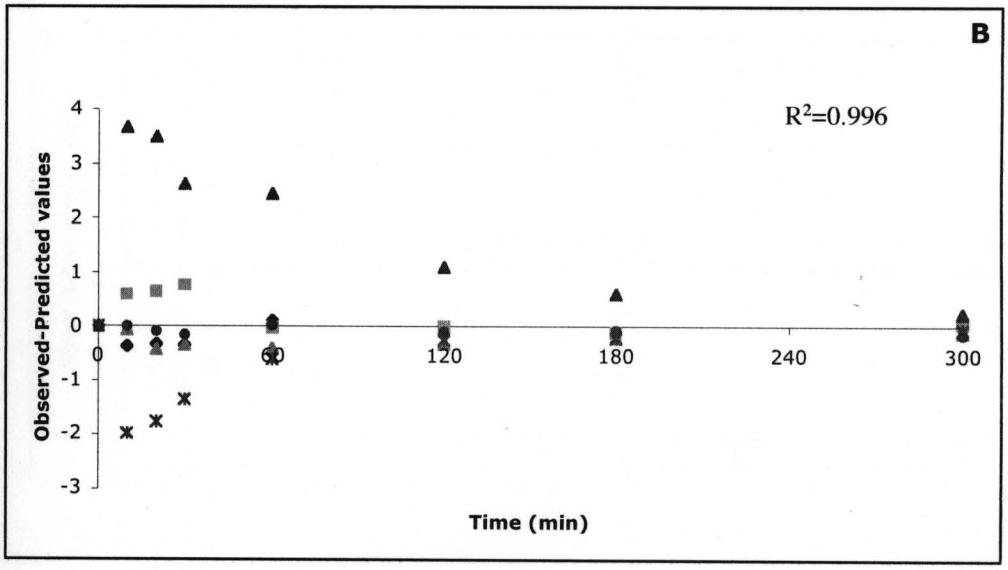

Figure 4-B-6: Plots of residuals versus time : (A) Control phenol red and (B) phenol red + 1%SDS

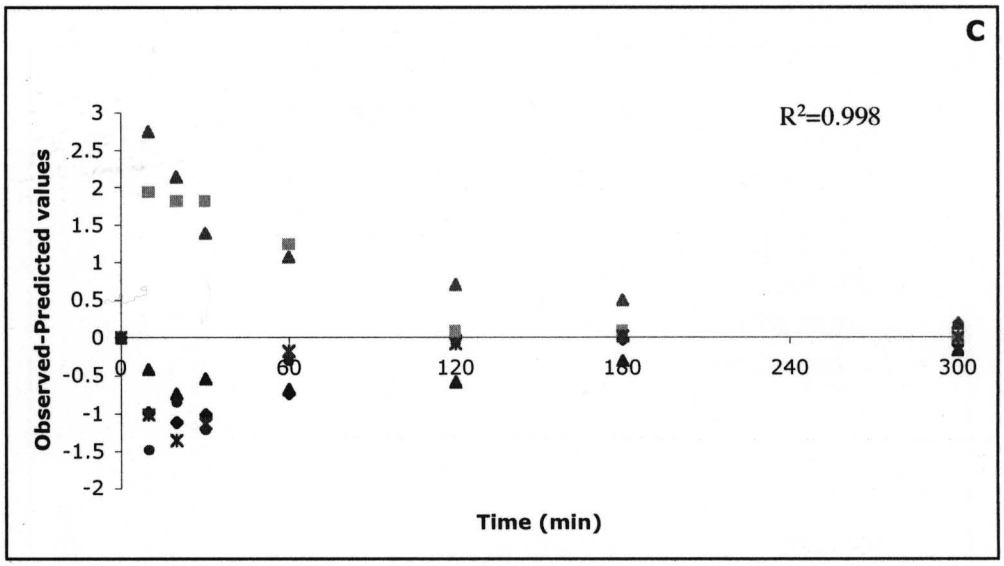

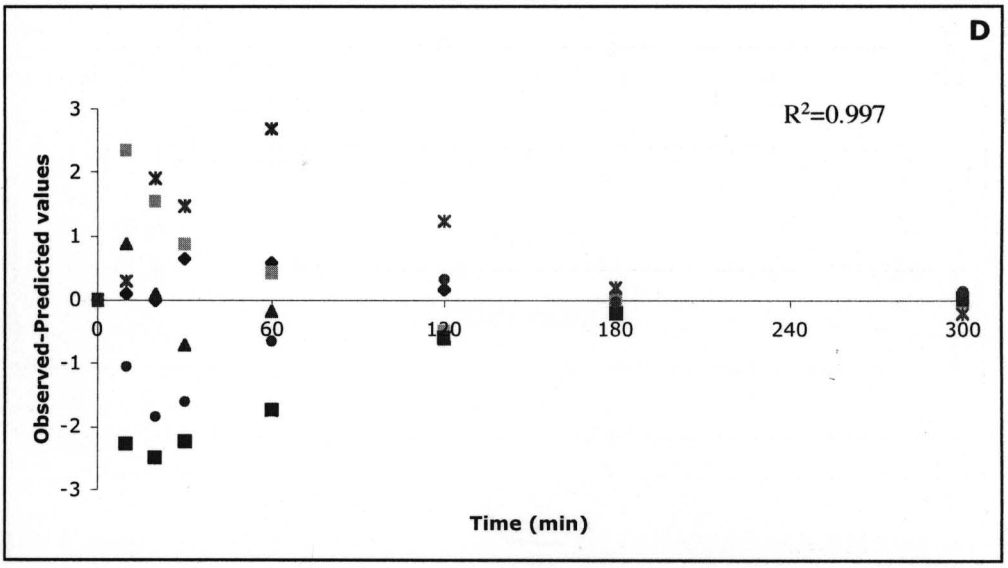

Figure 4-B-6: Plots of residuals versus time: (C) Phenol red + 1.5% SDS and (D) phenol red + 2% SDS

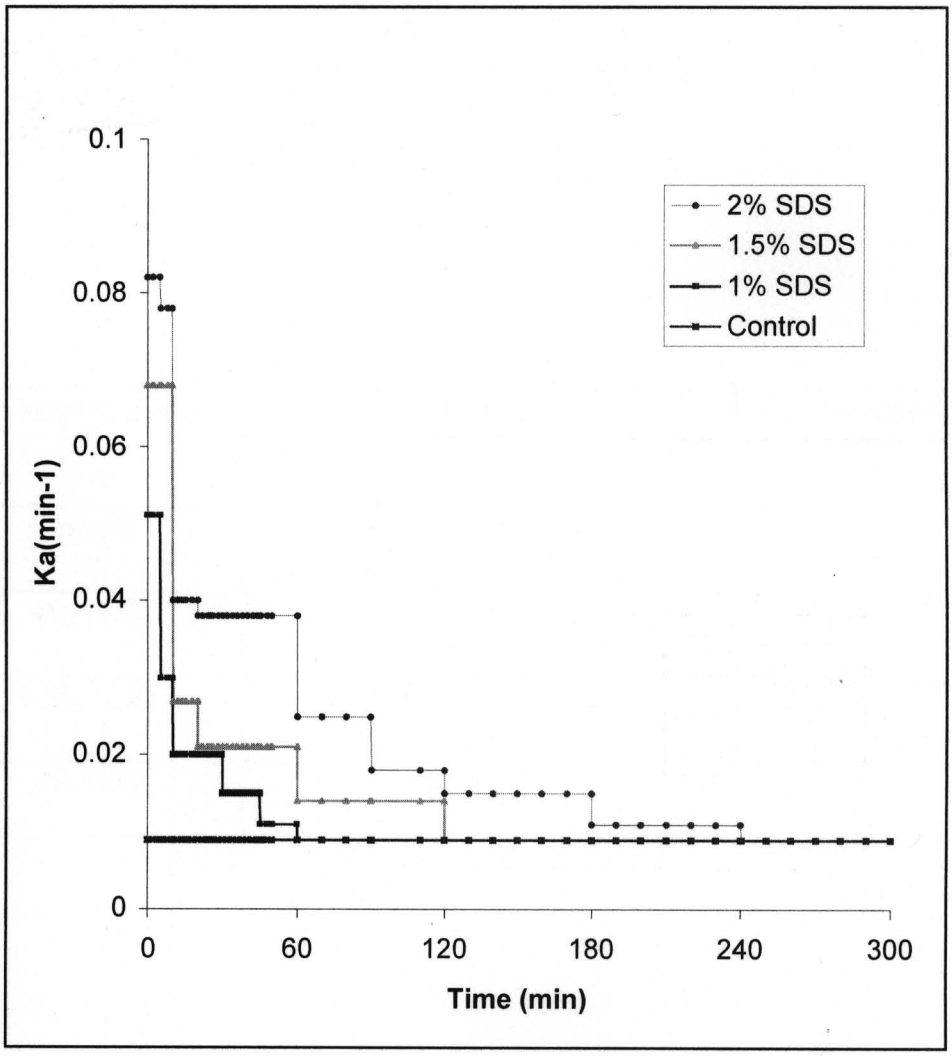

Figure 4-B-7: Change in oral absorption rate constant (K_a) of phenol red with respect to time when co-administered with SDS, as estimated by two-compartment model fitting using a step-function analysis

Treatment group	K_a (maximum) (min^{-1})	Time of Recovery
Control	0.009	-
1% SDS	0.051	1 hr
1.5% SDS	0.068	2 hrs
2% SDS	0.082	4 hrs

Table 4-B-3: Comparison of changes in absorption rate constant of phenol red upon co-administration with SDS

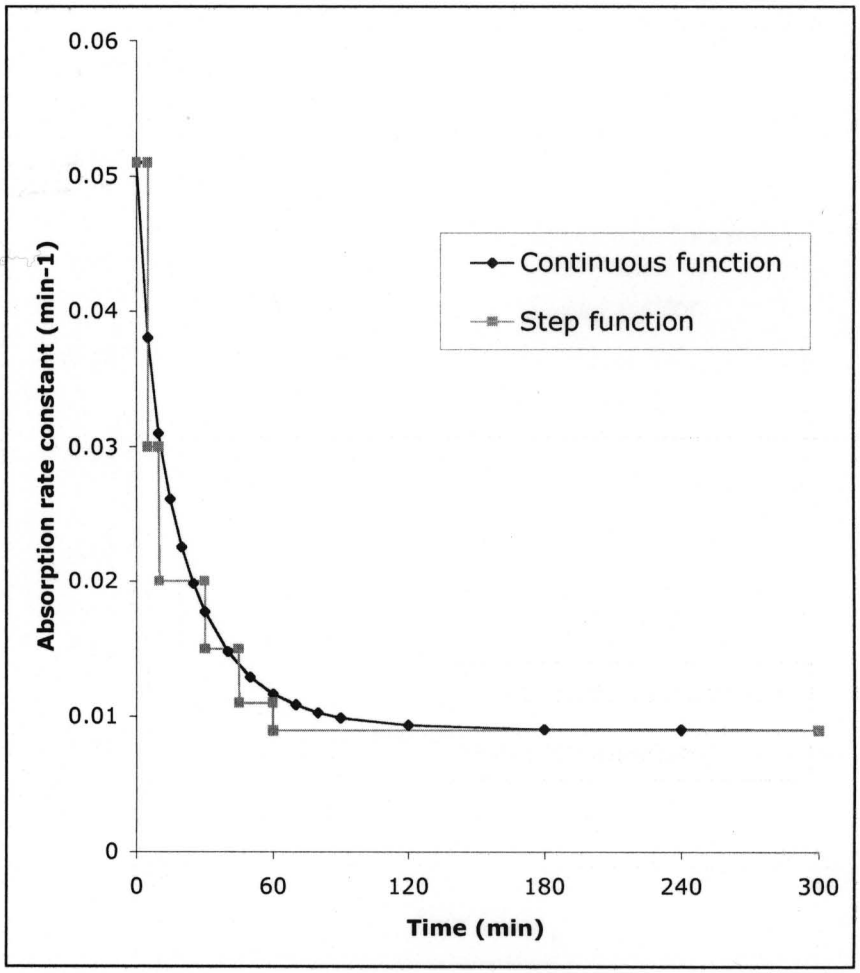

Figure 4-B-8: Estimation of K_a for 1% SDS treatment using a continuous exponential function

The following equation with two variables a & b were used to model K_a.

$K_a = K_{a0} + A*\exp(-a*time^b)$

Where K_a = predicted absorption rate constant
K_{a0} = control K_a (0.009 min-1)
A = 0.042 (Taken from step function analysis and held constant to reduce the number of variables)
a = 0.1
b = 0.81

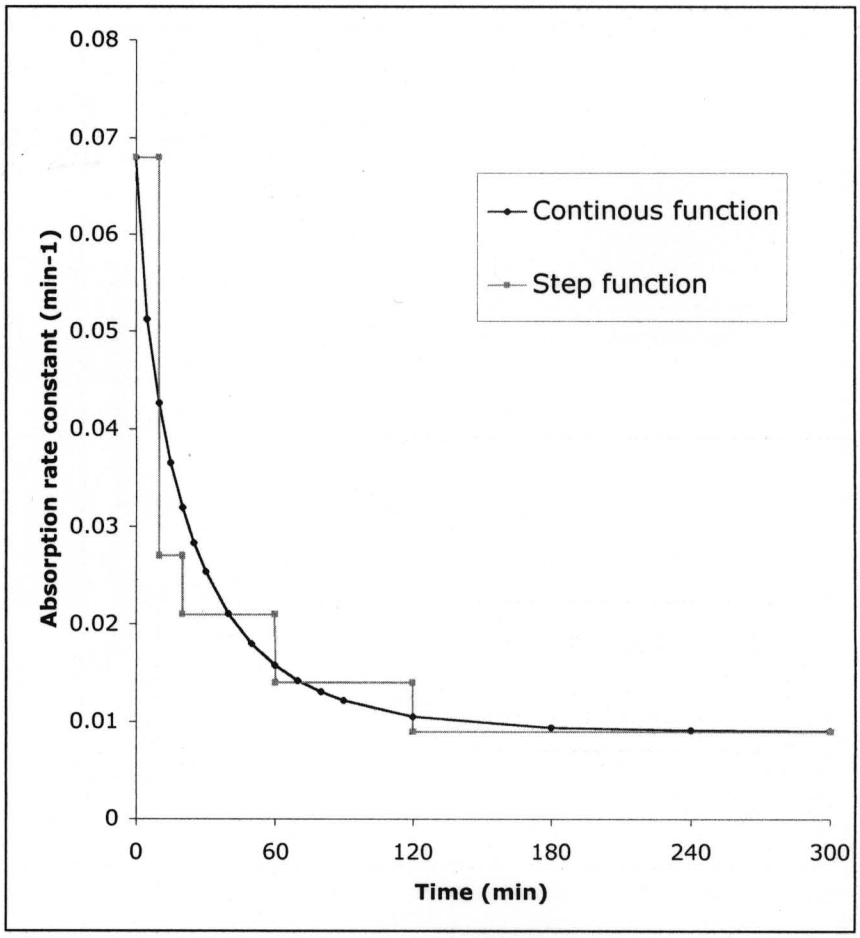

Figure 4-B-9: Estimation of K_a for 1.5% SDS treatment using a continuous exponential function

The following equation with two variables a & b were used to model K_a.

$K_a = K_{a0} + A*\exp(-a*time^b)$

Where K_a = predicted absorption rate constant
K_{a0} = control K_a (0.009 min-1)
A = 0.059 (Taken from step function analysis and held constant to reduce the number of variables)
a = 0.1
b = 0.75

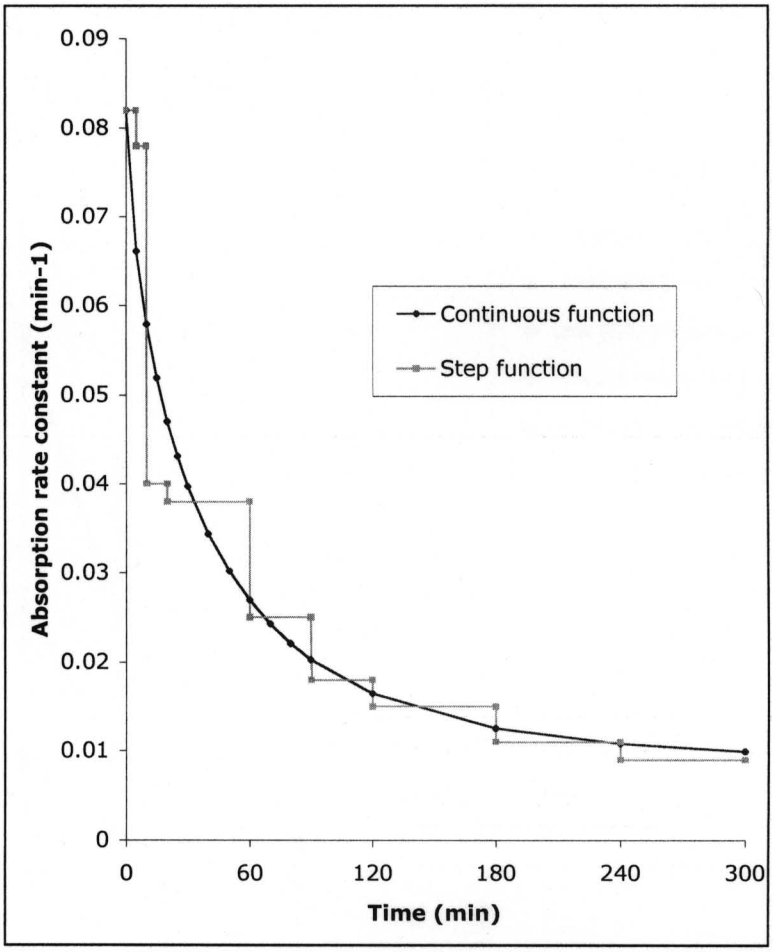

Figure 4-B-10: Estimation of K_a for 2% SDS treatment using a continuous exponential function

The following equation with two variables a & b were used to model K_a.

$K_a = K_{a0} + A*\exp(-a*time^b)$

Where K_a = predicted absorption rate constant
K_{a0} = control K_a (0.009 min-1)
A = 0.073 (Taken from step function analysis and held constant to reduce the number of variables)
a = 0.08
b = 0.7

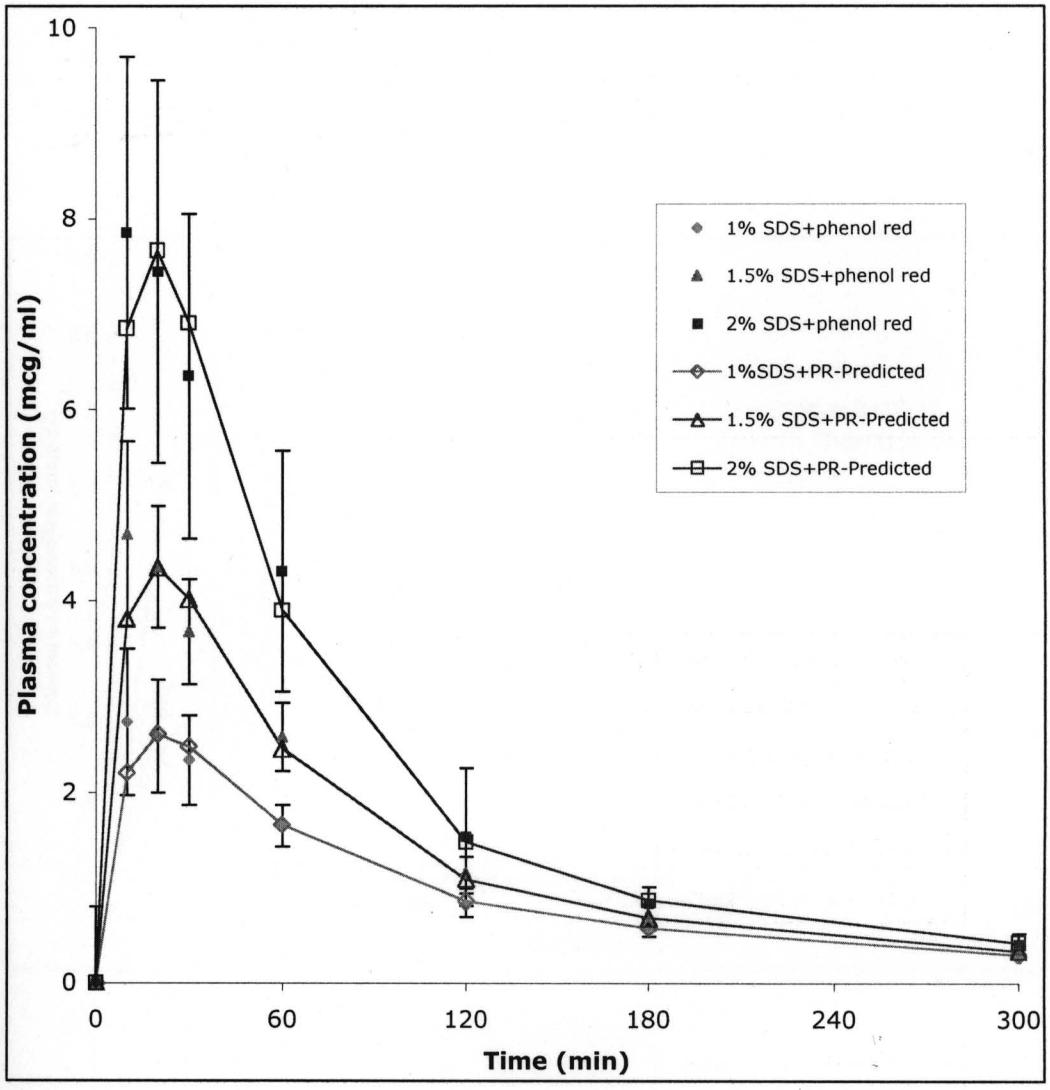

Figure 4-B-11: Observed and predicted plasma concentrations of phenol red obtained using K_a estimated from a continuous function

Each point represents Mean ± S.D.

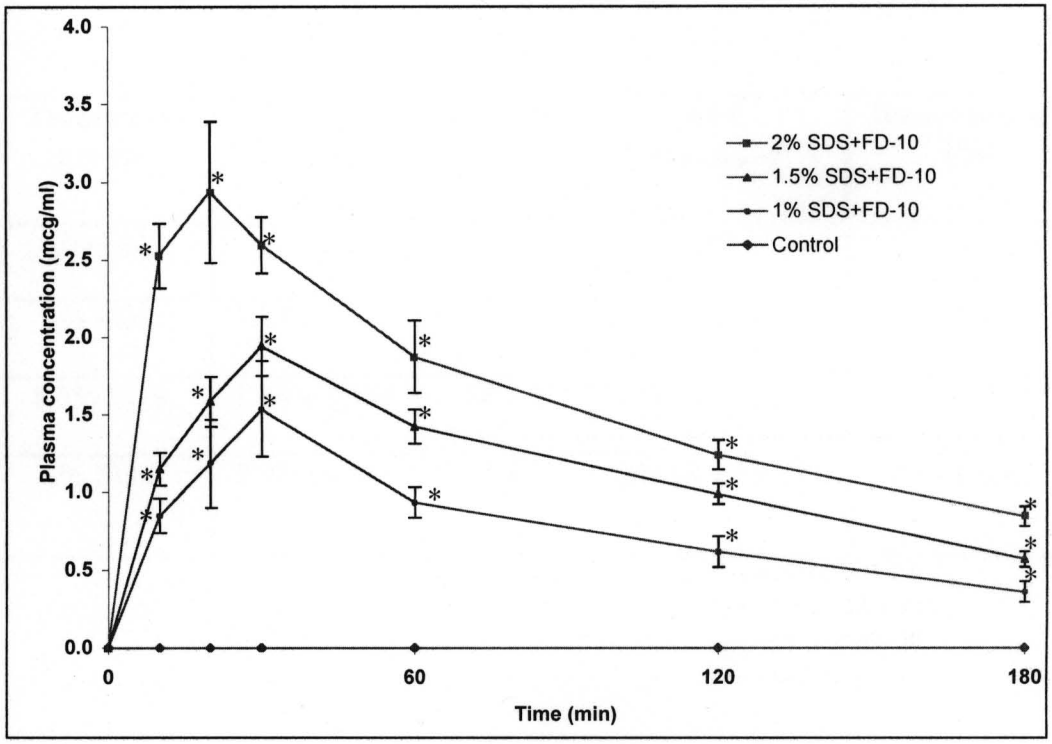

Figure 4-B-12: Plasma concentration-time profile of FD-10 when orally administered with and without SDS.

(Control: N = 12, SDS treatment: N = 6, Each point represents Mean ± S.E.

* Statistically significant difference from the control values at $p<0.05$)

Treatment group	C_{max} (mcg/ml)	T_{max} (min)	AUC ($t_{0\text{-}180\ min}$)	Bioavailability (%)
Control	0.0	0.0	0.0	0.0
1% SDS	1.53 ± 0.31*	30 ± 0	141.04 ± 14.18*	1.47 ± 0.26*
1.5% SDS	1.94 ± 0.19*	28 ± 2	195.45 ± 5.10*	2.04 ± 0.38*
2% SDS	2.93 ± 0.46*	23 ± 3	269.63 ± 18.59*	2.81 ± 0.62*

Table 4-B-4: Effect of SDS on oral absorption of FD-10.

(C_{max} and T_{max} are the averages calculated from the observed data. AUC was calculated using the linear trapezoidal rule from the observed data. Bioavailability was calculated by extrapolating the AUC to infinity.

Control: N = 12, SDS treatment: N = 6, Values are expressed as Mean ± S.E.

* Statistically significant difference from the control values at $p<0.05$)

Chapter 4-C: Evaluation of Absorption Barrier Recovery Using Marker Molecules (Objective II)

1. Materials

Materials used in this section are same as described in chapter 4-B.

2. Methods

Methods employed in this section were similar to those described in chapter 4-B. A variation was made in administration of oral gavage of surfactant and marker molecules. Rats were given an oral gavage of 2 ml of 1% SDS. After a specific recovery time that was assigned to each group of animals i.e. 15 minutes, 30 minutes, 1 hour and 3 hours, rats received an oral dose of marker molecules (phenol red and FD-10, 6 mg each dissolved in 2ml). After administration of marker molecules blood samples were drawn from the jugular vein at 0, 10, 20, 30, 60, 120, 180 and 300 minutes. Plasma was separated and assayed as described before. Pharmacokinetic parameters estimated for recovery groups and were compared with those of the control group (no prior exposure to SDS).

For positive control, 3-hour recovery experiments were performed using 1.5% and 2% SDS.

Statistical moment analysis and two-compartment analysis was performed on oral absorption data for phenol red using WinNonlin and MATLAB® 5 (Appendices F through K) respectively.

3. Results and Discussion

I. Recovery experiments with the small molecular weight marker

As explained in Chapter 3, 1% SDS was selected as a treatment and 1.5% and 2% SDS were selected as positive controls.

Results obtained for this experiment with phenol red are depicted in figure 4-C-1. C_{max}, T_{max} and AUC values are summarized in table 4-C-1. Since actual experimental values were obtained till 300 minutes, AUC values were calculated only till 300 minutes and were not extrapolated to infinity. C_{max} and AUC values decreased and T_{max} increased with increasing length of recovery times. After 15 and 30-minute recovery periods, the pharmacokinetic parameters for phenol red are still significantly different from the negative control indicating that absorption barrier recovery was partial. After 1-hour recovery time, the pharmacokinetic parameters are similar to that of the negative control, indicating that the absorption barrier recovery was complete by this time. This observation was confirmed by performing 3-hour recovery experiments. Statistical moment (non-compartment) analysis showed that MRT and MAT values after 1 and 3-hour recovery periods, were similar to those of the negative control but not for 15 and 30 minutes (table 4-C-2). The results showed that for low molecular weight molecules, absorption barrier recovery was complete for 1% SDS in 1 hour.

The C_{max}, T_{max} , AUC, MRT and MAT values for 1 hour recovery groups for 1% SDS were statistically comparable at 5% significance level, when 6 animals were used per group. This indicated that absorption barrier for phenol red was similar after recovery as compared to the negative control. To make sure that the difference in data for these groups is solely due to individual variability and not due to difference in the treatment, power analysis was performed at 80% and significance level of 5%. The number of animals required for each experimental group was calculated to be 12. Hence, 12 rats were used each for 1-hour recovery group with 1% SDS and the negative control group.

3-hour recovery experiments were done for the positive control SDS concentrations. Results obtained for this set of experiments for phenol red are depicted in figure 4-C-2. C_{max}, T_{max} and AUC values are summarized in table 4-C-3. C_{max}, T_{max} and AUC values for 1% and 1.5% SDS after 3-hour recovery are statistically comparable to that of the negative control whereas for 2% SDS, C_{max} and AUC were significantly higher and T_{max} was earlier as compared to the negative control values. Statistical moment analysis showed that MRT and MAT values for 1% and 1.5% SDS after 3-hour recovery, were similar to those of the negative control but not for 2% SDS (table 4-C-4). In summary, for low molecular weight markers, absorption barrier recovery was complete for 1% and 1.5% SDS in 3 hours but not for 2% SDS.

Two-compartment analysis was performed on recovery data for phenol red using MATLAB® 5 software with the freedom of changing K_a with time. The model fits are shown in figures 4-C-3 and 4-C-5. The changes in K_a with respect to time are shown in figures 4-C-4 and 4-C-6. The residual plots and regression coefficients are shown in figures 4-C-7, A through F.

For 1% SDS, after 15 and 30-minute recovery periods, the absorption rate constant (K_a) came to the control level in 45 and 30 minutes respectively (total 1-hour each). For the 1-hour recovery group, K_a was comparable to that of the control group.

For 3-hour recovery groups, K_a was comparable to the control value for 1% and 1.5% SDS, whereas for 2% SDS it came to the control level in 1 hour for 2% SDS (total 4 hours).

As described in Chapter 4-B, the two-compartment pharmacokinetic analysis on phenol red data obtained after co-administration with SDS, revealed that for 1% and 1.5% SDS, the K_a came back to the control value in one hour and 2 hours respectively, whereas it

took 4 hours for 2% SDS. The experiments designed for absorption barrier recovery confirmed these results.

K_a estimated using a step function for 1% SDS-15 min recovery and 30-min recovery as well as 2% SDS-3 hr recovery, were in accordance with the K_as estimated at the corresponding time points using both step and continuous functions described in Chapter 4-B when phenol red was co-administered with SDS.

II. Recovery experiments with the high molecular weight marker

The recovery results for FD-10 are shown in figure 4-C-8 and table 4-C-6. In absorption enhancement experiments described in chapter 4-B, FD-10 was not detected in plasma when administered alone. FD-10 could be quantified in plasma when it was co-administered with 1%, 1.5% and 2% SDS.

With 1% SDS, FD-10 was detected in plasma in the 15-minute recovery group but not in the 30-minute, 1-hour and 3-hour recovery groups, whereas with phenol red, the recovery was complete in 1 hour with 1% SDS. FD-10 was not detected in plasma after 3-hour recovery for both 1.5% and 2% SDS, whereas absorption recovery was not complete against the small molecular weight marker (phenol red) with 2% SDS after 3 hours. These results indicate that the absorption barrier possibly recovered against large molecular weight molecules before it did against small molecular weight molecules. However, this tentative conclusion needs to be validated by using a more sensitive analytical technique like radioactivity measurements.

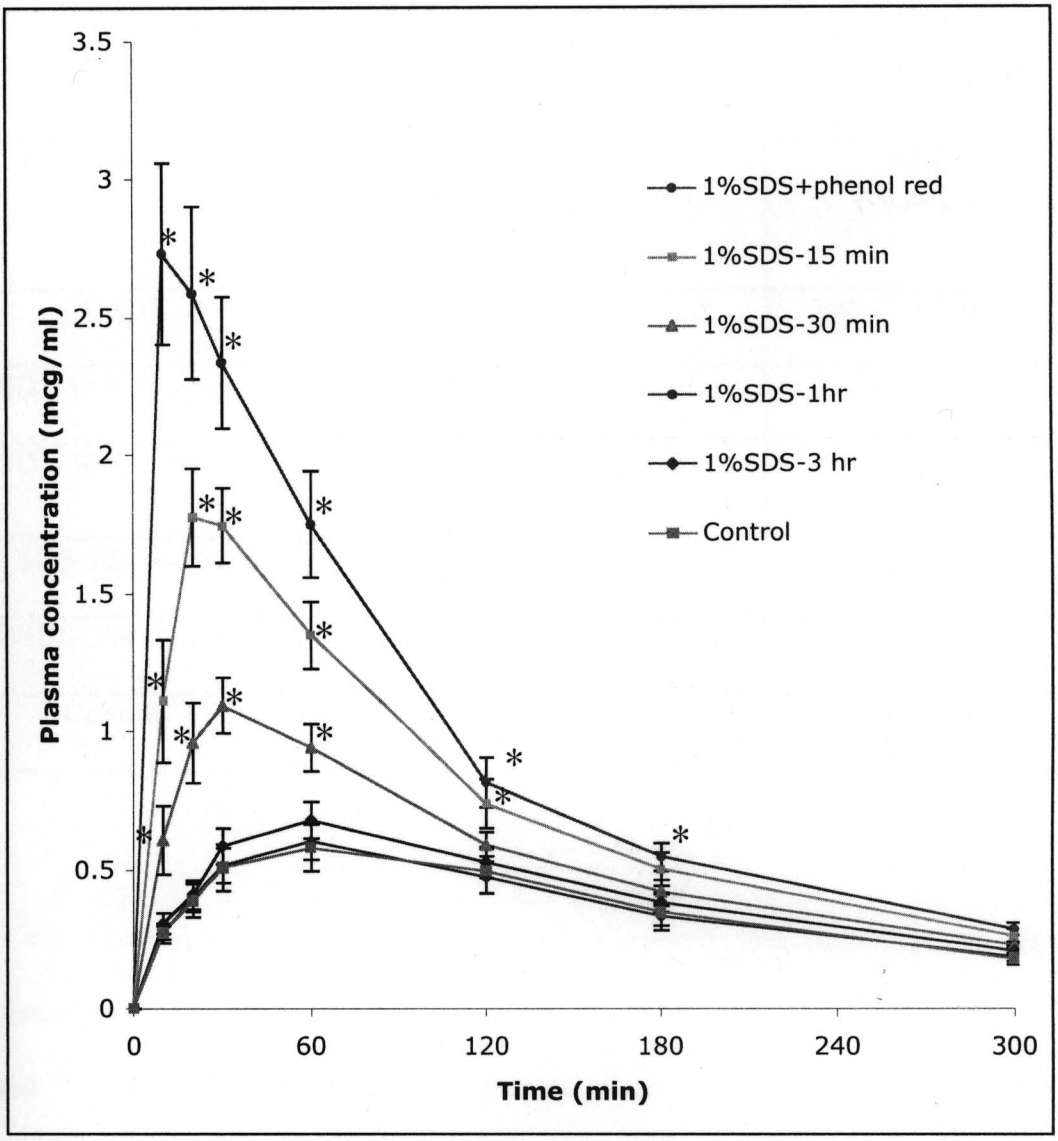

Figure 4-C-1: Plasma concentration-time profile of phenol red after different recovery periods upon administration of 1% SDS.

(Control & 1% SDS-1 hr recovery: N=12, other treatments: N=6, Each point represents Mean ± S.E., * Statistically significant difference from the control values at $p<0.05$)

Treatment group	C_{max} (mcg/ml)	T_{max} (min)	AUC ($t_{0\text{-}300\ min}$)
1% SDS	2.73 ± 0.33 *	13 ± 2	294.22 ± 30.44 *
1% SDS-15 min recovery	1.78 ± 0.17*	24 ± 2	241.60 ± 20.81 *
1% SDS-30 min recovery	1.10 ± 0.10 *	31 ± 6	167.61 ± 13.13*
1% SDS-1 hr recovery	0.60 ± 0.06	60 ± 0	110.85 ± 11.65
1% SDS-3 hr recovery	0.68 ± 0.08	60 ± 0	130.58 ± 15.56
Control	0.58 ± 0.08	60 ± 0	108.74 ± 15.72

Table 4-C-1: Oral absorption of phenol red after different recovery periods upon administration of 1% SDS.

C_{max} and T_{max} are the averages calculated from the observed data. AUC was calculated using the linear trapezoidal rule from the observed data.

(Control & 1% SDS-1 hr recovery: N=12, other treatments: N=6, Values are expressed as Mean ± S.E., * Statistically significant difference from the control values at $p<0.05$)

Treatment group	MRT (min)	MAT (min)	Bioavailability (%)
1% SDS	136.04 ± 5.2 *	60.23 ± 5.2 *	3.53 ± 0.23*
1% SDS-15 min recovery	152.07 ± 4.7 *	76.27 ± 4.7 *	2.71 ± 0.19*
1% SDS-30 min recovery	159.86 ± 3.31 *	84.05 ± 3.31 *	1.95 ± 0.15*
1% SDS-1 hr recovery	208.83 ± 9.4	133.02 ± 9.4	1.55 ± 0.11
1% SDS-3 hr recovery	200.43 ± 8.76	124.62 ± 8.76	1.65 ± 0.14
Control	208.88 ± 8.06	133.07 ± 8.06	1.51 ± 0.10

Table 4-C-2: Statistical moment analysis of oral absorption of phenol red after different recovery times upon administration of 1% SDS.

(MRT was calculated by extrapolating the AUC to infinity. MAT is the difference between the MRT of the respective treatment group and that after intravenous administration. Bioavailability was calculated by extrapolating AUC to infinity.

Control & 1% SDS-1 hr recovery: N=12, other treatments: N=6, Values are expressed as Mean ± S.E., * Statistically significant difference from the control values at $p<0.05$)

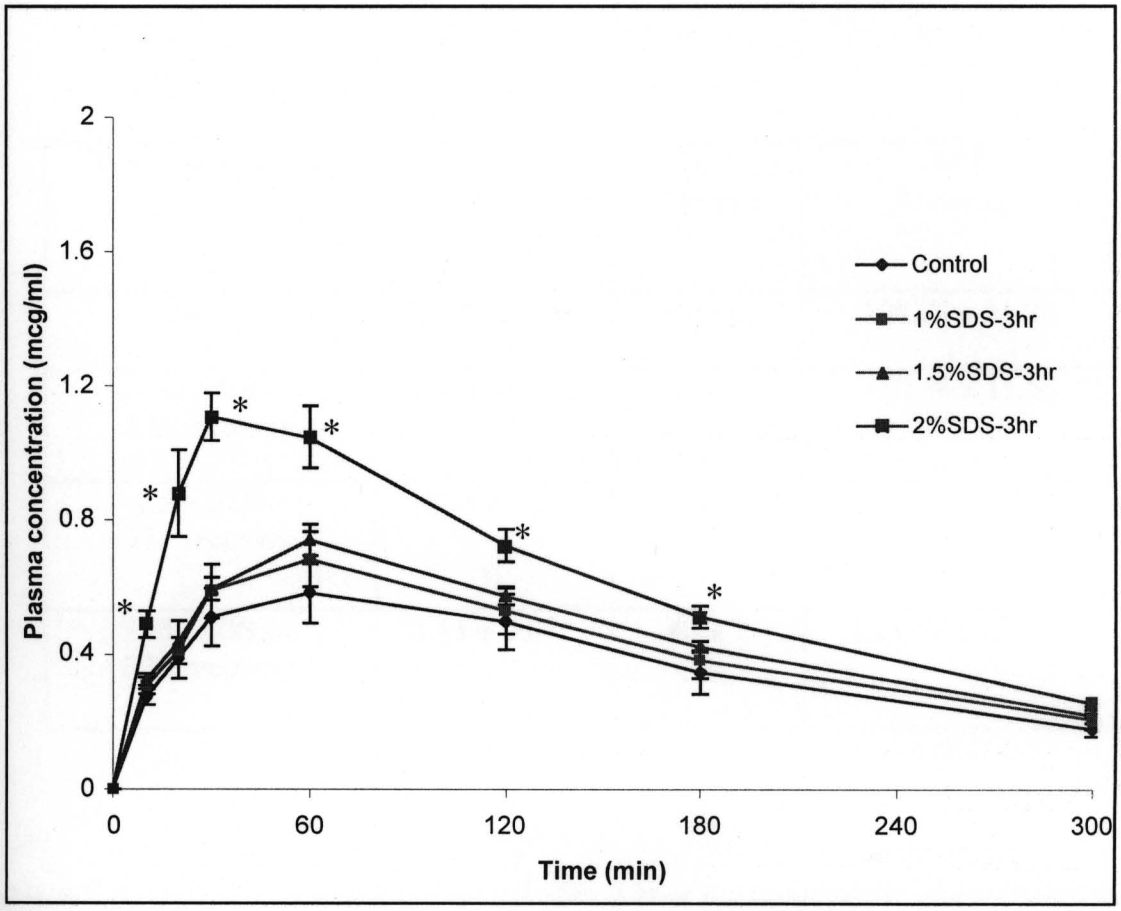

Figure 4-C-2: Plasma concentration-time profile of phenol red after 3-hour recovery periods upon oral administration of SDS.

(Control: N = 12, SDS treatment: N = 6, Each point represents Mean ± S.E.

* Statistically significant difference from the control values at $p<0.05$)

Treatment group	C_{max} (mcg/ml)	T_{max} (min)	AUC ($t_{0\text{-}300\ min}$)
Control	0.58 ± 0.08	60 ± 0	108.74 ± 15.72
1% SDS - 3 hr recovery	0.68 ± 0.08	60 ± 0	130.58 ± 15.56
1.5% SDS - 3 hr recovery	0.76 ± 0.08	60 ± 0	148.28 ± 14.86
2% SDS - 3 hr recovery	1.11 ± 0.07*	40 ± 7	228.63 ± 15.46*

Table 4-C-3: Oral absorption of phenol red after 3-hour recovery period upon administration of SDS.

(C_{max} and T_{max} are the averages calculated from the observed data. AUC was calculated using the linear trapezoidal rule from the observed data.

Control: N = 12, SDS treatment: N = 6, Values are expressed as Mean ± S.E.

* Statistically significant difference from the control values at $p<0.05$)

Treatment group	MRT (min)	MAT (min)	Bioavailability (%)
Control	208.88 ± 8.06	133.07 ± 8.06	1.51 ± 0.10
1% SDS-3 hr recovery	201.42 ± 21.47	125.61 ± 21.47	1.65 ± 0.12
1.5% SDS-3 hr recovery	203.01 ± 22.49	127.20 ± 22.49	1.71 ± 0.12
2% SDS-3 hr recovery	159.76 ± 13.25*	83.95 ± 13.25*	2.32 ± 0.14

Table 4-C-4: Statistical moment analysis of oral absorption of phenol red after 3-hour recovery upon administration of SDS

(MRT was calculated by extrapolating the AUC to infinity. MAT is the difference between the MRT of the respective treatment group and that after intravenous administration. Bioavailability was calculated by extrapolating AUC to infinity.

Control: N = 12, SDS treatment: N = 6, Values are expressed as Mean ± S.E.

* Statistically significant difference from the control values at $p<0.05$)

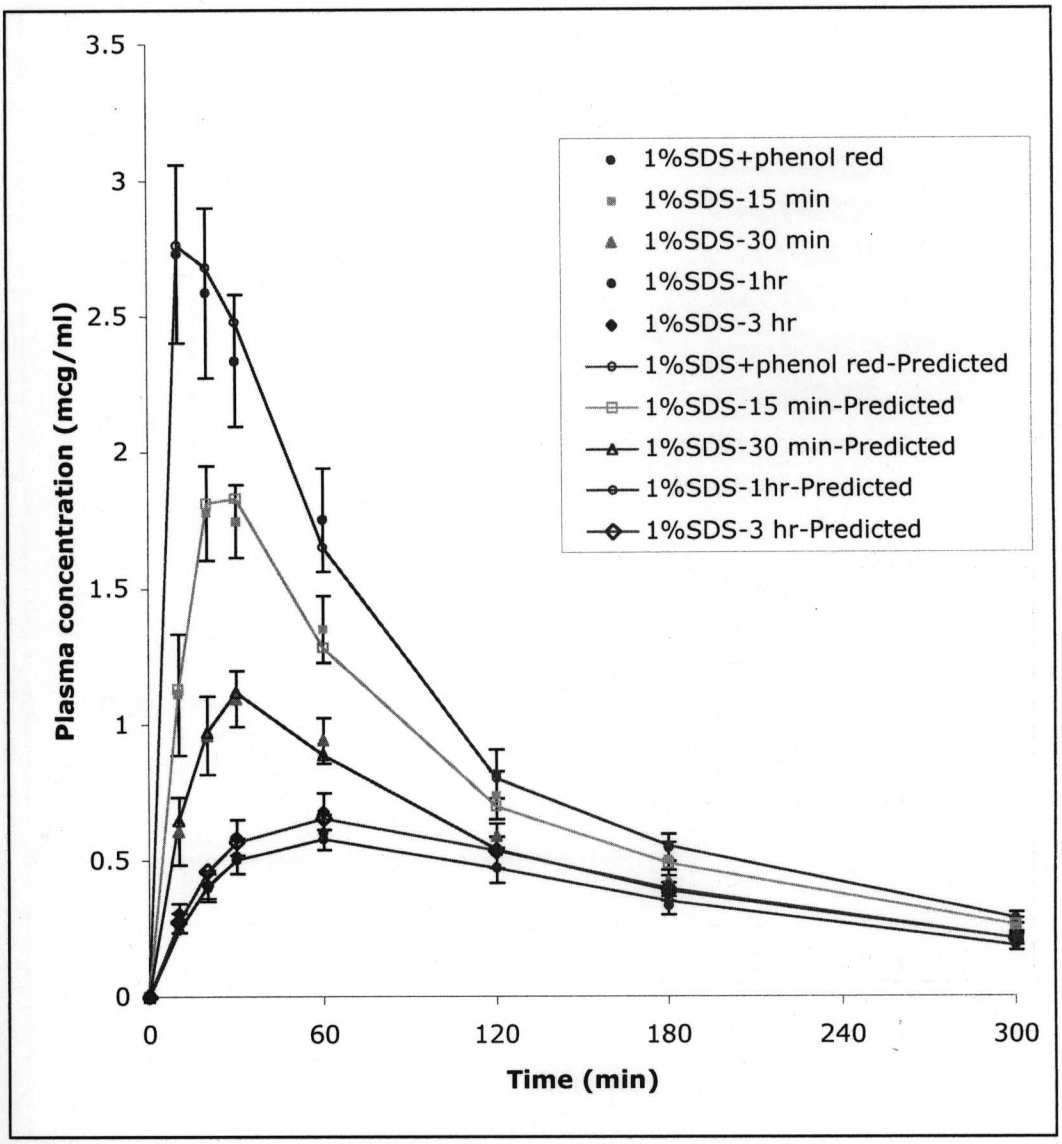

Figure 4-C-3: Observed and predicted plasma concentrations obtained by two-compartment model fitting using a step-function analysis for oral absorption of phenol red after different recovery times upon administration of 1% SDS.

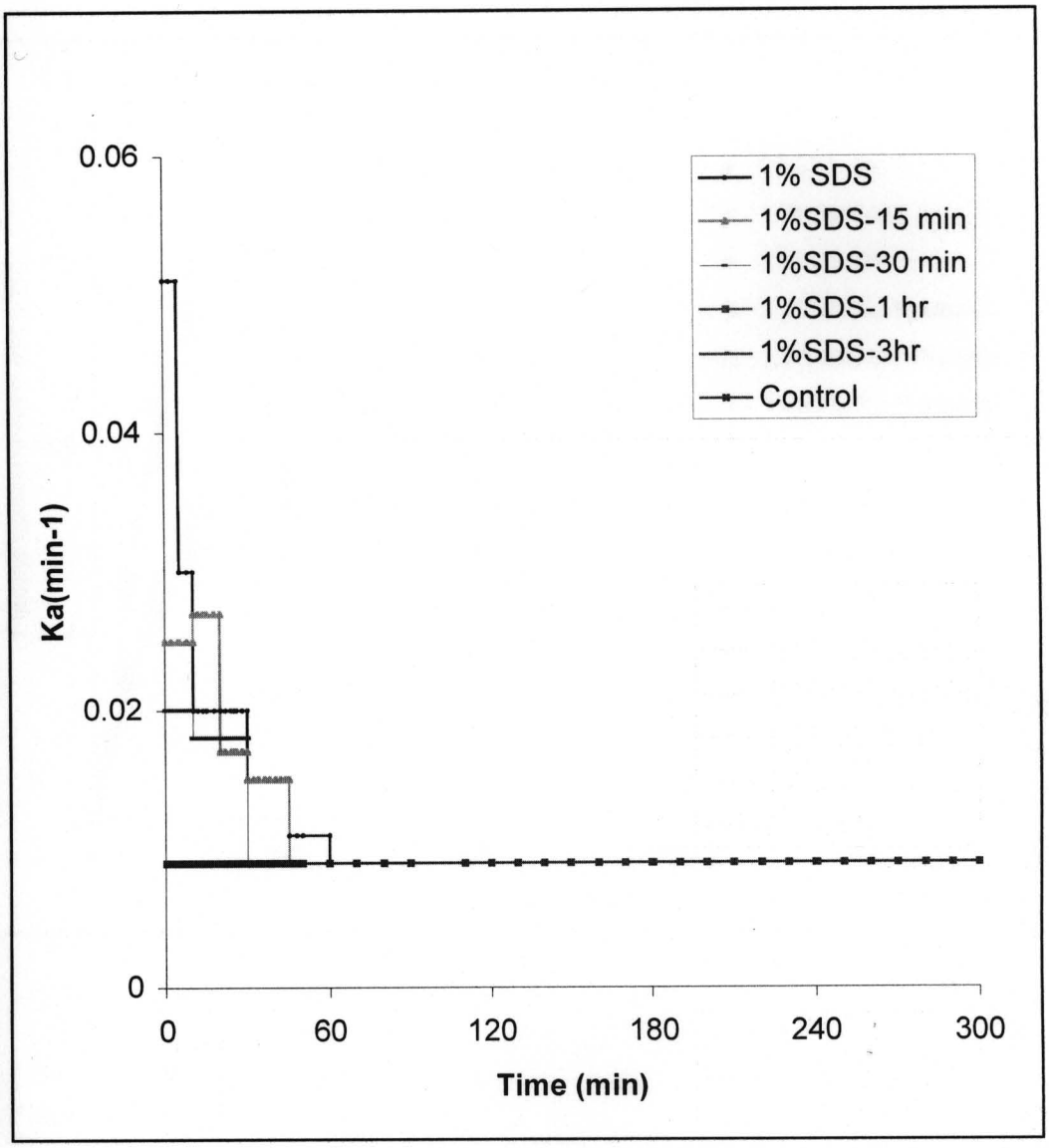

Figure 4-C-4: Change in oral absorption rate constant (K_a) with respect to time as estimated by two-compartment model fitting using a step-function analysis for phenol red after different recovery times upon administration of 1% SDS.

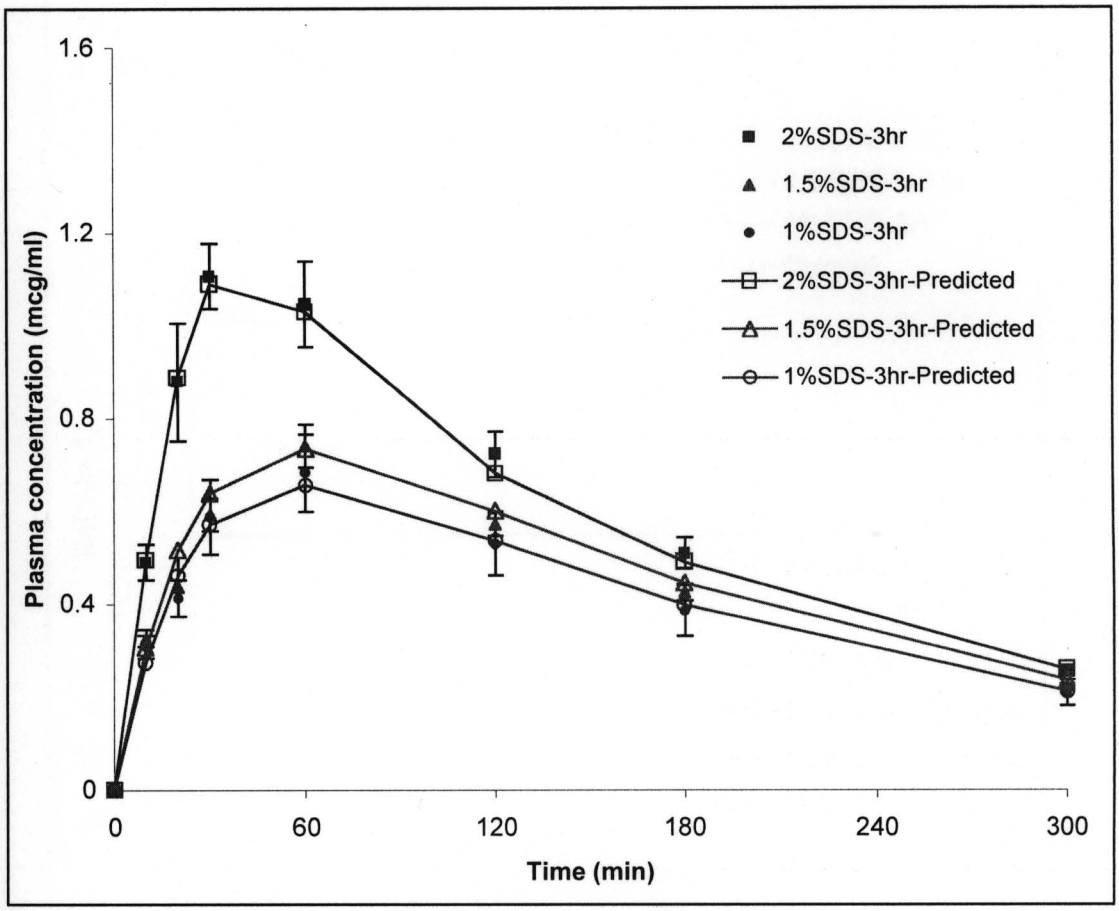

Figure 4-C-5: Observed and predicted plasma concentrations obtained by two-compartment model fitting using a step-function analysis for oral absorption of phenol red after 3-hour recovery period upon administration of SDS.

(N = 6, Each point represents Mean ± S.E.)

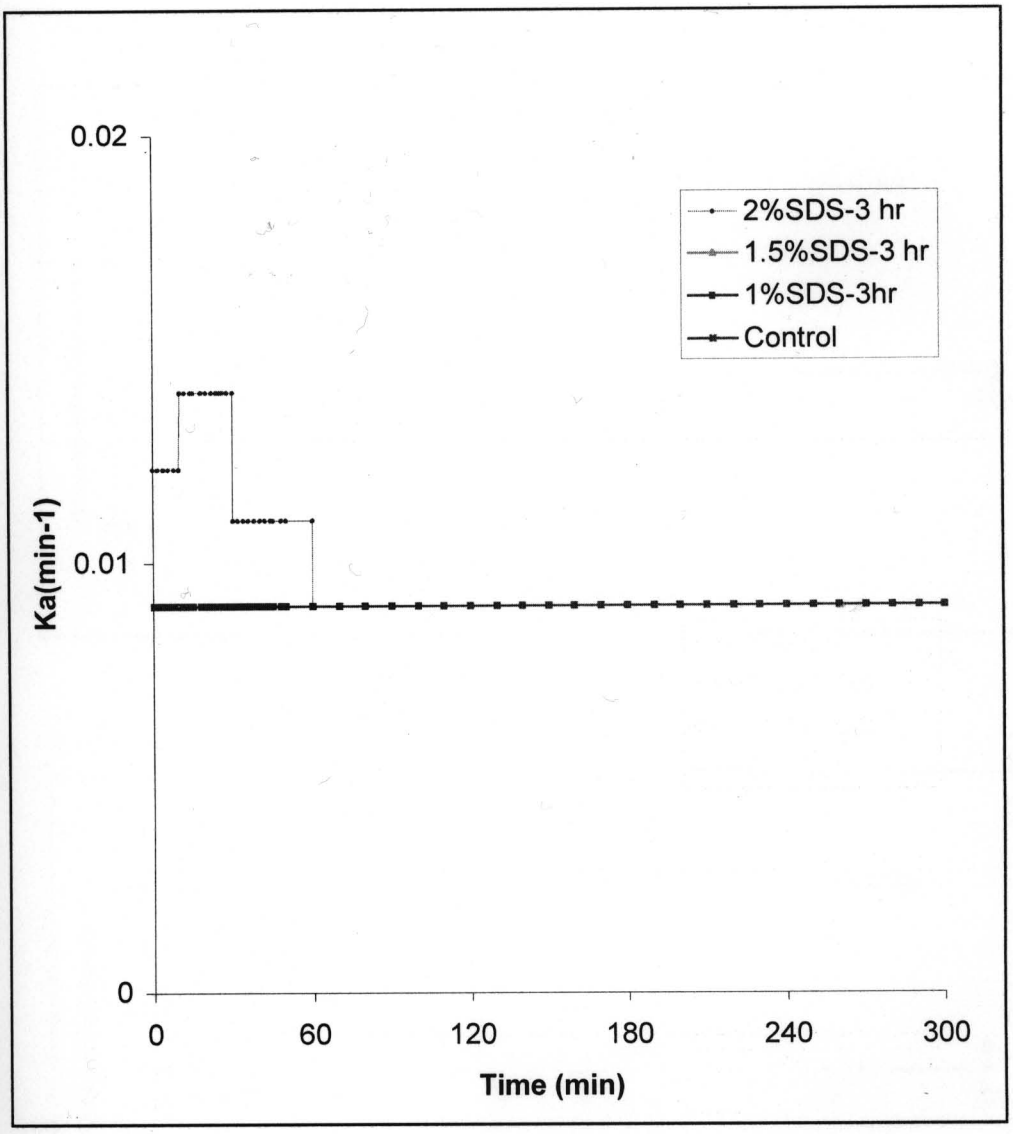

Figure 4-C-6: Change in oral absorption rate constant (K_a) with respect to time as estimated by two-compartment model fitting using a step-function analysis for phenol red after a 3-hour recovery upon administration of SDS.

(Note: Plots of K_a vs. time for control, 1% SDS-3hr and 1.5% SDS-3 hr recovery overlap)

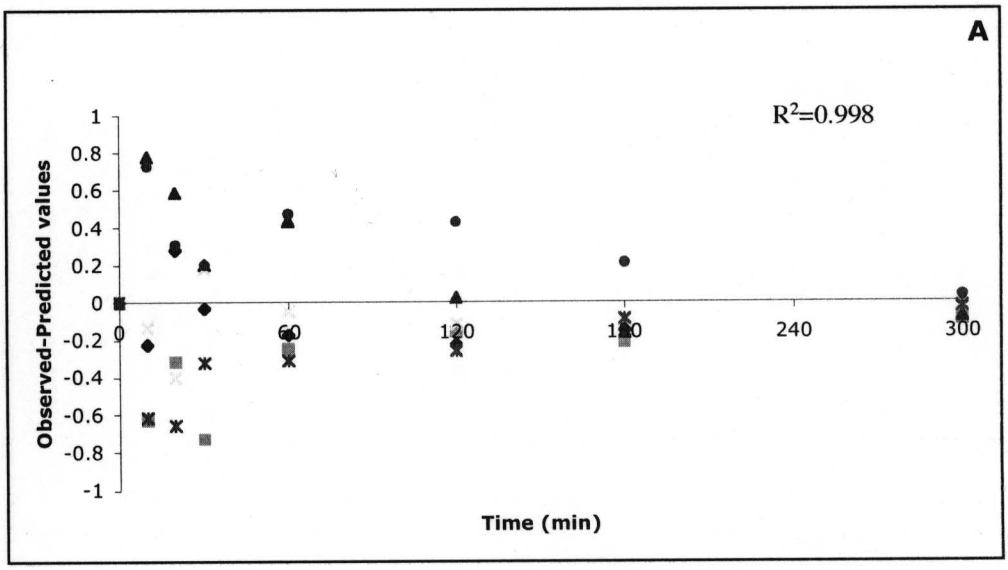

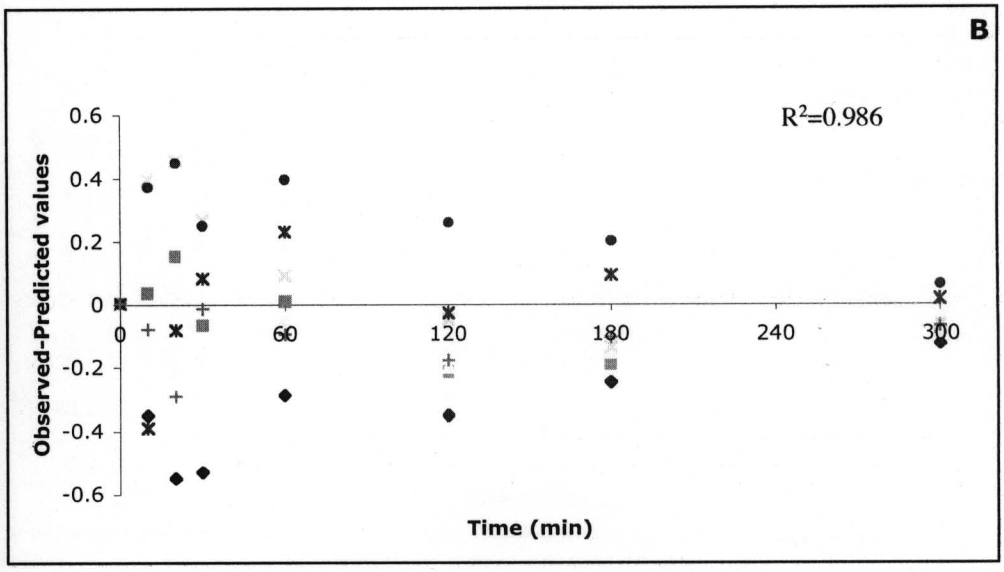

Figure 4-C-7: Plots of residuals versus time: (A) 1%SDS-15 min recovery and (B) 1%SDS-30 min recovery

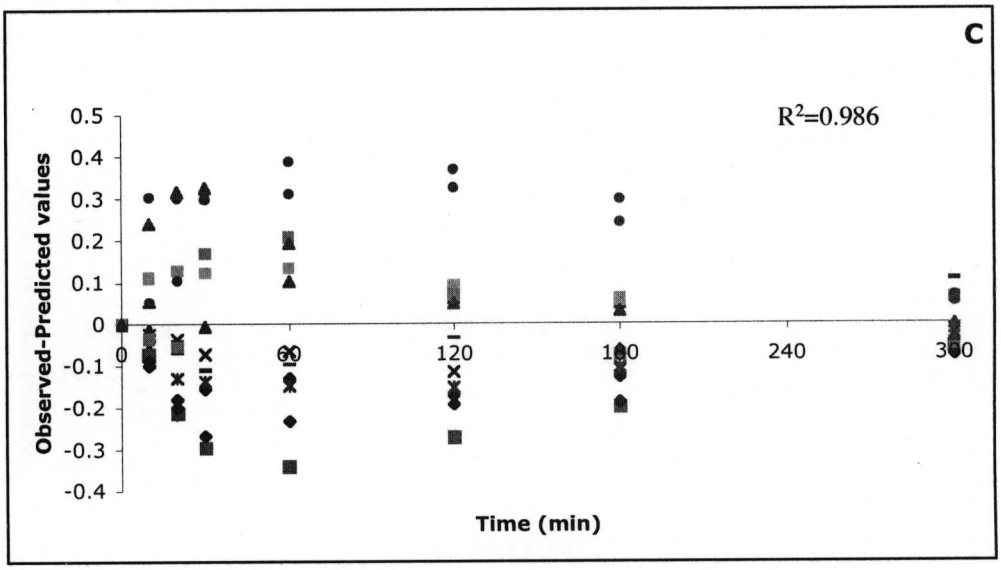

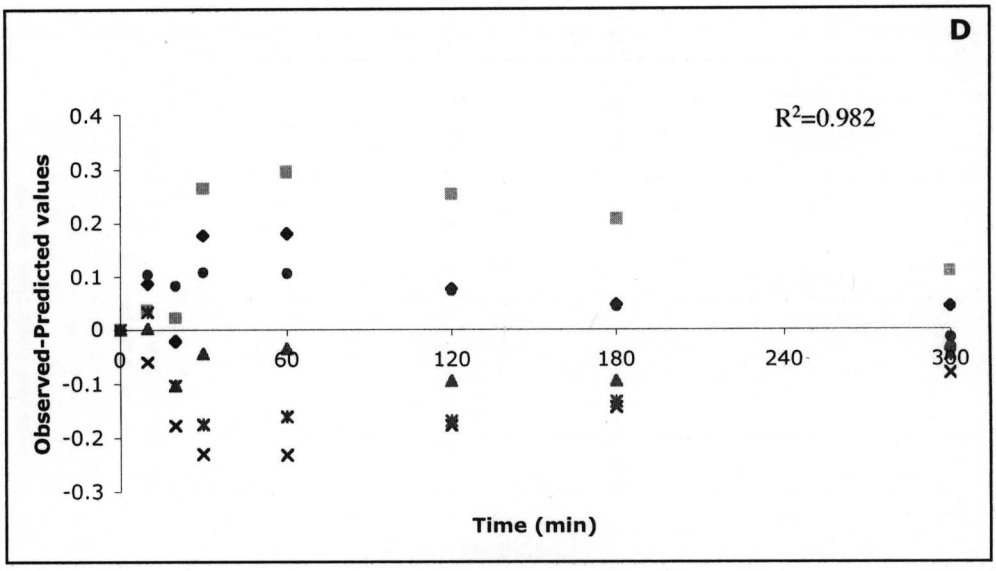

Figure 4-C-7: Plots of residuals versus time: (C) 1%SDS-1 hr recovery and (D) 1%SDS-3 hr recovery

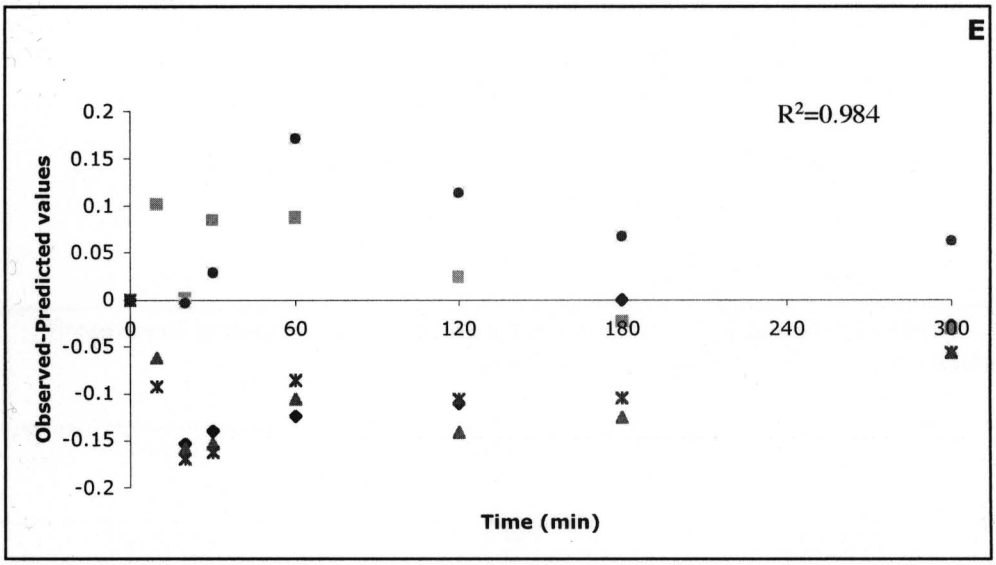

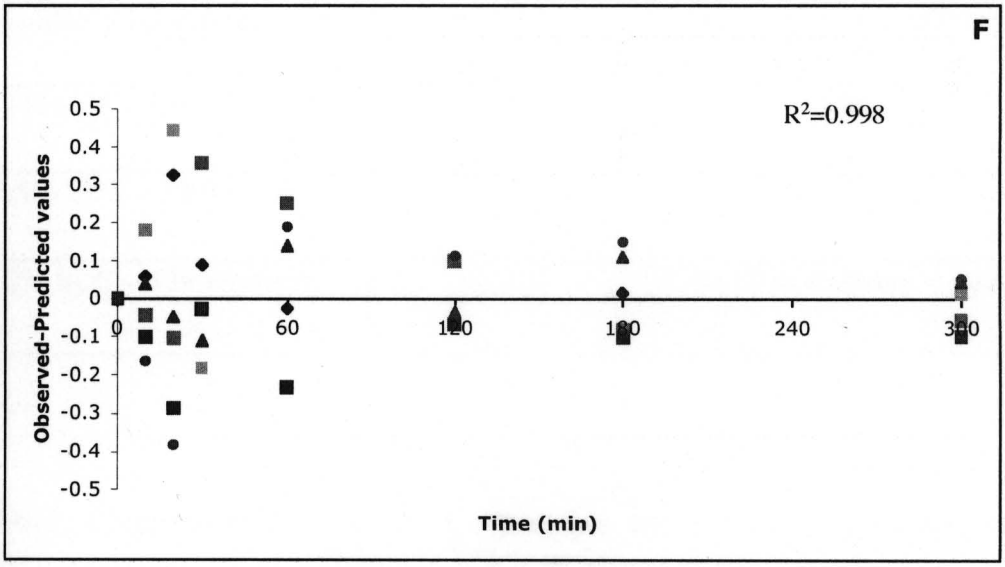

Figure 4-C-7: Plots of residuals versus time: (E) 1.5 % SDS- 3 hr recovery and (F) 2% SDS- 3 hr recovery

Treatment group	K_a (maximum) (min^{-1})	Time of Recovery estimated by curve fitting
Control	0.009	-
1% SDS	0.051	1 hr
1% SDS – 15 min recovery	0.027	45 min (+ 15 min recovery) = 1 hr
1% SDS – 30 min recovery	0.020	30 min (+ 30 min recovery) = 1 hr
1% SDS – 1 hr recovery	0.009	1 hr
1.5% SDS – 3 hr recovery	0.009	< 3 hrs
2% SDS – 3 hr recovery	0.014	1 hr (+3 hr recovery = 4 hrs)

Table 4-B-5: Comparison of changes in absorption rate constant of phenol red upon SDS administration as estimated using a step-function analysis .

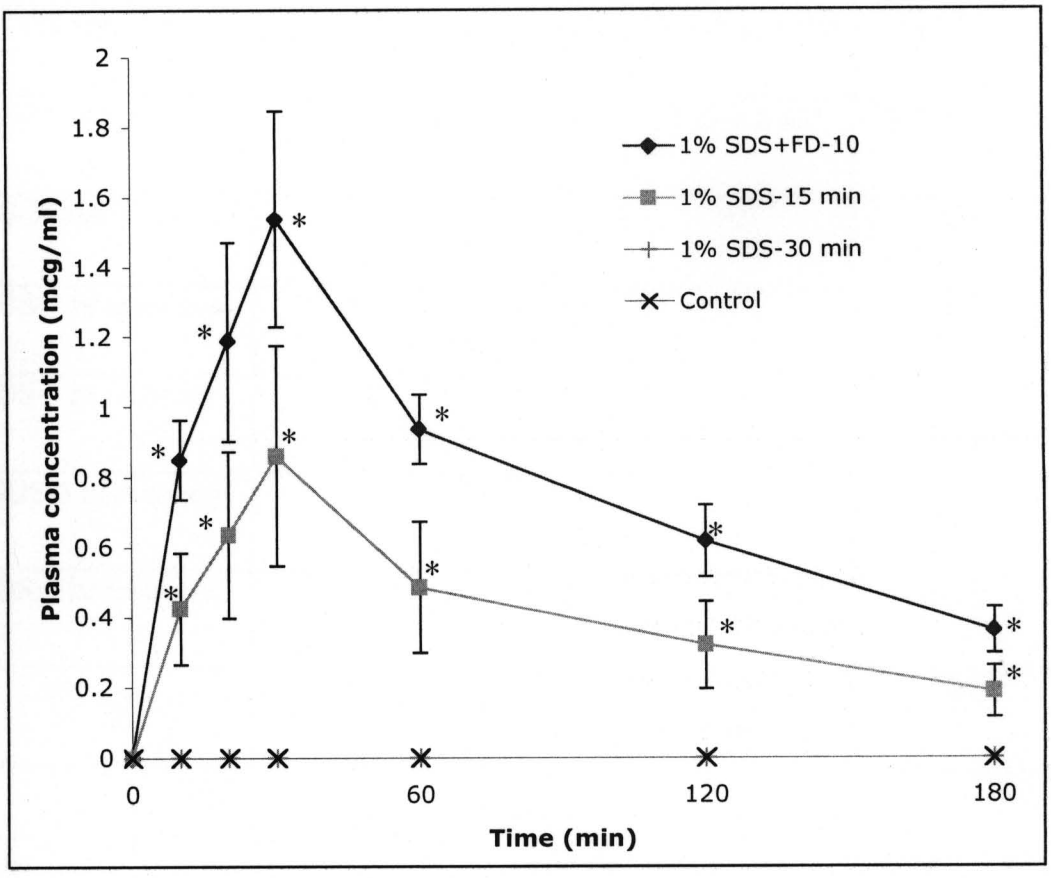

Figure 4-C-8: Oral absorption of FD-10 after different recovery times upon administration of 1% SDS.

(Control & 1% SDS-1 hr recovery: N= 12, Other SDS treatments: N= 6, Each point represents Mean ± S.E.

* Statistically significant difference from the control values at $p<0.05$)

Treatment group	C_{max} (mcg/ml)	T_{max} (min)	AUC ($t_{0\text{-}180\ min}$)	Bioavailability (%)
1% SDS	1.53 ± 0.31*	30 ± 0	141.04 ±14.18*	1.47 ± 0.26*
1% SDS-15 min recovery	0.86 ± 0.23*	30 ± 0	72.43 ± 8.43*	0.76 ± 0.17*
1% SDS-30 min recovery	0.0	0.0	0.0	0.0
1% SDS-1 hr recovery	0.0	0.0	0.0	0.0
1% SDS-3 hr recovery	0.0	0.0	0.0	0.0
1.5% SDS-3 hr recovery	0.0	0.0	0.0	0.0
2% SDS-3 hr recovery	0.0	0.0	0.0	0.0
Control	0.0	0.0	0.0	0.0

Table 4-C-6: Oral absorption of FD-10 after different recovery times upon oral administration of 1%, 1.5% and 2% SDS

(C_{max} and T_{max} are the averages calculated from the observed data. AUC was calculated using the linear trapezoidal rule from the observed data. Bioavailability was calculated by extrapolating AUC to infinity.

Control & 1% SDS-1 hr recovery: N= 12, Other SDS treatments: N= 6, Each point represents Mean ± S.E., *Statistically significant difference from the control values at $p<0.05$)

Chapter 4-D: Evaluation of Morphological Recovery Using Light and Transmission Electron Microscopy (Objective III)

1. Materials

Epon resin kit (Embed 812) was ordered from EMS, Hartfield, PA. 400 mesh Nickel grids were obtained from Ted Pella, California.

2. Methods

3 rats were used per group. The negative control group was given an oral gavage of water. The treatment groups were given an oral dose of 2 ml of 1% SDS. At specific time points (10 min, 15 min, 30 min, 1 hr or 3 hrs) rats were anesthetized with isoflurane as described in chapter 4-A. An incision was made in the abdomen and 1 cm of the duodenum was collected immediately below the pyloric sphincter. Similarly, 1 cm of the jejunum was collected, 10 cm from the pyloric sphincter. After tissue collection, the animals were sacrificed by excision of the heart.

The tissues were immediately washed with cold PBS (pH 7.0) and transferred into the 2.5% glutaraldehyde fixative solution in 0.1% cacodylate buffer (pH 7.0) and cut into small pieces. The samples were stored in the fixative solution overnight at 4^0C. The next day, they were stained with 1% osmium tetroxide in 0.1 M cacodylate buffer followed by two washings in 0.1% cacodylate buffer for 20 minutes each. The tissues were serially dehydrated in 30%, 50%, 70%, 90% and twice in 100% ethanol for 20 minutes each. The dehydrated tissues were then washed twice with propylene oxide for 20 minutes each and infiltrated with propylene oxide: Epon resin mixture (1:1) for 2 hours and with a 1:2 mixture overnight. The specimens were transferred into fresh resin twice for 3 hours each. The tissues were positioned in embedding molds in fresh EPON resin. The resin was then allowed to polymerize at 65^0C for 48 hours. 2μm sections were serially cut from the resin blocks using

an ultramicrotome (RMC, Arizona) equipped with a diamond knife, stained with 1% toluidine blue solution and viewed under a light microscope (Zeiss Axiovert 200 M). Control, 10 min, 15 min, 30 min, 1 hr and 3 hrs recovery sections were observed.

For transmission electron microscopy (TEM), 100 nm sections were cut and treated with 1% lead citrate solution for 20 seconds and then contrasted with 2% uranyl acetate in water for 10 minutes. The sections were mounted on 400 mesh grids and viewed under a transmission electron microscope (Zeiss EFTEM 912). Control, 30 min, 1 hr and 3 hrs recovery sections were observed.

3. Results and Discussion

I. Light microscopy

Figure 4-D-1 presents a cross section of control rat duodenal villi. Normal intestinal epithelium is observed, with well-aligned viable epithelial cells and some normal sloughing of cells at the tips. Figure 4-D-2 and 4-D-3 present cross sections of rat duodenal villi 10 and 15 minutes after administration of 1% SDS, respectively. The duodenal villi show signs of injury both after 10 and 15 minutes after treatment with the surfactant, implying that the action of SDS on the intestinal mucosa was quick. The villi are swollen and ruptured with damage extending to the lamina propria. Figure 4-D-4 presents rat duodenal villi 30 minutes after administration of 1% SDS. The damaged area on the villi look partially covered by the epithelial cells as compared to the villi 10 and 15 minutes after the treatment. Figure 4-D-5 presents rat duodenal villi 1 hour after administration of 1% SDS. The villi are covered with a continuous layer of epithelial cells. Light microscopy (LM) results show complete morphological recovery after 1 hour of treatment with 1% SDS for the duodenum. The

results were confirmed by observing morphology 3 hours after administration of 1% SDS. The results are shown in Figure 4-D-6.

Figure 4-D-7 presents a cross section of control rat jejunal villi. It shows normal jejunal villi covered with a continuous monolayer of epithelium. Figure 4-D-8 shows a section of jejunum, 10 minutes after treatment with 1% SDS. The villi still look normal under light microscopy, showing that the jejunum was still not affected by the penetration enhancer. Figure 4-D-9 shows abnormal jejunal villi 15 minutes after treatment with SDS. The intercellular spaces are dilated. Note that damage is not as extensive in the jejunum as it is seen in the duodenum at the same time. Figure 4-D-10 shows morphology of jejunal villi 30 minutes after administration of 1% SDS, the villi look normal and comparable to the control villi. Figure 4-D-11 and 4-D-12 present rat jejunal villi 1 and 3 hours after administration of 1% SDS. In both the figures, the villi are covered with a continuous layer of epithelial cells. LM results show complete morphological recovery after 30 minutes of treatment with 1% SDS for the jejunum.

The morphological recovery results were further confirmed with transmission electron microscopy (TEM).

II. Transmission electron microscopy

Upon a closer look under TEM, the control duodenal epithelium showed a surface covered with tall microvilli and normal tight junctions and adherens junctions between the normal duodenal epithelial cells (figure 4-D-13). For duodenal tissues obtained 30 minutes after treatment with 1% SDS, the epithelia surrounding the area of damage were observed under TEM. They had fewer microvilli on the surface and there were no defined junctional

complexes on the epithelial surface facing the damage (figure 4-D-14). This appearance is consistent with the restitution process that normally happens when damage is incurred by intestinal epithelium. The epithelial cells surrounding the area of damage lose polarity and microvilli disintegrate and start to migrate towards the zone of injury in order to cover it completely. Figure 4-D-15 shows appearance of duodenal epithelium 1 hour after treatment with SDS. The microvilli have started to regenerate and the paracellular junctions have started to reform. Even though the microvilli are not as tall as those seen for the control samples, the plasma membrane looks continuous and covered with microvilli. This means that the zone of injury is covered with intact epithelia and the transcellular and paracellular barrier have been re-established. Figure 4-D-16 shows duodenal epithelia 3 hours after treatment with SDS. The epithelial cells are covered with microvilli and paracellular junctions are normal.

Figure 4-D-17 shows normal jejunal epithelium covered with normal and tall microvilli and normal tight junctions and adherens junctions. 30 minutes after treatment with 1% SDS, the jejunal tissues appear normal as shown in Figure 4-D-18. The same observation was made 1 hour after treatment with 1% SDS for the jejunum (figure 4-D-19).

The morphological observations were consistent with the theory of restitution. The epithelial cells damaged by the surfactant, die of necrosis and are sloughed off from the villi into the lumen. The surrounding viable epithelial cells then disintegrate their junctional complexes and microvilli, thus losing their polarity and migrate over the zone of injury via contractile movement of the actin-myosin cable. Once cell-to-cell contact is established, junctional complexes are reformed and the microvilli start to re-grow [70-74]. This phenomenon was evident in the duodenum. 10 to 15 minutes after treatment with 1% SDS,

damage was evident in light microscopy in the duodenum. Discontinuity in the epithelial layer was probably because of shedding of the necrotized epithelial cells. 30 minutes after treatment with 1% SDS, partial recovery was seen in the duodenum in light microscopy and the epithelial cells bordering the zone of injury, did not show junctional complexes and microvilli in TEM images, which was consistent with the restitution hypothesis. 1 hour after treatment with 1% SDS, duodenal villi looked completely covered with epithelium in light microscopy. In TEM images, the junctional complexes were reestablished and the luminal surface of the epithelium had started to show growth of microvilli.

Sodium dodecyl sulfate (SDS) is an anionic surfactant. It is a commonly studied penetration enhancer, which has been shown to extract epithelial membrane components like proteins, phospholipids and cholesterol due to its surface-active behavior [108, 110, 142]. Below the critical micellar concentration, it opens up paracellular junctions by chelating Ca^{+2} ions, which are required to maintain the tight junctions [151]. In the jejunum only the paracellular spaces looked dilated in light microscopy. The membrane solubilizing action of SDS on the epithelium was confined to the duodenum due to the large concentration of SDS administered as an oral gavage. As the gavage solution traveled down to the jejunum the concentration of SDS was reduced (below the CMC) so that the action was limited to the paracellular pathway. Hudspeth et al showed that when injured, paracellular spaces could be repaired within 30 minutes *in vitro* [24]. In this study we found that it took about 15 minutes to repair the paracellular junctions in rat jejunum *in vivo.*

The results from absorption recovery studies were consistent with microscopy observations. Light microscopy results showed that damage occurred almost instantaneously (within 10 minutes) upon administration of 1% SDS which is consistent with the oral

absorption data where C_{max} was achieved within 10 minutes with the maximum K_a for phenol red after co-administration with 1% SDS. The epithelial cell layer was disrupted and was removed from the underlying lamina propria in some places, thus breaking down both the transcellular and paracellular barriers. 15 minutes after administration of the penetration enhancer, the mucosa in the duodenum still looked damaged. In the jejunum, only the paracellular spaces looked affected after 15 minutes. Partial mucosal repair was evident in the duodenum in 30 minutes as seen under light microscope and transmission electron microscope. In the jejunum, morphological recovery was complete in 30 minutes as seen in LM and TEM. This observation is in accordance with recovery data where oral absorption of markers was remarkably reduced after the 30-minute recovery period. The transcellular and paracellular repair was complete in the duodenum in one hour as seen under both LM and TEM. These observations were consistent with 1-hour recovery results where oral absorption of phenol red was comparable to that of the negative control. Similar observations were made after 3-hour recovery.

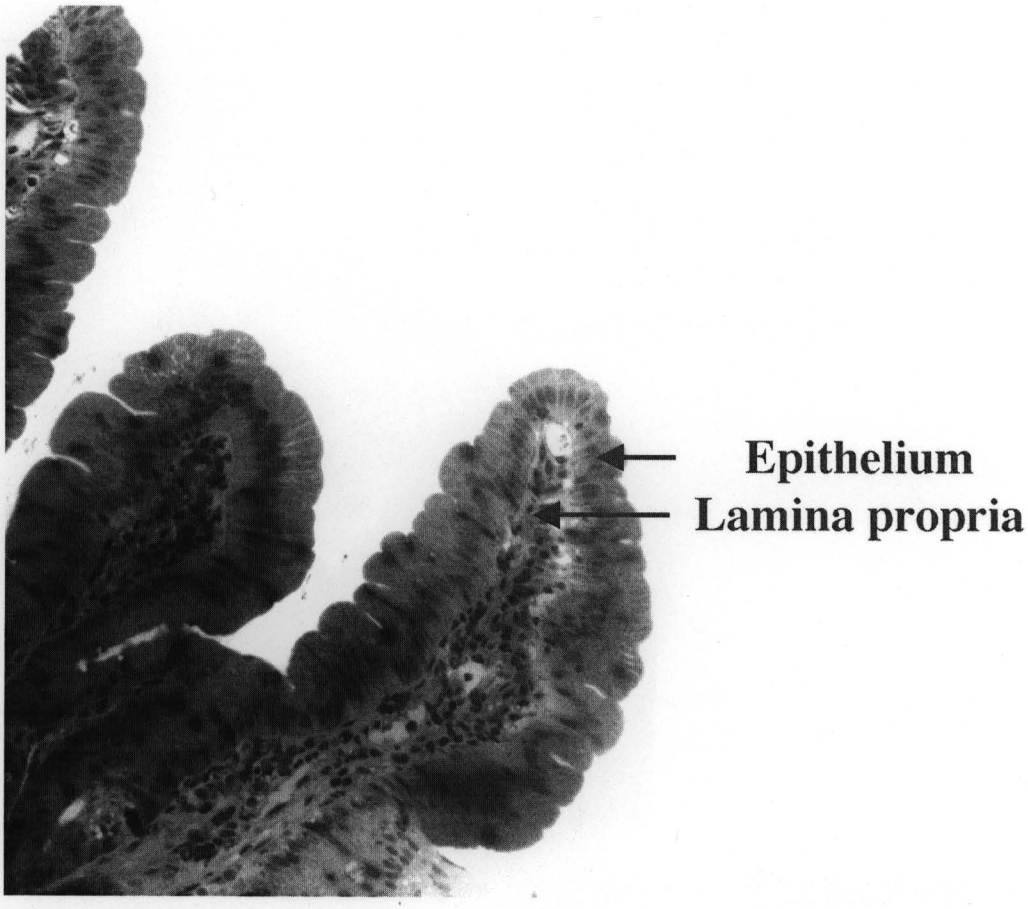

Figure 4-D-1: Light microscopy-Control duodenum (Magnification 100X)

Normal intestinal epithelium is observed, with well-aligned viable epithelial cells covering the surface of the villi.

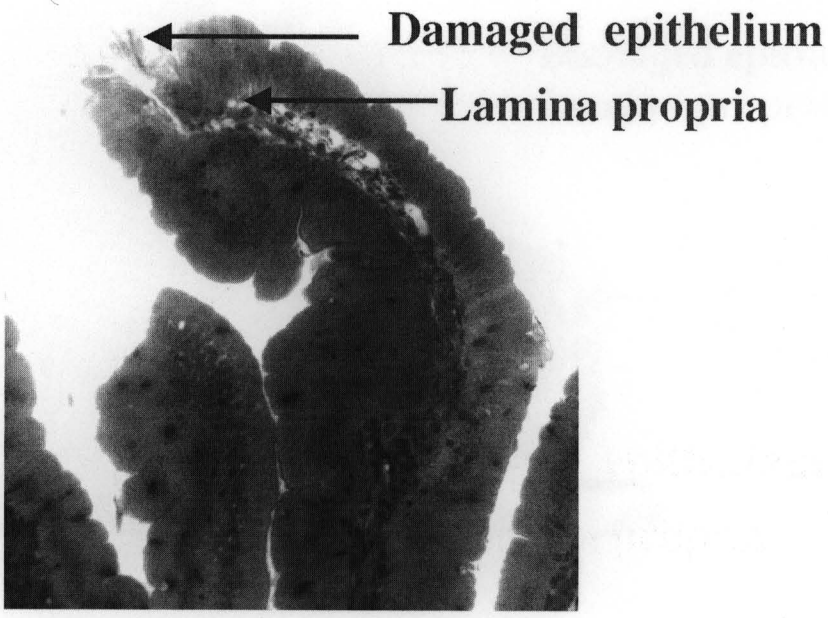

Figure 4-D-2: Light microscopy- Duodenum 10 min after administration of 1% SDS (Magnification 100X).

The epithelial layer is disrupted at the villus tip, the villus is slightly swollen with damage extending to the lamina propria.

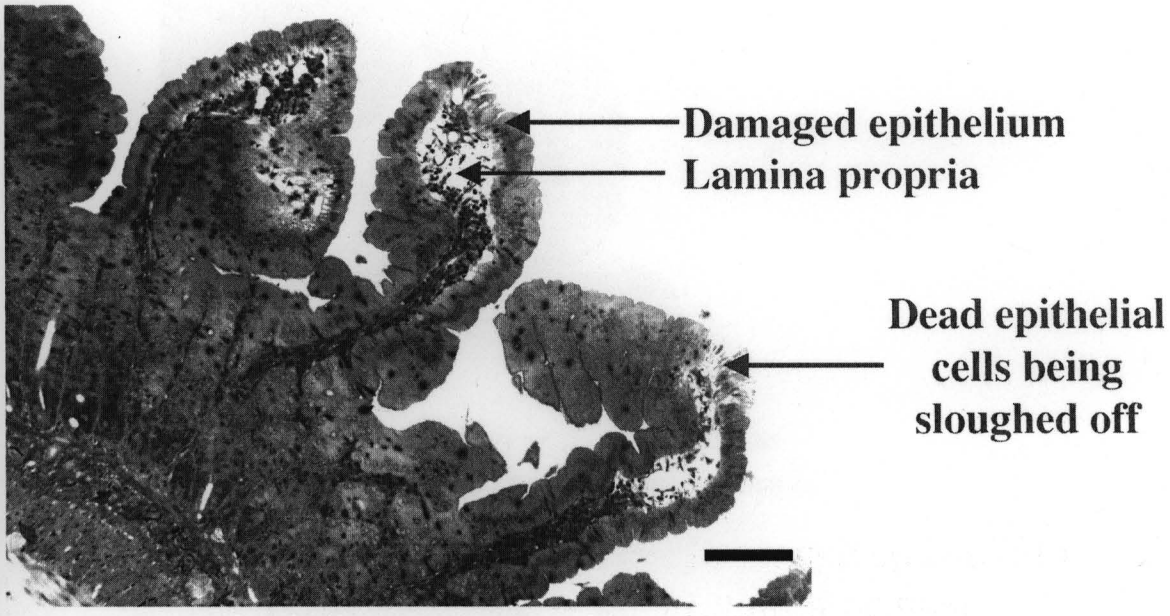

Figure 4-D-3: Light microscopy- Duodenum 15 min after administration of 1% SDS (Magnification 100X).

The villi are swollen and ruptured with damage extending to the lamina propria. The damaged epithelial cells are being sloughed off from the villus surface.

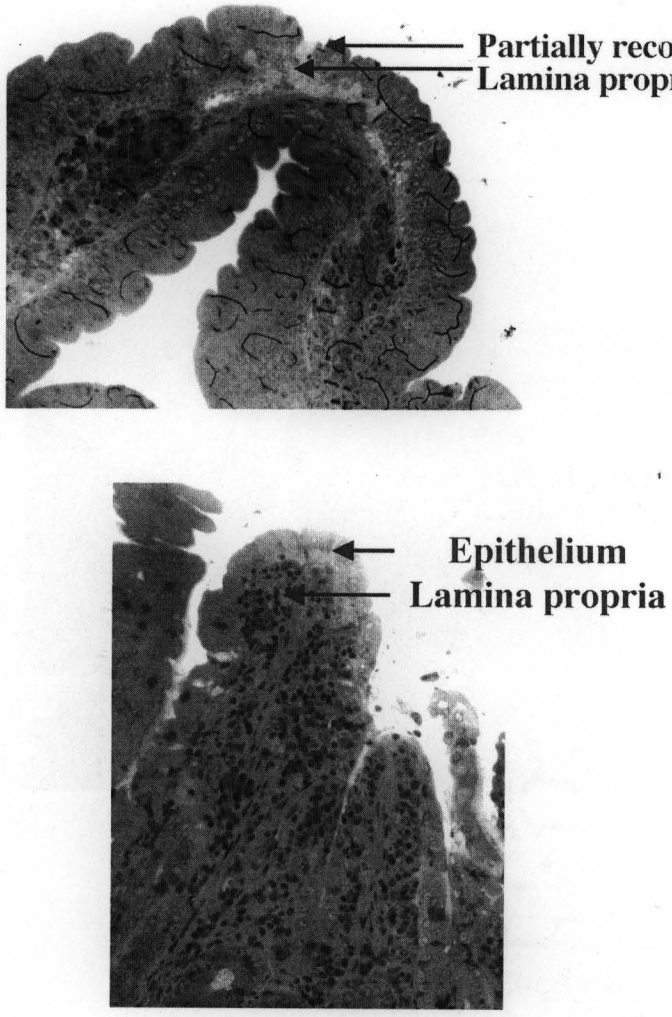

Figure 4-D-4: Light microscopy- Duodenum 30 min after administration of 1% SDS (Magnification 100X).

The results are variable with some villi covered with a continuous epithelial layer whereas some are partially covered by the epithelial cells as compared to the villi 10 and 15 minutes after the treatment.

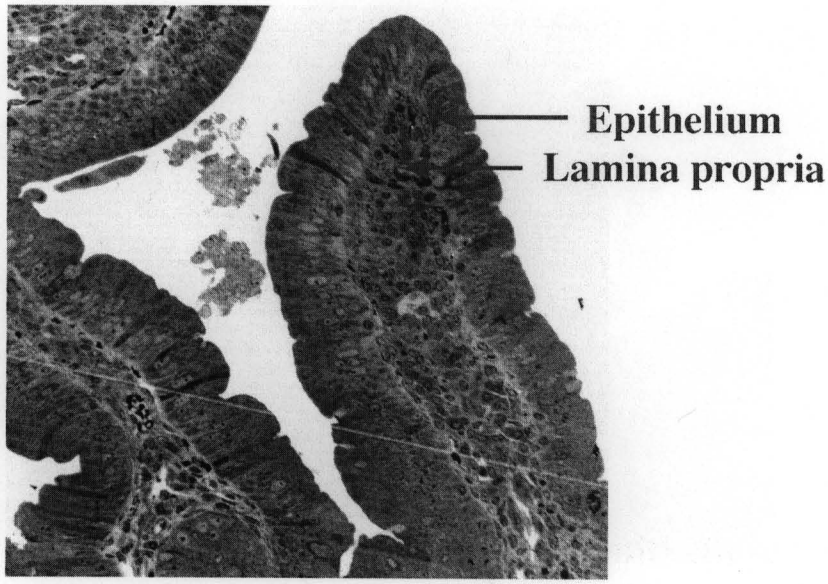

Figure 4-D-5: Light microscopy- Duodenum 1 hr after administration of 1% SDS (Magnification 100X).

The villi are covered with a continuous layer of epithelial cells appear normal.

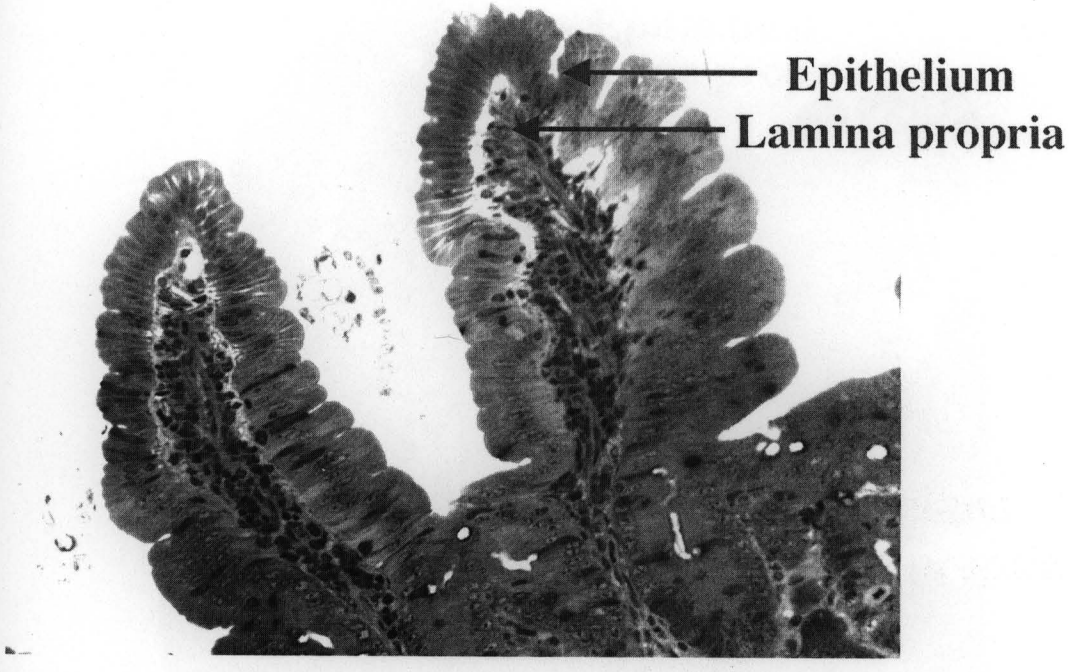

Figure 4-D-6: Light microscopy- Duodenum 3 hr after administration of 1% SDS (Magnification 100X).

The villi are covered with a continuous layer of epithelial cells appear normal.

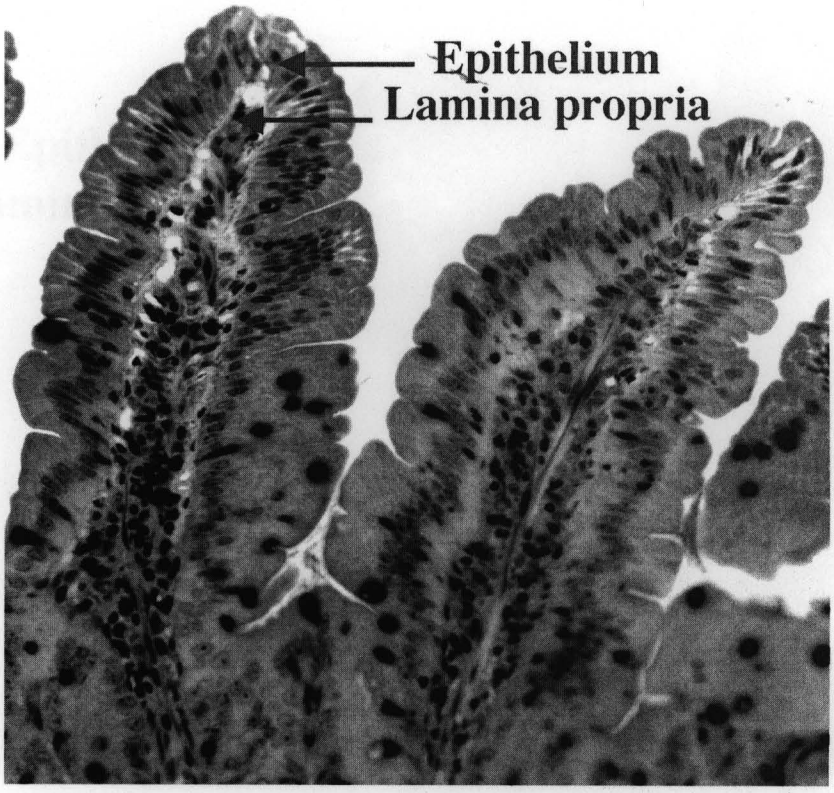

Figure 4-D-7: Light microscopy- Control Jejunum (Magnification 100X)

Villi are normal with a continuous layer of epithelial cells on the surface.

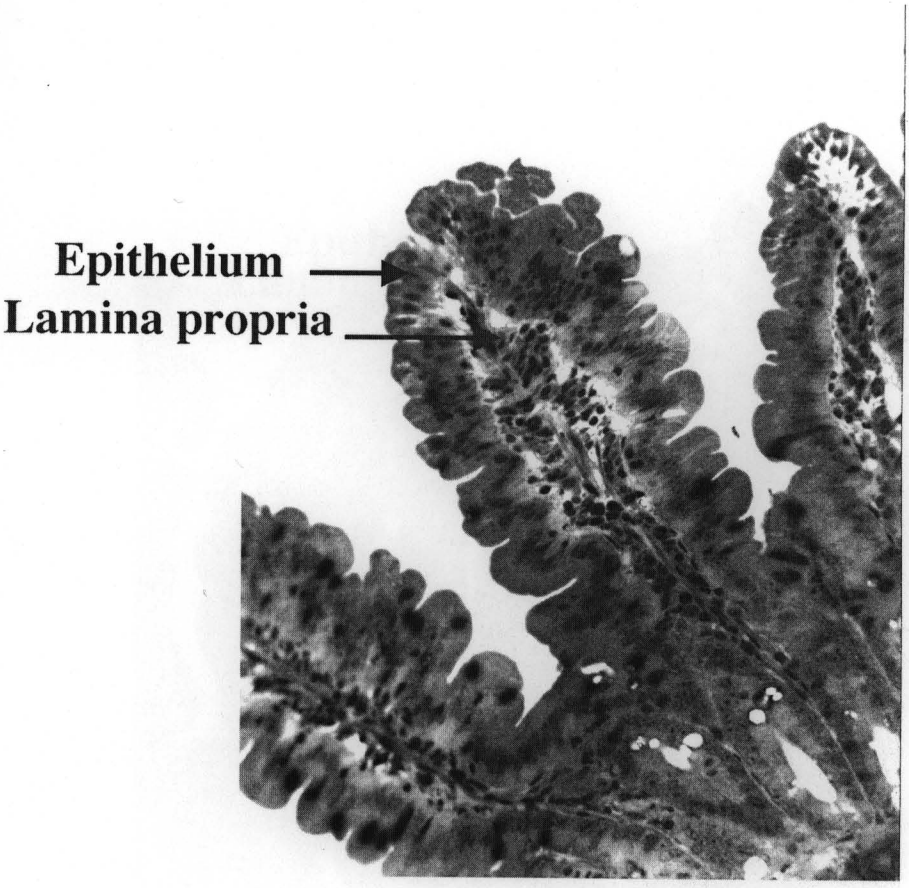

Figure 4-D-8: Light microscopy- Jejunum 10 min after administration of 1% SDS (Magnification 100X).

Intercellular spaces in the epithelium look dilated in some places but the appearance of the villi is not significantly different from the control.

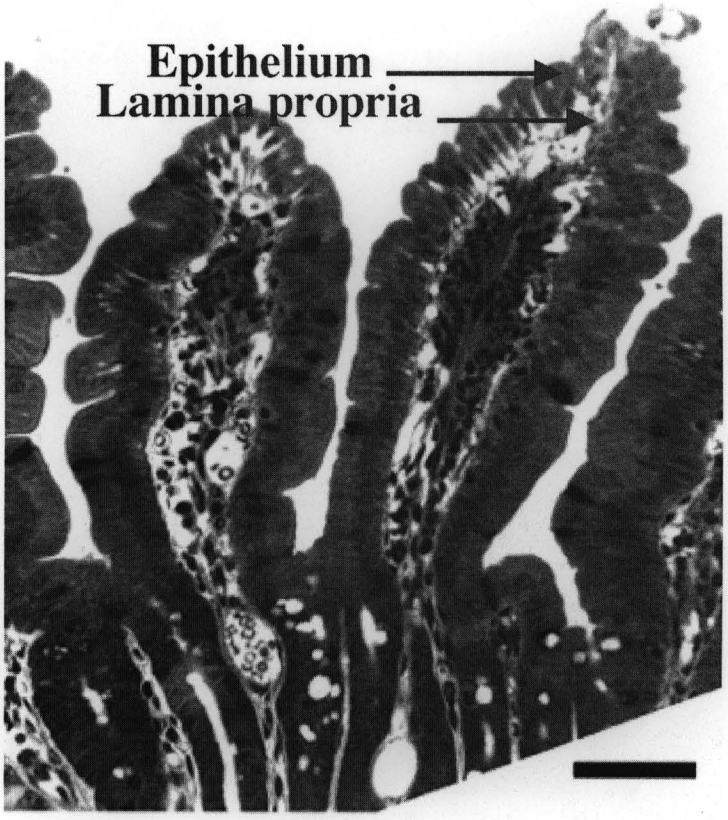

Figure 4-D-9: Light microscopy- Jejunum 15 min after administration of 1% SDS (Magnification 100X). The intercellular spaces in the epithelium are dilated especially at the tip of the villi. The effect of SDS on the jejunum is not as drastic as seen in the duodenum.

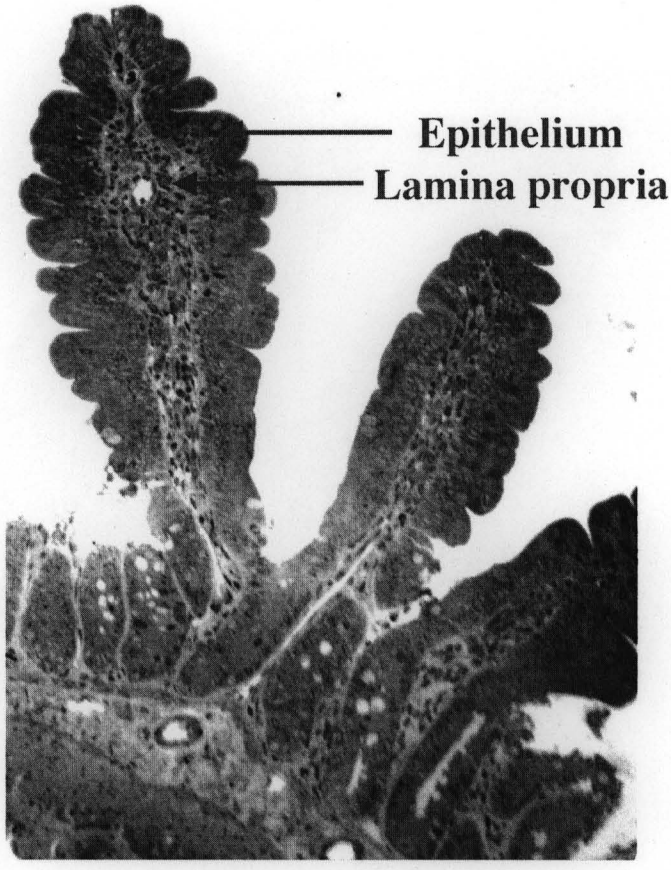

Figure 4-D-10: Light microscopy- Jejunum 30 min after administration of 1% SDS (Magnification 100X). The villi look normal with a continuous layer of epithelium on the surface.

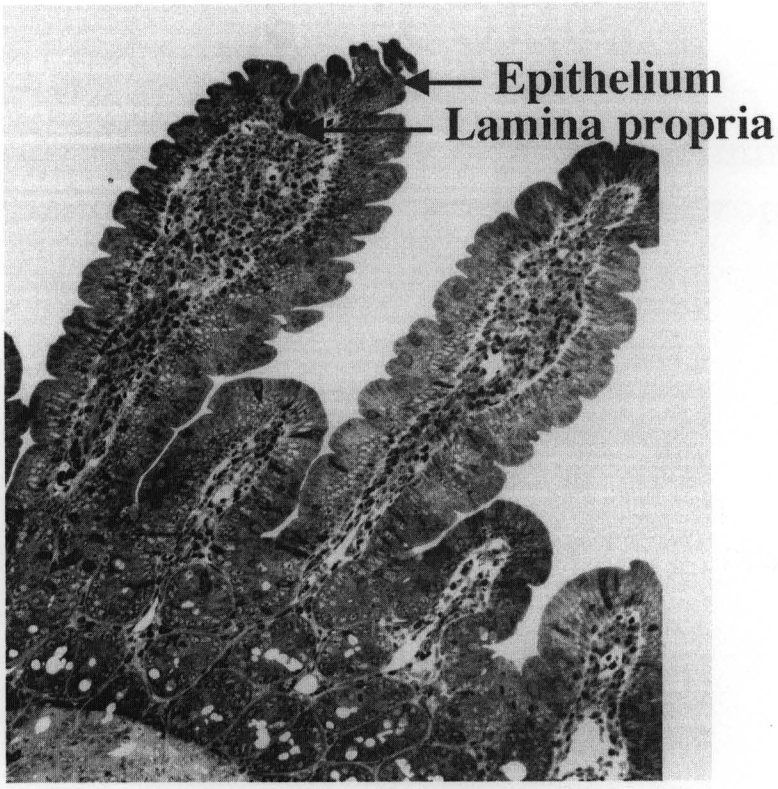

Figure 4-D-11: Light microscopy- Jejunum 1 hr after administration of 1% SDS (Magnification 100X).

The villi look normal with a continuous layer of epithelium on the surface.

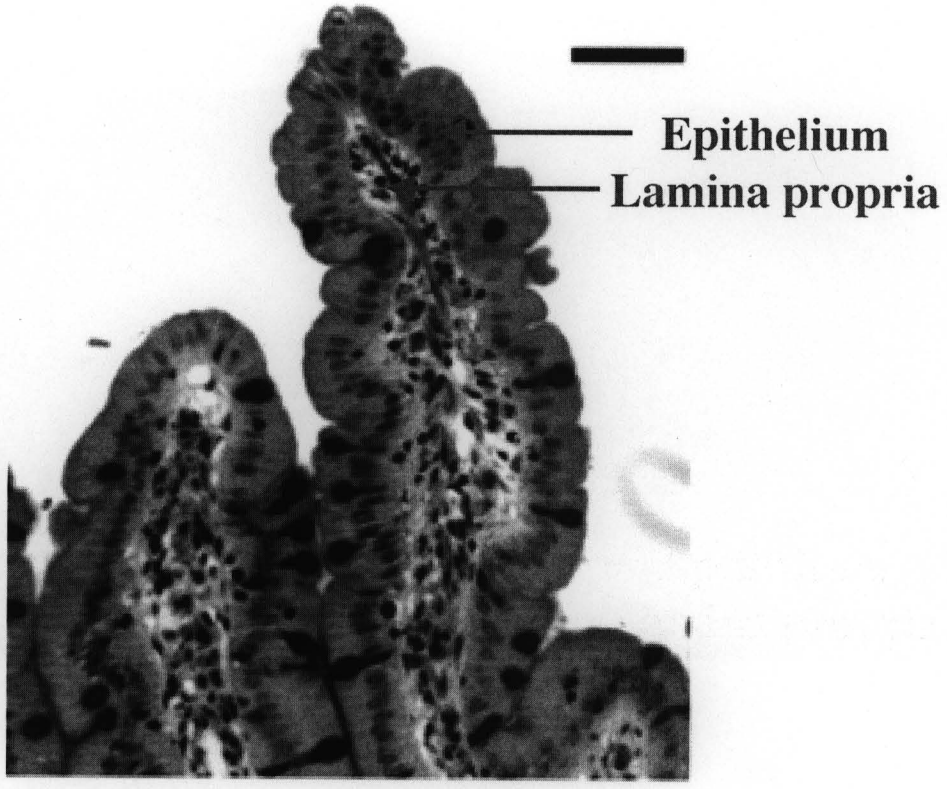

Figure 4-D-12: Light microscopy- Jejunum 3 hr after administration of 1% SDS (Magnification 100X). The villi look normal with a continuous layer of epithelium on the surface.

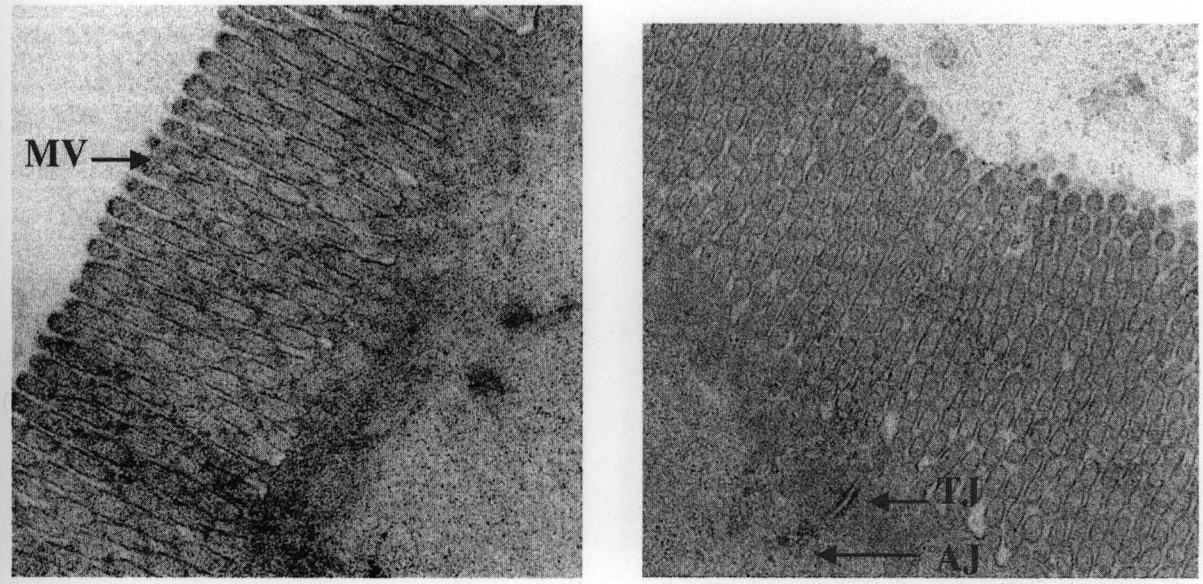

(A) (B)

Figure 4-D-13: Transmission electron microscopy- Control Duodenum

(A) MV- microvilli and (B) TJ- tight junctions, AJ- adherens junctions

(Magnification 1000,000 X).

The epithelial cell surface is covered with tall microvilli and the junctional complexes look normal.

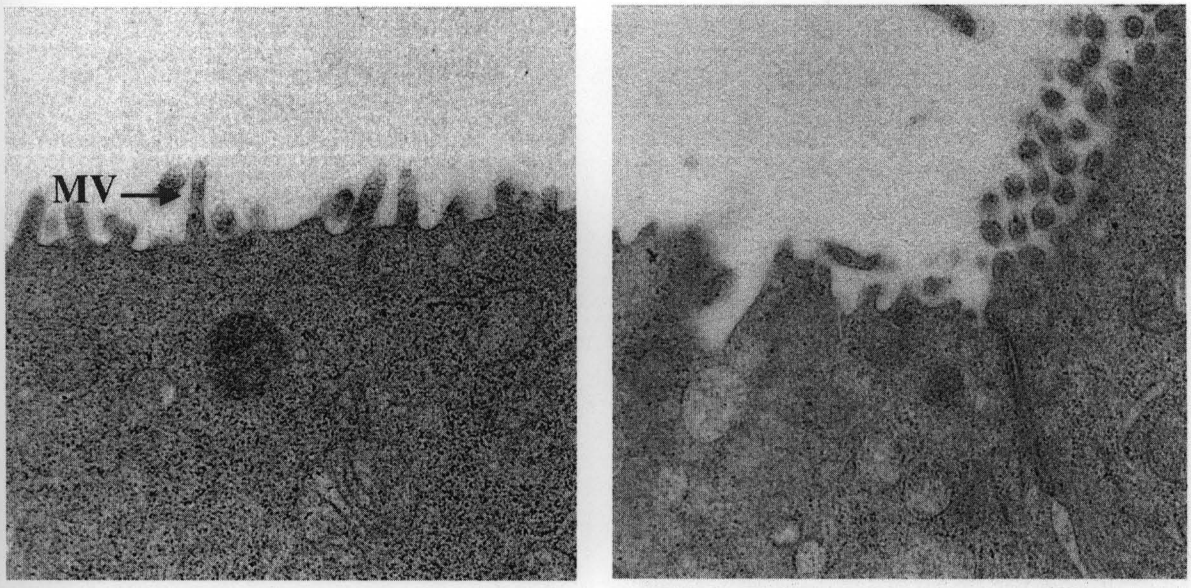

(A) (B)

Figure 4-D-14: Transmission electron microscopy- Duodenum 30 min after treatment with 1% SDS.

(A) MV - microvilli and (B) lack of intercellular junctions in the cells bordering zone of injury.

(Magnification 1000,000 X).

The epithelial cell bordering the zone of injury have disintegrated the microvilli from the surface and lack the junctional complex, a phenomena consistent with the restitution process.

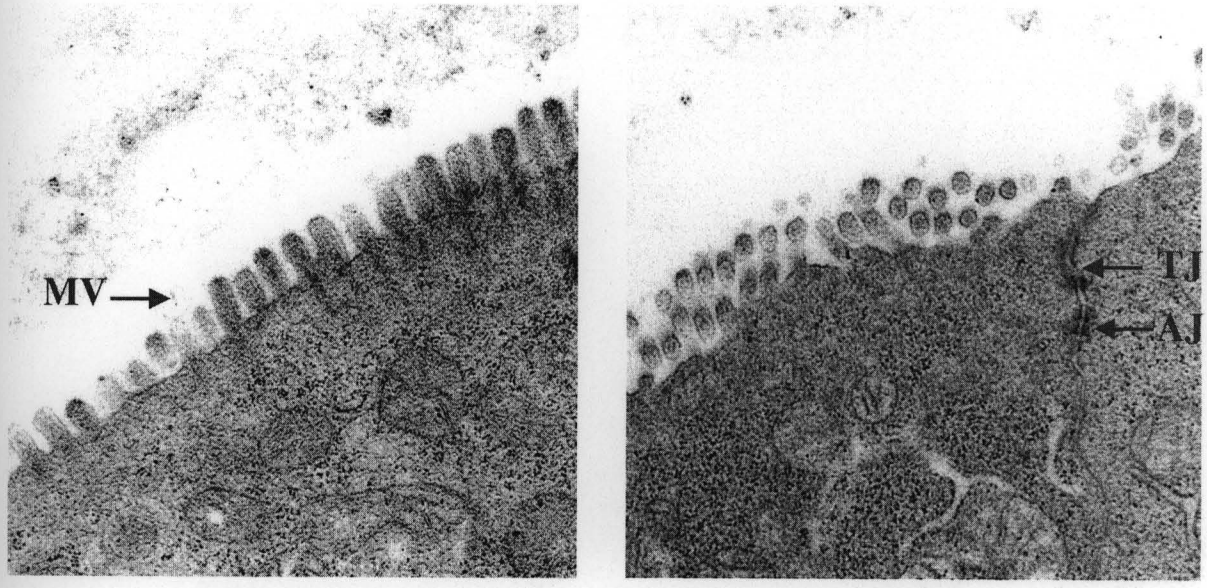

(A) (B)

Figure 4-D-15: Transmission electron microscopy- Duodenum 60 min after treatment with 1% SDS.

(A) MV - microvilli and (B) TJ- tight junctions, AJ - adherens junctions.

(Magnification 1000,000 X).

The epithelial cells at the tip of the villi have started to generate microvilli on the luminal surface and the junctional complexes with the adjacent epithelial cell.

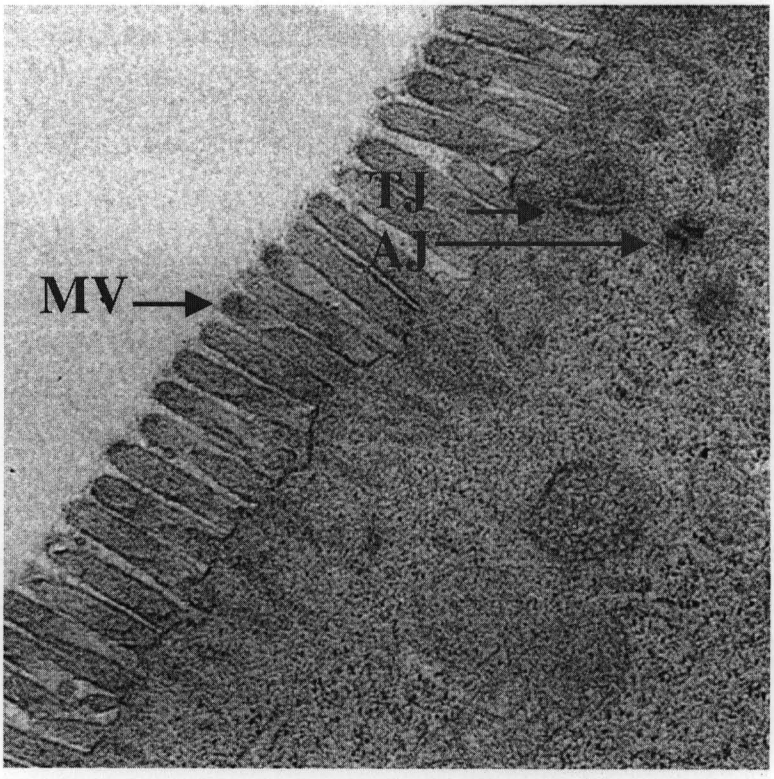

Figure 4-D-16: Transmission electron microscopy- Duodenum 3 hr after treatment with 1% SDS.

MV – microvilli, TJ – tight junctions and AJ - adheres junctions.

(Magnification 1000,000 X).

The microvilli on the luminal surface of epithelial cells at the tip of the villi have grown taller and the junctional complexes are formed.

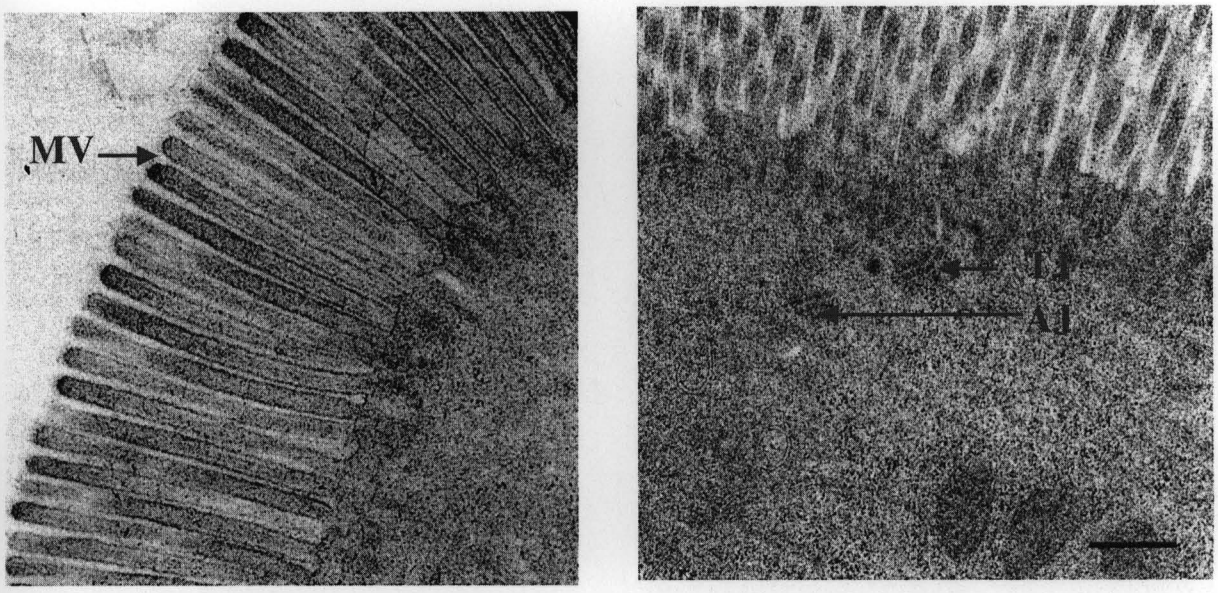

(A) (B)

Figure 4-D-17: Transmission electron microscopy: Control Jejunum.

(A) MV - microvilli and (B) TJ – tight junctions, AJ- adherens junctions.

(Magnification 1000,000 X).

The luminal surface of the epithelium is covered with tall microvilli and the junctional complexes look normal.

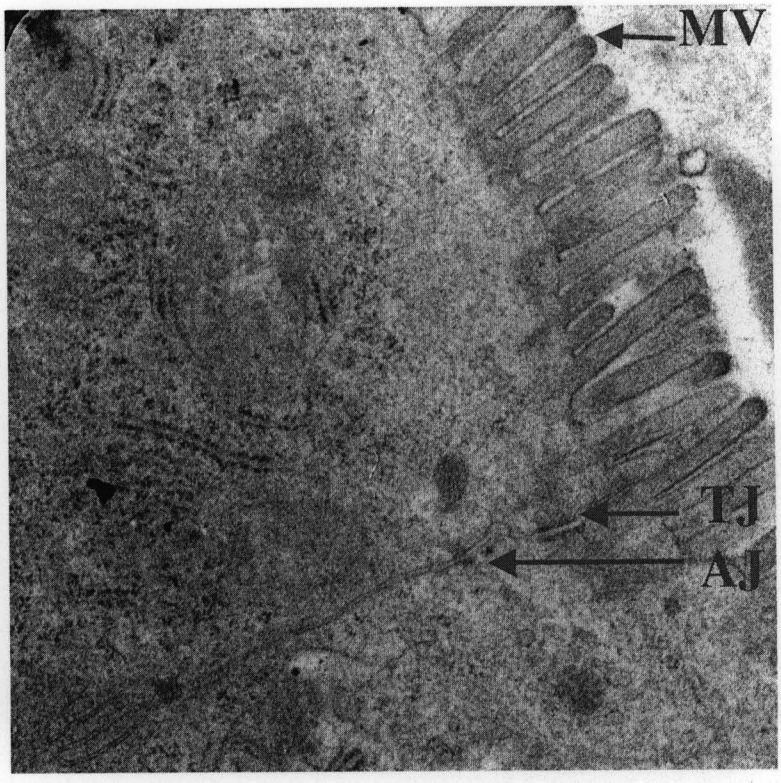

Figure 4-D-18: Transmission electron microscopy: Jejunum 30 min after treatment with 1% SDS

MV – microvilli, TJ – tight junctions and AJ - adherens junctions

(Magnification 1000,000 X)

The luminal surface of epithelial cells at the tip of the villi is covered with microvilli and the junctional complexes are formed.

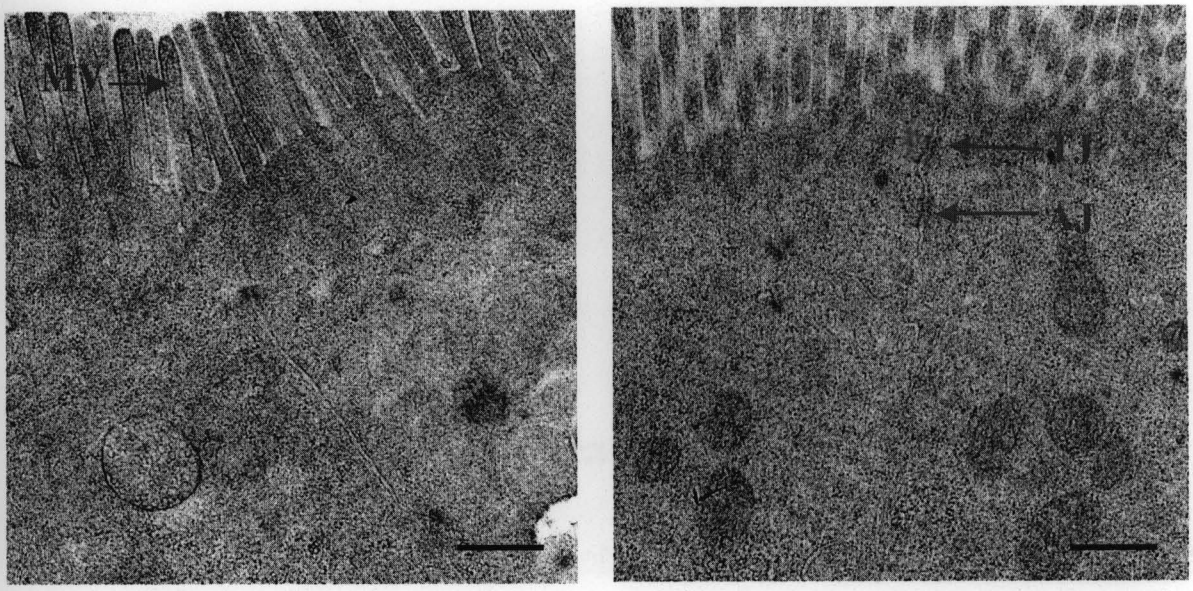

Figure 4-D-19: Transmission electron microscopy- Jejunum 60 min after treatment with 1% SDS.

(A) MV - microvilli and (B) TJ – tight junctions, AJ - adherens junctions.

(Magnification 1000,000 X).

The luminal surface of epithelial cells at the tip of the villi is covered with microvilli and the junctional complexes look normal.

Chapter 4-E: Repeated Exposure Study

(Objective IV)

1. Materials

Materials used in this section were same as described in chapters 4-B through 4-D.

2. Methods

I. Evaluation of absorption barrier after repeated exposure

12 rats were given an oral gavage of 2 ml of 1% SDS everyday for 14 days. On day 15, animals were given an oral dose of phenol red and FD-10 (6 mg each dissolved in 2 ml). Blood samples were drawn and plasma samples were assayed as described previously. Statistical moment (non-compartment) and two-compartment pharmacokinetic analysis was performed using WinNonlin and MATLAB® 5 respectively, as described in chapters 4-B through 4-C.

II. Evaluation of morphology after repeated exposure

For morphology experiments, 3 rats were used. All experimental methods were same as described in chapter 4-D.

3. Results and Discussion

I. Evaluation of absorption barrier

Results obtained for this experiment with phenol red are depicted in figure 4-E-1. Two-compartment analysis is shown in figure 4-E-2. Residual plots are shown in Figure 4-E-3. C_{max}, T_{max}, AUC, MRT, MAT and K_a values obtained after repeated exposure to 1% SDS are summarized in table 4-E-1. Since actual experimental values were obtained till 300 minutes, AUC values were calculated from time 0 to 300 minutes for comparison between treatment and control groups, and were not extrapolated to infinity.

C_{max}, T_{max}, AUC, MRT, MAT and K_a values for phenol red after repeated exposure experiment, are statistically comparable to those for the negative control. The results show that for low molecular weight molecules, absorption barrier remained unaltered after repeated exposure to 1% SDS for 14 days.

FD-10 was not detected in plasma samples in any rat. The results indicate that for high molecular weight molecules, absorption barrier probably remained unaltered after repeated exposure to 1% SDS for 14 days.

12 rats were used in this study to obtain 80% power for statistical analysis at 5% significance level for comparison between the treatment and control group.

II. Evaluation of morphology

Light microscopy results showed normal morphology of duodenal and jejunal villi covered with a continuous layer of epithelium. The results are shown in figures 4-E-4 and 4-E-5. Upon a closer look under transmission electron microscope, the epithelium looked normal and covered with microvilli (figures 4-E-6 and 4-E-7). The tight junctions and adherens junctions looked comparable to those of control animals (figures 4-E-6 and 4-E-7). The results from both absorption and microscopy experiments showed that the transcellular and paracellular barrier were intact after repeated oral gavage of 1% SDS to rats for 14 days.

In conclusion, no local toxicity was noted after repeated oral gavage of 1% SDS to rats for 14 days.

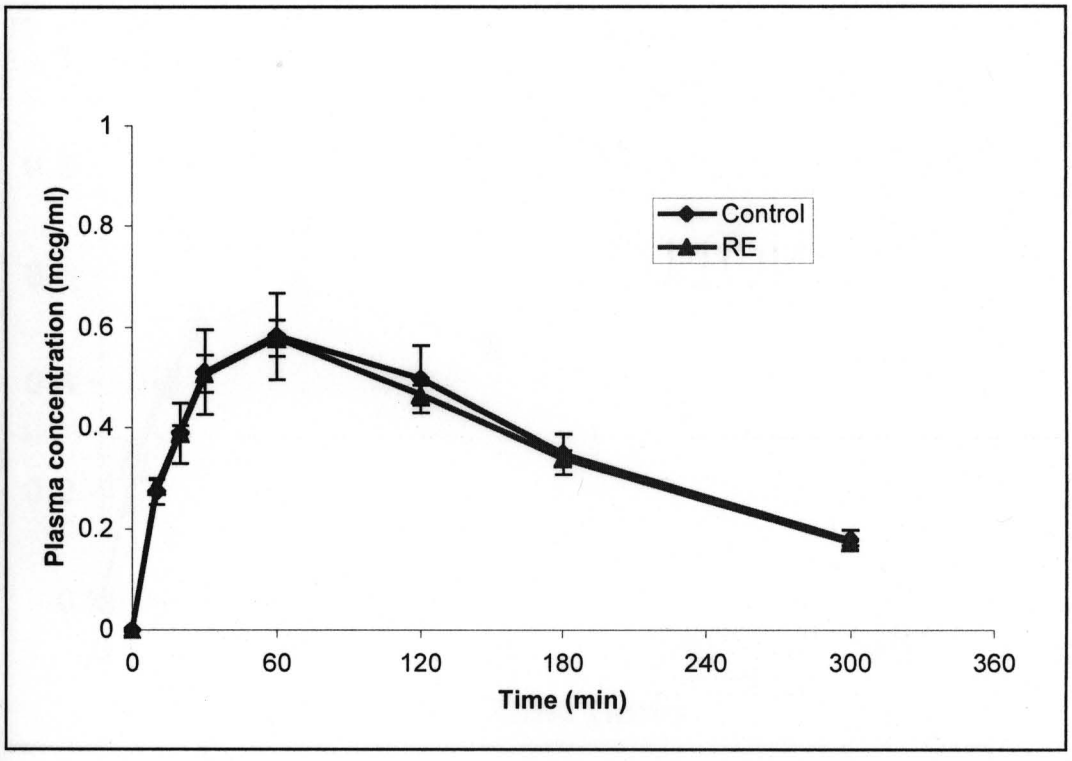

Figure 4-E-1: Oral absorption of phenol red after repeated exposure to 1% SDS.

(N= 12, Each point represents Mean ± S.E.)

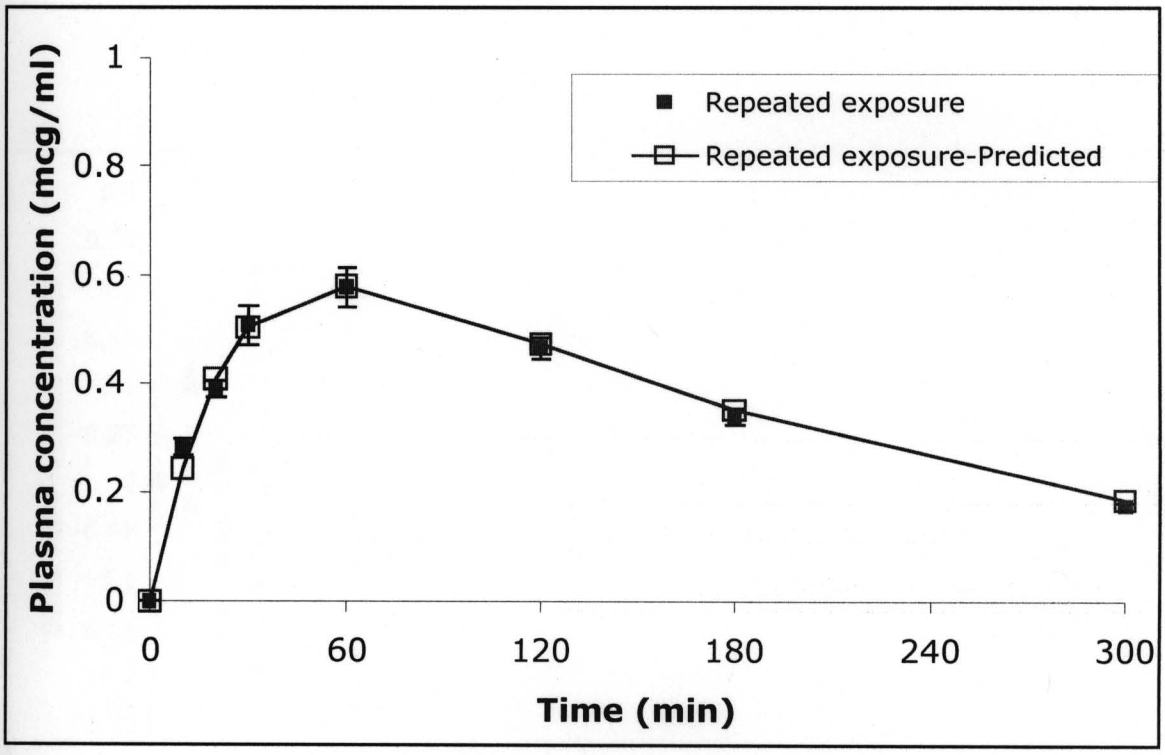

Figure 4-E-2: Observed and predicted plasma concentrations obtained by two-compartment model fitting using a step-function analysis for oral absorption of phenol red after repeated exposure to 1% SDS.

(N = 12, Each point represents Mean ± S.E.)

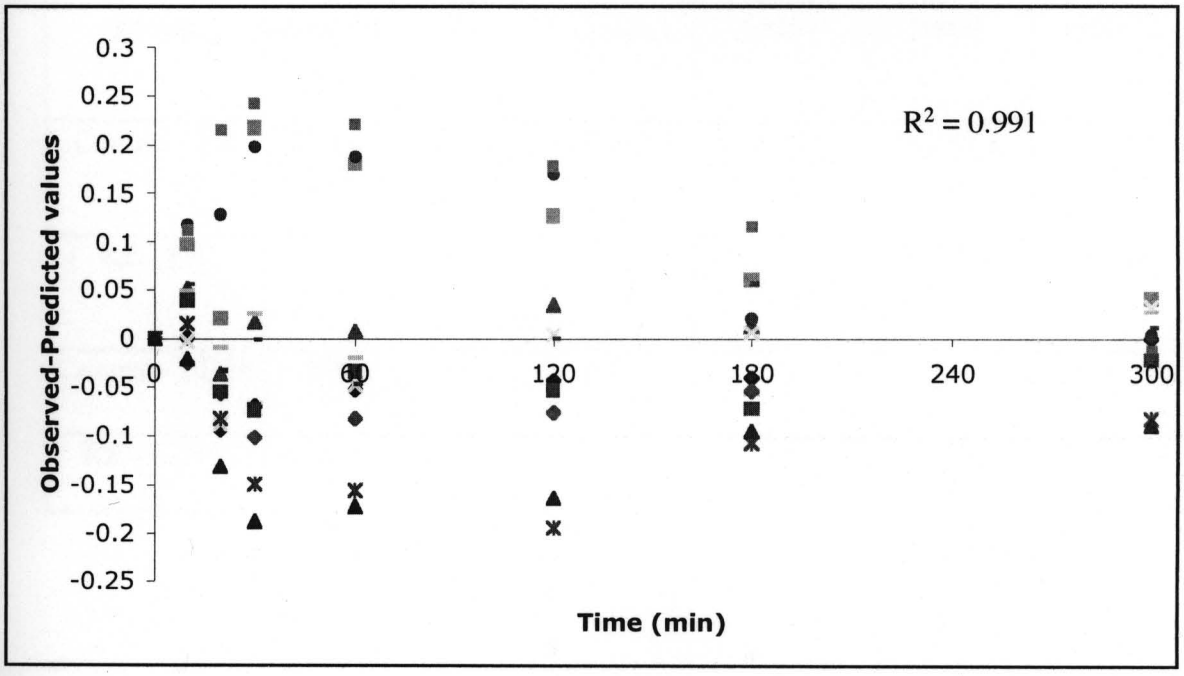

Figure 4-E-3: Plot of residuals versus time – Repeated exposure study

Treatment group	C_{max} (mcg/ml)	T_{max} (min)	AUC ($t_{0\text{-}300\ min}$)	MRT (min)	MAT (min)	K_a (min^{-1})
Control - PR	0.58 ± 0.08	60 ± 0	108.74 ± 15.72	208.88 ± 8.06	133.07 ± 8.06	0.009
RE - PR	0.56 ± 0.04	60 ± 0	104.33 ± 16.58	202.29 ± 13.58	127.2 ± 13.58	0.009
Control - FD10	0.0	0.0	0.0	0.0	0.0	-
RE - FD10	0.0	0.0	0.0	0.0	0.0	-

Table 4-E-1: Oral absorption of phenol red and FD-10 after repeated exposure to 1% SDS (C_{max} and T_{max} are the averages calculated from the observed data.

AUC was calculated using the linear trapezoidal rule from the observed data.

MRT was calculated by extrapolating the AUC to infinity. MAT is the difference between the MRT of the treatment group and that after intravenous administration.)

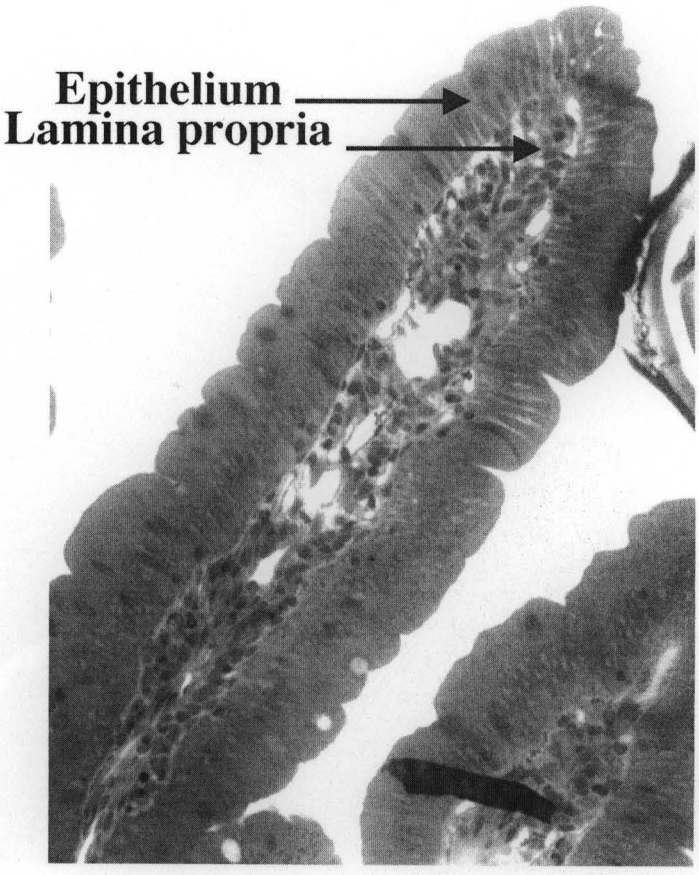

Figure 4-E-4: Light microscopy-Duodenum after repeated exposure to 1% SDS (Magnification 100X).

The villi look normal with a continuous layer of epithelial cells on the surface.

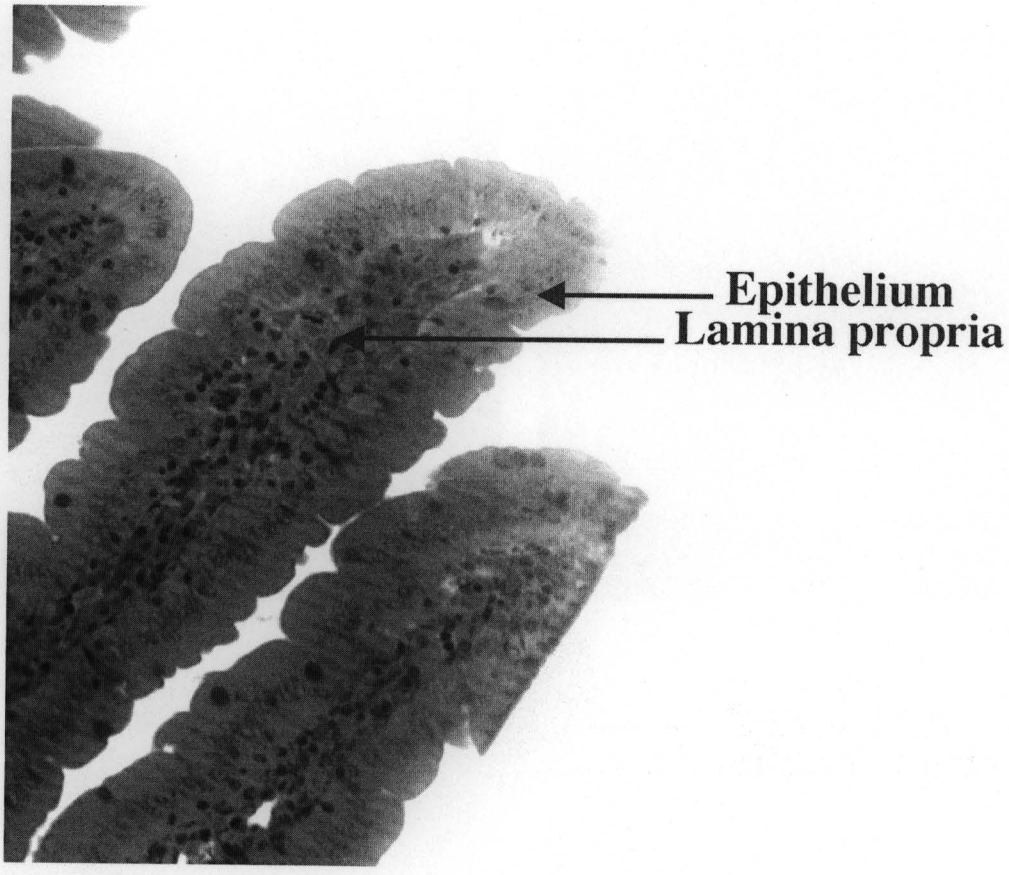

Figure 4-E-5: Light microscopy-Jejunum after repeated exposure to 1% SDS (Magnification 100 X).

The villi look normal with a continuous layer of epithelial cells on the surface.

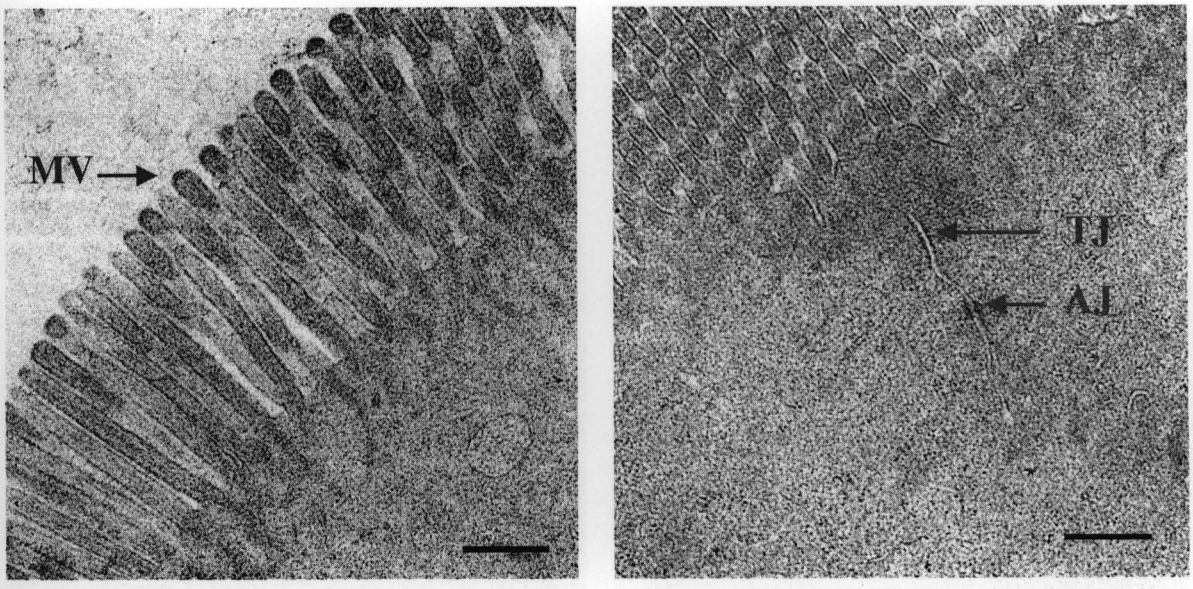

(A) (B)

Figure 4-E-6: Transmission electron microscopy-Duodenum after repeated exposure to 1% SDS.

(A) MV - microvilli and (B) TJ – tight junctions, AJ- adherens junctions.

(Magnification 1000,000 X).

The epithelial surface is covered with tall microvilli and the junctional complexes look normal.

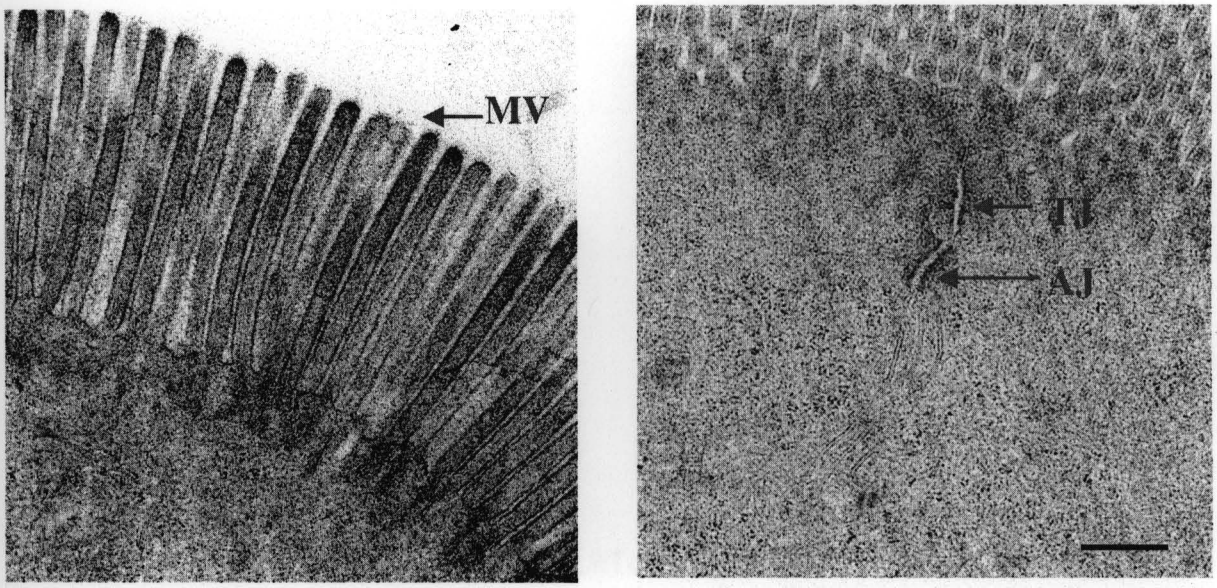

(A) (B)

Figure 4-E-7: Transmission electron microscopy-Jejunum after repeated exposure to 1% SDS. (A) MV-microvilli and (B) TJ-tight junctions, AJ-adherens junctions.

(Magnification 1000,000 X).

The epithelial surface is covered with tall microvilli and the junctional complexes look normal.

Chapter 4-F: How to Correlate Rat Data to Human Data?

An Experimental Design

In this study we showed that damage caused by 1% SDS is temporary and reversible. In order for the penetration enhancer approach to work, it is imperative to show that damage caused by them is temporary and reversible in humans as well. Extrapolating results from animals to humans is a huge challenge, especially correlating recovery after use of penetration enhancers, since it adds additional variables of epithelial cell migration and repair. In the literature, very few studies have been reported that use penetration enhancers in humans and almost none on recovery of the human gastrointestinal epithelium after damage from a penetration enhancer. Few studies have reported recovery from damage caused by alcohol using microscopy [68, 69]. Alcohol is not a conventional penetration enhancer and it is not easy to compare microscopy results from one lab to another. Since it was not practical for us to conduct studies in human volunteers, we are proposing here an experimental design that may be helpful for other researchers in correlating recovery kinetics between humans and rats.

1. Materials

Model penetration enhancer

The surfactant selected for this purpose is dioctyl sodium dodecyl sulfate (DOSS), which is used as a stool softener. It is an anionic surfactant and according to Martindale-the extra pharmacopoeia, could be used in divided doses up to 500 mg per day [159]. It is taken on a daily basis by patients with chronic constipation and cancer patients on opiates. Since it is a surfactant, it is contraindicated for co-administration with other drugs, especially mineral oil.

Permeation Markers

Phenol red is selected as a low molecular weight marker (PR, 354 D). Phenol red is a poorly absorbed marker molecule, which has been used to assess gut permeability in patients suffering from coeliac disease, patients undergoing gastrointestinal surgery and cancer patients receiving radiochemotherapy [160-162].

2. Dose calculations

DOSS- Since 500 mg per day is approved for use in humans, 5 different doses selected for humans are: 100, 200, 300, 400 and 500 mg. Using allometry method (Appendix Q) [174, 175], corresponding surfactant doses calculated for rats are as follows, 2.6 mg, 5.2 mg, 7.8 mg, 10.4 mg and 13 mg.

Markers- Phenol red dose was calculated to be 230 mg for humans (70 kg body weight) and 6 mg for rats (300 gm body weight). The dose selected for rats is same as used in this work. The corresponding human dose was calculated using allometry method.

3. Methods

I. Evaluation of absorption enhancement

Administer the markers orally to humans and rats, draw blood samples and generate plasma concentration-time profiles. Estimate pharmacokinetic parameters (C_{max}, T_{max}, AUC, MAT, MRT and K_a). This is the negative control, which will be used for comparison with treatment groups for the following experiments. Measure absorption enhancement for the marker by administering it orally to humans and rats with 5 different doses of DOSS. Estimate pharmacokinetic parameters for absorption enhancement groups (C_{max}, T_{max}, AUC,

MAT, MRT and K_a). These results are the positive controls for subsequent recovery experiments.

II. Evaluation of absorption barrier recovery

Perform absorption barrier recovery experiments in both humans and rats, by administering DOSS orally and then administering marker at different recovery times. Recovery times should be selected based on the two-compartment pharmacokinetic modeling in Section I. Draw blood samples and generate plasma concentration-time profiles. Estimate pharmacokinetic parameters (C_{max}, T_{max}, AUC, MAT, MRT and K_a) and compare with the respective negative control values to determine the recovery times for all the five doses of DOSS in humans and rats.

III. Evaluation of morphology

Perform morphology experiments in both humans and rats using light and transmission electron spectroscopy. From human volunteers, the intestinal samples can be collected using an endoscope as described in the literature [68, 69]. Evaluate morphology at different recovery times as determined in section II, after administration of all 5 doses of DOSS.

IV. Correlation between human and rat data

Correlate recovery in humans to rats by plotting human recovery times vs. rat recovery times for 5 doses of DOSS and performing regression analysis (linear or non-linear).

Using this correlation plot, it would be possible to predict recovery results in humans if recovery kinetics in rats is evaluated for any other penetration enhancer, the underlying assumption being that once local damage is caused by any penetration enhancer, the subsequent recovery mechanism remains same.

Chapter 5: Concluding Remarks and Suggested Future Work

The oral route of administration is the most preferred route due to its convenience and low cost. However, it is not always possible to incorporate drugs into oral drug delivery systems if oral absorption of drugs is limited by their poor permeation through the intestinal mucosa.

This problem is becoming more prominent as more protein and peptide drugs are becoming available with the advent of biotechnology. Moreover, the newer synthetic molecules tend to be more hydrophobic. Both these classes of drugs show poor oral bioavailability due to their low partition coefficient and low water solubility, respectively. These drugs either have to be administered parenterally as in the case of certain hormones, antibiotics, antifungal and anticancer drugs increasing the healthcare cost, or are rendered useless as happens to some new drugs in the pipeline, which are difficult to test due to their poor water solubility. The third problem associated with poor oral absorption is variability in bioavailability as in the case of phenytoin and cyclosporin, depending upon fed vs. fasted state and formulations from one manufacturer to another due to differences in the excipients used. These problems could be solved to some extent, if oral absorption of these drugs is improved, which can be achieved by modifying the drug properties or using a suitable drug delivery vehicle. In the cases where these approaches are not feasible, an alternative is to modify the mucosal membrane using penetration enhancers.

In spite of huge amount of work that has been done on penetration enhancers over the last five decades, there is a gap in understanding of recovery kinetics after their action on the mucosa. In this work, we have attempted to address the issues that will hopefully help in a better design of future studies involving use of penetration enhancers and better understanding of their effects on the mucosal membrane.

After an extensive literature search, we identified the following three areas to explore further: 1) measuring kinetics of functional recovery through absorption of markers across the mucosa, during various stages of recovery, after treatment with a penetration enhancer in an intact animal, 2) correlating functional recovery (absorption barrier recovery) with morphological recovery and 3) evaluating effects of a penetration enhancer on the mucosa after repeated use.

A review of the literature revealed that damage of the intestinal mucosa by food and some drugs is a common occurrence. We undertook the study with an assumption that if penetration enhancer-induced local damage is similar to that induced by food, then it is possible to use penetration enhancers to improve drug absorption.

We were able to show absorption barrier recovery quantitatively by measuring absorption of markers in terms of their pharmacokinetic parameters (C_{max}, T_{max}, AUC, MRT, MAT and K_a). The results showed that the local effects of penetration enhancers could be temporary and reversible. As can be imagined, the time of recovery would be dependent on the kind and concentration of penetration enhancers. With 1% SDS solution the absorption recovery took place within one hour for phenol red (a small molecular weight marker). We also found that the time for absorption barrier recovery was dependent on the molecular weight of the permeant as well. It was shorter for FD-10 (about 30 minutes with 1% SDS). A tentative conclusion can be made that the breakdown of absorption barrier by penetration enhancers would be shorter against large molecular weight toxic molecules compared to small molecular weight drug molecules. But this assumption needs to be verified by using a more sensitive analytical technique and if possible, by using the actual toxins as a large molecular weight marker. Endotoxemia in alcoholism is studied by giving an oral gavage of

alcohol and endotoxins (up to 10 mg/kg dose) in rats [176]. Similar studies could be conducted in rats by substituting alcohol with penetration enhancers and measuring subsequent uptake of endotoxins along with a model drug into the systemic circulation after an oral gavage.

In the present study, we estimated changes in K_a with respect to time by fitting the phenol red data to a two-compartment model using Matlab software, which was a useful tool as it allowed measuring functional recovery (absorption barrier recovery) temporally. Two-compartment modeling of the absorption enhancement data (Objective I) revealed that at all the three concentrations, action of SDS on the intestinal mucosa was almost instantaneous, giving rise to the highest K_a value in the beginning. The K_a reduced with time, as the mucosa recovered and it came to the control level in 1 hour, 2 hours and 4 hours for 1%, 1.5% and 2% SDS respectively. Experiments designed for absorption barrier recovery studies (Objective II) confirmed these results.

Morphological recovery evaluated using light and transmission electron microscopy with 1% SDS showed a good correlation with functional recovery. The damaging effect on the membrane was immediate (about 10 minutes) as noted both in absorption measurements of phenol red and in morphology in the duodenum. The epithelial layer was uniformly disrupted in 15 minutes after administration of SDS. Interestingly, absorption was still maximum for markers when co-administered with SDS and not after 15-minute recovery. This is probably because when a penetration enhancer and a drug are presented together to the mucosal surface, maximum drug can cross the biological barrier upon damage by the penetration enhancer due to the intimate contact between the drug and the damaged site.

30 minutes after administration of SDS, there was evidence of repair. The epithelial layer was discontinuous in few villi whereas it was continuous in others. Concurrently, the C_{max} and AUC values were smaller and T_{max} was longer for this recovery period. The effect of penetration enhancers on morphology was mainly confined to the duodenum, which accounts for 5% of the total length of the small intestine. The effect in the proximal jejunum was seen on the paracellular spaces in 15 minutes and the tissue (both the tight junctions and the microvilli) looked normal within 30 minutes. This observation was consistent with the pharmacokinetic analysis of phenol red, where absorption rate constant (K_a) was highest for the first 10 minutes and became smaller later as the gavage solution traveled down the intestinal tract.

Absorption barrier recovered in one hour for phenol red. As seen in light and electron microscopy, the villi were covered by a continuous monolayer of epithelial cells and the tight junctions between the epithelial cells had started to reform. The microvilli were intact but short as compared to the negative control specimen. It was not surprising that at this time, the absorption profile for a paracellular marker like phenol red was similar to the negative control, since the paracellular spaces were similar to those in the negative control. It should be kept in mind that the total transcellular surface area available for absorption in the duodenum at this time is probably lesser than that in the control tissue. It will be interesting to see how absorption of a transcellular marker will be affected if it is administered at this time. The results from these studies will help set guidelines for subsequent administration of other drugs for patients on a multi-drug regimen.

Finally, a repeated exposure study was performed with 1% SDS for 14 days. No permanent local effects in terms of permeability and morphology were observed in the small

intestine. However, longer exposure studies (about 2 years for chronic toxicity) are needed to establish feasibility of penetration enhancer approach.

Despite decades of work done on penetration enhancers, they have not found practical utility in formulations due to safety concerns. These concerns originated from lack of understanding in how penetration enhancers affect the barrier function of the gastrointestinal mucosa because of inability to quantify the effect. This work was attempted to fill this gap in understanding by establishing a pharmacokinetic tool to evaluate functional recovery of the gastrointestinal mucosa after use of a penetration enhancer.

Appendix A

Formulae used for statistical moment analysis (non-compartment analysis) [163]:

$$AUC = \int_0^\infty C_p \, dt$$

$$AUMC = \int_0^\infty tC_p \, dt$$

$$MRT = \frac{AUMC}{AUC}$$

$$MAT = MRT_{oral} - MRT_{IV}$$

$$\text{Bioavailability} = \frac{AUC_{oral} \text{ X } Dose_{IV}}{AUC_{IV} \text{ X } Dose_{oral}}$$

Abbreviations

AUC - Area under the curve

AUMC - Area under moment curve

MRT - Mean residence time

MAT - Mean absorption time

Appendix B

Matlab program used to estimate K_a for Control

```
clear; % PK22.m
n = 300; % Number of steps
kao = 0.009; % ka in min-1
ke = 0.0245; % k in min-1
k23 = 0.0138; % K23 in min-1
K32 = 0.01; % K32 in min-1
dt = 300/n; % Let experiment run for 300 min and calculate dt from 300 min.

for i = 1:n % Initialize arrays;
   t(i) = 0;
   kaa(i) = 0;
   Acc(i) = 0;
   Atc(i) = 0;
   Aac(i) = 0;
   Ace(i) = 0;
   Ate(i) = 0;
   Aae(i) = 0;
end;

Fc = 0.015; % Bioavailability of control.
Fe = 0.035; % Bioavailability of experiment.
Vc=25;
Aac(1) = Fc*6000; % Initial control amount at absorption site = 6000 mcg
Acc(1) = 0; % Initial control amount in central compartment = 0 mcg.
Atc(1) = 0; % Intial control amount in tissue compartment = 0 mg.
Aae(1) = Fe*6000; % Initial experiment amount at absorption site = 6000 mg
Ace(1) = 0; % Initial experiment amount in central compartment = 0 mg.
Ate(1) = 0; % Intial experiment amount in tissue compartment = 0 mg.

for i = 1:n-1; % Calculation of Aa (amount at absorption site) and A (amount in body)
   t(i+1) = t(i) + dt;
   if t(i+1) < 10;
      ka = 0.051;
   elseif t(i+1) >= 10 & t(i+1) < 20;
      ka = .020;
   elseif t(i+1) >= 20 & t(i+1) < 30;
      ka = 0.018;
   elseif t(i+1) >= 30 & t(i+1) < 45;
      ka = 0.015;
   elseif t(i+1) >= 45 & t(i+1) < 60;
      ka = 0.011;
```

```
  elseif t(i+1) >= 60 & t(i+1) < 300;
    ka = kao;
  elseif t(i+1) >= 300;
    ka = kao;
  end;
  Aac(i+1) = Aac(i) - kao*Aac(i)*dt;
  Acc(i+1) = Acc(i) + (kao*Aac(i) - (ke + K23)*Acc(i) + K32*Atc(i))*dt;
  Atc(i+1) = Atc(i) + (K23*Acc(i) - K32*Atc(i))*dt;
  Aae(i+1) = Aae(i) - ka*Aae(i)*dt;
  Ace(i+1) = Ace(i) + (ka*Aae(i) - (ke + K23)*Ace(i) + K32*Ate(i))*dt;
  Ate(i+1) = Ate(i) + (K23*Ace(i) - K32*Ate(i))*dt;
end;

Cc=Acc/Vc; %negative control
Ce=Ace/Vc; %1%SDS
Cc

plot(t,Cc,t,Ce); % Plot Plasma conc vs t and Plasma conc vs t;
axis([0,300,0,10]);
grid;
xlabel('Time(min)');
ylabel('Amount');
```

Appendix C

Matlab program used to estimate K_a for phenol red +1% SDS

```
clear; % PK22.m
n = 300; % Number of steps
kao = 0.009; % ka in min-1
ke = 0.0245; % k in min-1
K23 = 0.0138; % K23 in min-1
K32 = 0.01; % K32 in min-1
dt = 300/n; % Let experiment run for 300 min and calculate dt from 300 min.

for i = 1:n % Initialize arrays;
   t(i) = 0;
   kaa(i) = 0;
   Acc(i) = 0;
   Atc(i) = 0;
   Aac(i) = 0;
   Ace(i) = 0;
   Ate(i) = 0;
   Aae(i) = 0;
end;

Fc = 0.015; % Bioavailability of control.
Fe = 0.035; % Bioavailability of experiment.
Vc=25;
Aac(1) = Fc*6000; % Initial control amount at absorption site = 6000 mcg
Acc(1) = 0; % Initial control amount in central compartment = 0 mcg.
Atc(1) = 0; % Intial control amount in tissue compartment = 0 mcg.
Aae(1) = Fe*6000; % Initial experiment amount at absorption site = 6000 mcg
Ace(1) = 0; % Initial experiment amount in central compartment = 0 mcg.
Ate(1) = 0; % Intial experiment amount in tissue compartment = 0 mcg.

for i = 1:n-1; % Calculation of Aa (amount at absorption site) and A (amount in body)
   t(i+1) = t(i) + dt;
   if t(i+1) < 10;
      ka = 0.051;
   elseif t(i+1) >= 10 & t(i+1) < 20;
      ka = .020;
   elseif t(i+1) >= 20 & t(i+1) < 30;
      ka = 0.018;
   elseif t(i+1) >= 30 & t(i+1) < 45;
      ka = 0.015;
   elseif t(i+1) >= 45 & t(i+1) < 60;
```

```
    ka = kao;
  elseif t(i+1) >= 60 & t(i+1) < 300;
    ka = kao;
  elseif t(i+1) >= 300;
    ka = kao;
  end;
  Aac(i+1) = Aac(i) - kao*Aac(i)*dt;
  Acc(i+1) = Acc(i) + (kao*Aac(i) - (ke + K23)*Acc(i) + K32*Atc(i))*dt;
  Atc(i+1) = Atc(i) + (K23*Acc(i) - K32*Atc(i))*dt;
  Aae(i+1) = Aae(i) - ka*Aae(i)*dt;
  Ace(i+1) = Ace(i) + (ka*Aae(i) - (ke + K23)*Ace(i) + K32*Ate(i))*dt;
  Ate(i+1) = Ate(i) + (K23*Ace(i) - K32*Ate(i))*dt;
end;

Cc=Acc/Vc; %negative control
Ce=Ace/Vc; %1%SDS
Ce

plot(t,Cc,t,Ce); % Plot Plasma conc vs t and Plasma conc vs t;
axis([0,300,0,10]);
grid;
xlabel('Time(min)');
ylabel('Amount');
```

Appendix D

Matlab program used to estimate K_a for phenol red +1.5% SDS

```
clear; % PK22.m
n = 300; % Number of steps
kao = 0.009; % ka in min-1
ke = 0.0245; % k in min-1
K23 = 0.0138; % K23 in min-1
K32 = 0.01; % K32 in min-1
dt = 300/n; % Let experiment run for 300 min and calculate dt from 300 min.

for i = 1:n % Initialize arrays;
   t(i) = 0;
   kaa(i) = 0;
   Acc(i) = 0;
   Atc(i) = 0;
   Aac(i) = 0;
   Ace(i) = 0;
   Ate(i) = 0;
   Aae(i) = 0;
end;

Fc = 0.015; % Bioavailability of control.
Fe = 0.048; % Bioavailability of experiment.
Vc=25;
Aac(1) = Fc*6000; % Initial control amount at absorption site = 6000 mcg
Acc(1) = 0; % Initial control amount in central compartment = 0 mcg.
Atc(1) = 0; % Intial control amount in tissue compartment = 0 mcg.
Aae(1) = Fe*6000; % Initial experiment amount at absorption site = 6000 mcg
Ace(1) = 0; % Initial experiment amount in central compartment = 0 mcg.
Ate(1) = 0; % Intial experiment amount in tissue compartment = 0 mcg.

for i = 1:n-1; % Calculation of Aa (amount at absorption site) and A (amount in body)
   t(i+1) = t(i) + dt;
   if t(i+1) < 10;
      ka = .068;
   elseif t(i+1) >= 10 & t(i+1) < 20;
      ka = .027;
   elseif t(i+1) >= 20 & t(i+1) < 30;
      ka = 0.021;
   elseif t(i+1) >= 30 & t(i+1) < 60;
      ka = .021;
   elseif t(i+1) >= 60 & t(i+1) < 120;
```

```
    ka = .014;
  elseif t(i+1) >= 120 & t(i+1) < 300;
    ka = kao;
  elseif t(i+1) >= 300;
    ka = kao;
  end;
  Aac(i+1) = Aac(i) - kao*Aac(i)*dt;
  Acc(i+1) = Acc(i) + (kao*Aac(i) - (ke + K23)*Acc(i) + K32*Atc(i))*dt;
  Atc(i+1) = Atc(i) + (K23*Acc(i) - K32*Atc(i))*dt;
  Aae(i+1) = Aae(i) - ka*Aae(i)*dt;
  Ace(i+1) = Ace(i) + (ka*Aae(i) - (ke + K23)*Ace(i) + K32*Ate(i))*dt;
  Ate(i+1) = Ate(i) + (K23*Ace(i) - K32*Ate(i))*dt;
end;

Cc=Acc/Vc; %negative control
Ce=Ace/Vc; %1.5%SDS
Ce

plot(t,Cc,t,Ce); % Plot Plasma conc vs t and Plasma conc vs t;
axis([0,300,0,10]);
grid;
xlabel('Time(min)');
ylabel('Amount');
```

Appendix E

Matlab program used to estimate K_a for phenol red +2% SDS

```
clear; % PK22.m
n = 300; % Number of steps
kao = 0.009; % ka in min-1
ke = 0.0245; % k in min-1
K23 = 0.0138; % K23 in min-1
K32 = 0.01; % K32 in min-1
dt = 300/n; % Let experiment run for 300 min and calculate dt from 300 min.

for i = 1:n % Initialize arrays;
   t(i) = 0;
   kaa(i) = 0;
   Acc(i) = 0;
   Atc(i) = 0;
   Aac(i) = 0;
   Ace(i) = 0;
   Ate(i) = 0;
   Aae(i) = 0;
end;

Fc = 0.015; % Bioavailability of control.
Fe = 0.072; % Bioavailability of experiment.
Vc=25;
Aac(1) = Fc*6000; % Initial control amount at absorption site = 6000 mcg
Acc(1) = 0; % Initial control amount in central compartment = 0 mcg.
Atc(1) = 0; % Intial control amount in tissue compartment = 0 mcg.
Aae(1) = Fe*6000; % Initial experiment amount at absorption site = 6000 mcg
Ace(1) = 0; % Initial experiment amount in central compartment = 0 mcg.
Ate(1) = 0; % Intial experiment amount in tissue compartment = 0 mcg.

for i = 1:n-1; % Calculation of Aa (amount at absorption site) and A (amount in body)
   t(i+1) = t(i) + dt;
   if t(i+1) < 10;
      ka = 0.082;
   elseif t(i+1) >= 10 & t(i+1) < 20;
      ka = .04;
   elseif t(i+1) >= 20 & t(i+1) < 60;
      ka = 0.035;
   elseif t(i+1) >= 60 & t(i+1) < 180;
      ka = 0.032;
   elseif t(i+1) >= 180 & t(i+1) < 240;
```

```
    ka = .015;
  elseif t(i+1) >= 300;
    ka = kao;
  end;
  Aac(i+1) = Aac(i) - kao*Aac(i)*dt;
  Acc(i+1) = Acc(i) + (kao*Aac(i) - (ke + K23)*Acc(i) + K32*Atc(i))*dt;
  Atc(i+1) = Atc(i) + (K23*Acc(i) - K32*Atc(i))*dt;
  Aae(i+1) = Aae(i) - ka*Aae(i)*dt;
  Ace(i+1) = Ace(i) + (ka*Aae(i) - (ke + K23)*Ace(i) + K32*Ate(i))*dt;
  Ate(i+1) = Ate(i) + (K23*Ace(i) - K32*Ate(i))*dt;
end;

Cc=Acc/Vc; %negative control
Ce=Ace/Vc; %2%SDS
Ce

plot(t,Cc,t,Ce); % Plot Plasma conc vs t and Plasma conc vs t;
axis([0,300,0,10]);
grid;
xlabel('Time(min)');
ylabel('Amount');
```

Appendix F

Matlab program used to estimate K_a for1%SDS-15 min recovery

```
clear; % PK22.m
n = 300; % Number of steps
kao = 0.009; % ka in min-1
ke = 0.0245; % k in min-1
K23 = 0.0138; % K23 in min-1
K32 = 0.01; % K32 in min-1
dt = 300/n; % Let experiment run for 300 min and calculate dt from 300 min.

for i = 1:n % Initialize arrays;
   t(i) = 0;
   kaa(i) = 0;
   Acc(i) = 0;
   Atc(i) = 0;
   Aac(i) = 0;
   Ace(i) = 0;
   Ate(i) = 0;
   Aae(i) = 0;
end;

Fc = 0.015; % Bioavailability of control.
Fe = 0.027; % Bioavailability of experiment.
Vc=25;
Aac(1) = Fc*6000; % Initial control amount at absorption site = 6000 mcg
Acc(1) = 0; % Initial control amount in central compartment = 0 mcg.
Atc(1) = 0; % Intial control amount in tissue compartment = 0 mcg.
Aae(1) = Fe*6000; % Initial experiment amount at absorption site = 6000 mcg
Ace(1) = 0; % Initial experiment amount in central compartment = 0 mcg.
Ate(1) = 0; % Intial experiment amount in tissue compartment = 0 mcg.

for i = 1:n-1; % Calculation of Aa (amount at absorption site) and A (amount in body)
   t(i+1) = t(i) + dt;
   if t(i+1) < 10;
      ka = 0.025;
   elseif t(i+1) >= 10 & t(i+1) < 20;
      ka = .027;
   elseif t(i+1) >= 20 & t(i+1) < 30;
      ka = .017;
   elseif t(i+1) >= 30 & t(i+1) < 45;
      ka = 0.015;
```

```
   elseif t(i+1) >= 45 & t(i+1) < 60;
      ka = kao;
   elseif t(i+1) >= 60 & t(i+1) < 300;
      ka = kao;
   elseif t(i+1) >= 300;
      ka = kao;
   end;
   Aac(i+1) = Aac(i) - kao*Aac(i)*dt;
   Acc(i+1) = Acc(i) + (kao*Aac(i) - (ke + K23)*Acc(i) + K32*Atc(i))*dt;
   Atc(i+1) = Atc(i) + (K23*Acc(i) - K32*Atc(i))*dt;
   Aae(i+1) = Aae(i) - ka*Aae(i)*dt;
   Ace(i+1) = Ace(i) + (ka*Aae(i) - (ke + K23)*Ace(i) + K32*Ate(i))*dt;
   Ate(i+1) = Ate(i) + (K23*Ace(i) - K32*Ate(i))*dt;
end;

Cc=Acc/Vc; %negative control
Ce=Ace/Vc; %1% SDS-15 min
Ce

plot(t,Cc,t,Ce); % Plot Plasma conc vs t and Plasma conc vs t;
axis([0,300,0,10]);
grid;
xlabel('Time(min)');
ylabel('Amount');
```

Appendix G

Matlab program used to estimate K_a for1%SDS-30 min recovery

```
clear; % PK22.m
n = 300; % Number of steps
kao = 0.009; % ka in min-1
ke = 0.0245; % k in min-1
K23 = 0.0138; % K23 in min-1
K32 = 0.01; % K32 in min-1
dt = 300/n; % Let experiment run for 300 min and calculate dt from 300 min.

for i = 1:n % Initialize arrays;
   t(i) = 0;
   kaa(i) = 0;
   Acc(i) = 0;
   Atc(i) = 0;
   Aac(i) = 0;
   Ace(i) = 0;
   Ate(i) = 0;
   Aae(i) = 0;
end;

Fc = 0.015; % Bioavailability of control.
Fe = 0.019; % Bioavailability of experiment.
Vc=25;
Aac(1) = Fc*6000; % Initial control amount at absorption site = 6000 mcg
Acc(1) = 0; % Initial control amount in central compartment = 0 mcg.
Atc(1) = 0; % Intial control amount in tissue compartment = 0 mcg.
Aae(1) = Fe*6000; % Initial experiment amount at absorption site = 6000 mcg
Ace(1) = 0; % Initial experiment amount in central compartment = 0 mcg.
Ate(1) = 0; % Intial experiment amount in tissue compartment = 0 mcg.

for i = 1:n-1; % Calculation of Aa (amount at absorption site) and A (amount in body)
   t(i+1) = t(i) + dt;
   if t(i+1) < 10;
      ka = 0.020;
   elseif t(i+1) >= 10 & t(i+1) < 20;
      ka = .018;
   elseif t(i+1) >= 20 & t(i+1) < 30;
      ka = .018;
   elseif t(i+1) >= 30 & t(i+1) < 45;
      ka = kao;
   elseif t(i+1) >= 45 & t(i+1) < 60;
```

```
    ka = kao;
  elseif t(i+1) >= 60 & t(i+1) < 300;
    ka = kao;
  elseif t(i+1) >= 300;
    ka = kao;
  end;
  Aac(i+1) = Aac(i) - kao*Aac(i)*dt;
  Acc(i+1) = Acc(i) + (kao*Aac(i) - (ke + K23)*Acc(i) + K32*Atc(i))*dt;
  Atc(i+1) = Atc(i) + (K23*Acc(i) - K32*Atc(i))*dt;
  Aae(i+1) = Aae(i) - ka*Aae(i)*dt;
  Ace(i+1) = Ace(i) + (ka*Aae(i) - (ke + K23)*Ace(i) + K32*Ate(i))*dt;
  Ate(i+1) = Ate(i) + (K23*Ace(i) - K32*Ate(i))*dt;
end;

Cc=Acc/Vc; %negative control
Ce=Ace/Vc; %1%SDS-30 min
Ce

plot(t,Cc,t,Ce); % Plot Plasma conc vs t and Plasma conc vs t;
axis([0,300,0,10]);
grid;
xlabel('Time(min)');
ylabel('Amount');
```

Appendix H

Matlab program used to estimate K_a for1%SDS-1 hr recovery

```
clear; % PK22.m
n = 300; % Number of steps
kao = 0.009; % ka in min-1
ke = 0.0245; % k in min-1
K23 = 0.0138; % K23 in min-1
K32 = 0.01; % K32 in min-1
dt = 300/n; % Let experiment run for 300 min and calculate dt from 300 min.

for i = 1:n % Initialize arrays;
   t(i) = 0;
   kaa(i) = 0;
   Acc(i) = 0;
   Atc(i) = 0;
   Aac(i) = 0;
   Ace(i) = 0;
   Ate(i) = 0;
   Aae(i) = 0;
end;

Fc = 0.015; % Bioavailability of control.
Fe = 0.015; % Bioavailability of experiment.
Vc=25;
Aac(1) = Fc*6000; % Initial control amount at absorption site = 6000 mcg
Acc(1) = 0; % Initial control amount in central compartment = 0 mcg.
Atc(1) = 0; % Intial control amount in tissue compartment = 0 mcg.
Aae(1) = Fe*6000; % Initial experiment amount at absorption site = 6000 mcg
Ace(1) = 0; % Initial experiment amount in central compartment = 0 mcg.
Ate(1) = 0; % Intial experiment amount in tissue compartment = 0 mcg.

for i = 1:n-1; % Calculation of Aa (amount at absorption site) and A (amount in body)
   t(i+1) = t(i) + dt;
   if t(i+1) < 10;
      ka = kao;
   elseif t(i+1) >= 10 & t(i+1) < 20;
      ka = kao;
   elseif t(i+1) >= 20 & t(i+1) < 30;
      ka = kao;
   elseif t(i+1) >= 30 & t(i+1) < 45;
      ka = kao;
   elseif t(i+1) >= 45 & t(i+1) < 60;
```

```
    ka = kao;
  elseif t(i+1) >= 60 & t(i+1) < 300;
    ka = kao;
  elseif t(i+1) >= 300;
    ka = kao;
  end;
  Aac(i+1) = Aac(i) - kao*Aac(i)*dt;
  Acc(i+1) = Acc(i) + (kao*Aac(i) - (ke + K23)*Acc(i) + K32*Atc(i))*dt;
  Atc(i+1) = Atc(i) + (K23*Acc(i) - K32*Atc(i))*dt;
  Aae(i+1) = Aae(i) - ka*Aae(i)*dt;
  Ace(i+1) = Ace(i) + (ka*Aae(i) - (ke + K23)*Ace(i) + K32*Ate(i))*dt;
  Ate(i+1) = Ate(i) + (K23*Ace(i) - K32*Ate(i))*dt;
end;

Cc=Acc/Vc; %negative control
Ce=Ace/Vc; %1%SDS-60 min
Ce

plot(t,Cc,t,Ce); % Plot Plasma conc vs t and Plasma conc vs t;
axis([0,300,0,10]);
grid;
xlabel('Time(min)');
ylabel('Amount');
```

Appendix I

Matlab program used to estimate K_a for1%SDS-3 hr recovery

```
clear; % PK22.m
n = 300; % Number of steps
kao = 0.009; % ka in min-1
ke = 0.0245; % k in min-1
K23 = 0.0138; % K23 in min-1
K32 = 0.01; % K32 in min-1
dt = 300/n; % Let experiment run for 300 min and calculate dt from 300 min.

for i = 1:n % Initialize arrays;
   t(i) = 0;
   kaa(i) = 0;
   Acc(i) = 0;
   Atc(i) = 0;
   Aac(i) = 0;
   Ace(i) = 0;
   Ate(i) = 0;
   Aae(i) = 0;
end;

Fc = 0.015; % Bioavailability of control.
Fe = 0.0165; % Bioavailability of experiment.
Vc=25;
Aac(1) = Fc*6000; % Initial control amount at absorption site = 6000 mcg
Acc(1) = 0; % Initial control amount in central compartment = 0 mcg.
Atc(1) = 0; % Intial control amount in tissue compartment = 0 mcg.
Aae(1) = Fe*6000; % Initial experiment amount at absorption site = 6000 mcg
Ace(1) = 0; % Initial experiment amount in central compartment = 0 mcg.
Ate(1) = 0; % Intial experiment amount in tissue compartment = 0 mcg.

for i = 1:n-1; % Calculation of Aa (amount at absorption site) and A (amount in body)
   t(i+1) = t(i) + dt;
   if t(i+1) < 10;
      ka = kao;
   elseif t(i+1) >= 10 & t(i+1) < 20;
      ka = kao;
   elseif t(i+1) >= 20 & t(i+1) < 30;
      ka = kao;
   elseif t(i+1) >= 30 & t(i+1) < 45;
      ka = kao;
   elseif t(i+1) >= 45 & t(i+1) < 60;
```

```
    ka = kao;
  elseif t(i+1) >= 60 & t(i+1) < 300;
    ka = kao;
  elseif t(i+1) >= 300;
    ka = kao;
  end;
  Aac(i+1) = Aac(i) - kao*Aac(i)*dt;
  Acc(i+1) = Acc(i) + (kao*Aac(i) - (ke + K23)*Acc(i) + K32*Atc(i))*dt;
  Atc(i+1) = Atc(i) + (K23*Acc(i) - K32*Atc(i))*dt;
  Aae(i+1) = Aae(i) - ka*Aae(i)*dt;
  Ace(i+1) = Ace(i) + (ka*Aae(i) - (ke + K23)*Ace(i) + K32*Ate(i))*dt;
  Ate(i+1) = Ate(i) + (K23*Ace(i) - K32*Ate(i))*dt;
end;

Cc=Acc/Vc; %negative control
Ce=Ace/Vc; %1%SDS-180 min
Ce

plot(t,Cc,t,Ce); % Plot Plasma conc vs t and Plasma conc vs t;
axis([0,300,0,10]);
grid;
xlabel('Time(min)');
ylabel('Amount');
```

Appendix J

Matlab program used to estimate K_a for1.5%SDS-3 hr recovery

```
clear; % PK22.m
n = 300; % Number of steps
kao = 0.009; % ka in min-1
ke = 0.0245; % k in min-1
K23 = 0.0138; % K23 in min-1
K32 = 0.01; % K32 in min-1
dt = 300/n; % Let experiment run for 300 min and calculate dt from 300 min.

for i = 1:n % Initialize arrays;
   t(i) = 0;
   kaa(i) = 0;
   Acc(i) = 0;
   Atc(i) = 0;
   Aac(i) = 0;
   Ace(i) = 0;
   Ate(i) = 0;
   Aae(i) = 0;
end;

Fc = 0.015; % Bioavailability of control.
Fe = 0.0171; % Bioavailability of experiment.
Vc=25;
Aac(1) = Fc*6000; % Initial control amount at absorption site = 6000 mcg
Acc(1) = 0; % Initial control amount in central compartment = 0 mcg.
Atc(1) = 0; % Intial control amount in tissue compartment = 0 mcg.
Aae(1) = Fe*6000; % Initial experiment amount at absorption site = 6000 mcg
Ace(1) = 0; % Initial experiment amount in central compartment = 0 mcg.
Ate(1) = 0; % Intial experiment amount in tissue compartment = 0 mcg.

for i = 1:n-1; % Calculation of Aa (amount at absorption site) and A (amount in body)
   t(i+1) = t(i) + dt;
   if t(i+1) < 10;
      ka = kao;
   elseif t(i+1) >= 10 & t(i+1) < 20;
      ka = kao;
   elseif t(i+1) >= 20 & t(i+1) < 30;
      ka = kao;
   elseif t(i+1) >= 30 & t(i+1) < 45;
      ka = kao;
   elseif t(i+1) >= 45 & t(i+1) < 60;
```

```
    ka = kao;
  elseif t(i+1) >= 60 & t(i+1) < 300;
    ka = kao;
  elseif t(i+1) >= 300;
    ka = kao;
  end;
  Aac(i+1) = Aac(i) - kao*Aac(i)*dt;
  Acc(i+1) = Acc(i) + (kao*Aac(i) - (ke + K23)*Acc(i) + K32*Atc(i))*dt;
  Atc(i+1) = Atc(i) + (K23*Acc(i) - K32*Atc(i))*dt;
  Aae(i+1) = Aae(i) - ka*Aae(i)*dt;
  Ace(i+1) = Ace(i) + (ka*Aae(i) - (ke + K23)*Ace(i) + K32*Ate(i))*dt;
  Ate(i+1) = Ate(i) + (K23*Ace(i) - K32*Ate(i))*dt;
end;

Cc=Acc/Vc; %negative control
Ce=Ace/Vc; %1.5%SDS-180 min
Ce

plot(t,Cc,t,Ce); % Plot Plasma conc vs t and Plasma conc vs t;
axis([0,300,0,10]);
grid;
xlabel('Time(min)');
ylabel('Amount');
```

Appendix K

Matlab program used to estimate K_a for 2%SDS-3 hr recovery

```
clear; % PK22.m
n = 300; % Number of steps
kao = 0.009; % ka in min-1
ke = 0.0245; % k in min-1
K23 = 0.0138; % K23 in min-1
K32 = 0.01; % K32 in min-1
dt = 300/n; % Let experiment run for 300 min and calculate dt from 300 min.

for i = 1:n % Initialize arrays;
   t(i) = 0;
   kaa(i) = 0;
   Acc(i) = 0;
   Atc(i) = 0;
   Aac(i) = 0;
   Ace(i) = 0;
   Ate(i) = 0;
   Aae(i) = 0;
end;

Fc = 0.015; % Bioavailability of control.
Fe = 0.023; % Bioavailability of experiment.
Vc=25;
Aac(1) = Fc*6000; % Initial control amount at absorption site = 6000 mcg
Acc(1) = 0; % Initial control amount in central compartment = 0 mcg.
Atc(1) = 0; % Intial control amount in tissue compartment = 0 mcg.
Aae(1) = Fe*6000; % Initial experiment amount at absorption site = 6000 mcg
Ace(1) = 0; % Initial experiment amount in central compartment = 0 mcg.
Ate(1) = 0; % Intial experiment amount in tissue compartment = 0 mcg.

for i = 1:n-1; % Calculation of Aa (amount at absorption site) and A (amount in body)
   t(i+1) = t(i) + dt;
   if t(i+1) < 10;
      ka = 0.0122;
   elseif t(i+1) >= 10 & t(i+1) < 30;
      ka = .014;
   elseif t(i+1) >= 30 & t(i+1) < 60;
      ka = 0.011;
   elseif t(i+1) >= 60 & t(i+1) < 300;
      ka = kao;
   elseif t(i+1) >= 300;
```

```
    ka = kao;
  end;
  Aac(i+1) = Aac(i) - kao*Aac(i)*dt;
  Acc(i+1) = Acc(i) + (kao*Aac(i) - (ke + K23)*Acc(i) + K32*Atc(i))*dt;
  Atc(i+1) = Atc(i) + (K23*Acc(i) - K32*Atc(i))*dt;
  Aae(i+1) = Aae(i) - ka*Aae(i)*dt;
  Ace(i+1) = Ace(i) + (ka*Aae(i) - (ke + K23)*Ace(i) + K32*Ate(i))*dt;
  Ate(i+1) = Ate(i) + (K23*Ace(i) - K32*Ate(i))*dt;
end;

Cc=Acc/Vc; %negative control
Ce=Ace/Vc; %2%SDS-180 min
Ce

plot(t,Cc,t,Ce); % Plot Plasma conc vs t and Plasma conc vs t;
axis([0,300,0,10]);
grid;
xlabel('Time(min)');
ylabel('Amount');
```

Appendix L

Matlab program used to estimate K_a for1%SDS-repeated exposure

```
clear; % PK22.m
n = 300; % Number of steps
kao = 0.009; % ka in min-1
ke = 0.0245; % k in min-1
K23 = 0.0138; % K23 in min-1
K32 = 0.01; % K32 in min-1
dt = 300/n; % Let experiment run for 300 min and calculate dt from 300 min.

for i = 1:n % Initialize arrays;
   t(i) = 0;
   kaa(i) = 0;
   Acc(i) = 0;
   Atc(i) = 0;
   Aac(i) = 0;
   Ace(i) = 0;
   Ate(i) = 0;
   Aae(i) = 0;
end;

Fc = 0.015; % Bioavailability of control.
Fe = 0.015; % Bioavailability of experiment.
Vc=25;
Aac(1) = Fc*6000; % Initial control amount at absorption site = 6000 mcg
Acc(1) = 0; % Initial control amount in central compartment = 0 mcg.
Atc(1) = 0; % Intial control amount in tissue compartment = 0 mcg.
Aae(1) = Fe*6000; % Initial experiment amount at absorption site = 6000 mcg
Ace(1) = 0; % Initial experiment amount in central compartment = 0 mcg.
Ate(1) = 0; % Intial experiment amount in tissue compartment = 0 mcg.

for i = 1:n-1; % Calculation of Aa (amount at absorption site) and A (amount in body)
   t(i+1) = t(i) + dt;
   if t(i+1) < 10;
      ka = kao;
   elseif t(i+1) >= 10 & t(i+1) < 20;
      ka = kao;
   elseif t(i+1) >= 20 & t(i+1) < 30;
      ka = kao;
   elseif t(i+1) >= 30 & t(i+1) < 45;
      ka = kao;
   elseif t(i+1) >= 45 & t(i+1) < 60;
```

```
    ka = kao;
  elseif t(i+1) >= 60 & t(i+1) < 300;
    ka = kao;
  elseif t(i+1) >= 300;
    ka = kao;
  end;
  Aac(i+1) = Aac(i) - kao*Aac(i)*dt;
  Acc(i+1) = Acc(i) + (kao*Aac(i) - (ke + K23)*Acc(i) + K32*Atc(i))*dt;
  Atc(i+1) = Atc(i) + (K23*Acc(i) - K32*Atc(i))*dt;
  Aae(i+1) = Aae(i) - ka*Aae(i)*dt;
  Ace(i+1) = Ace(i) + (ka*Aae(i) - (ke + K23)*Ace(i) + K32*Ate(i))*dt;
  Ate(i+1) = Ate(i) + (K23*Ace(i) - K32*Ate(i))*dt;
end;

Cc=Acc/Vc; %negative control
Ce=Ace/Vc; %repeated exposure
Ce

plot(t,Cc,t,Ce); % Plot Plasma conc vs t and Plasma conc vs t;
axis([0,300,0,10]);
grid;
xlabel('Time(min)');
ylabel('Amount');
```

Appendix M

Formulae used to test Goodness-of-fit statistics

$$R^2 = \frac{SSR}{SST} = 1 - \frac{SSE}{SST} \qquad \text{(Since SST=SSR+SSE)}$$

Where SST = Total sum of squares
SSR = Sum of squares of regression
SSE = Sum of squares due to error

$$SSE = \sum_{i=1}^{n} w_i (y_i - \hat{y}_i)^2$$

Where, $w_i = 1/s^2$ (s^2 = sample variance)

$\hat{y}_i$ = predicted value

$$SSR = \sum_{i=1}^{n} w_i (\hat{y}_i - \bar{y})^2$$

Where, $\bar{y}$ = mean value

$$SST = \sum_{i=1}^{n} w_i (y_i - \bar{y})^2$$

Appendix N

Matlab program used to optimize Ka for phenol red when co-administered with 1% SDS using an exponential function

```
clear; % SDS3b.m for 1% SDS
n = 3100; % Number of integration steps
ke = 0.0245; % ke in min-1
k12 = 0.0138; % k12 in min-1
k21 = 0.01; % k21 in min-1
Dose = 6000; %Dose in micrograms
Vc = 25; % V of the central compartment in mL
dt = 310/n; % Let experiment run for 300 min and calculate dt from 300 min.
F = 0.035; % Bioavailability after oral dose with 1% SDS
b = 0.0775;

for i = 1:n % Initialize arrays;
   t(i) = 0;
   ka(i) = 0;
   Aa(i) = 0;
   Ac(i) = 0;
   C(i) = 0;
   At(i) = 0;
end;

Aa(1) = F*Dose; % Initial amount at absorption site.
Ac(1) = 0; % Initial amount in central compartment = 0 mcg.
At(1) = 0; % Intial amount in tissue compartment = 0 mcg.

tt(1) = 10;
tt(2) = 20;
tt(3) = 30;
tt(4) = 60;
tt(5) = 120;
tt(6) = 180;
tt(7) = 300;

Ce(1) = 2.731;
Ce(2) = 2.587;
Ce(3) = 2.336;
Ce(4) = 1.551;
Ce(5) = 0.818;
Ce(6) = 0.548;
Ce(7) = 0.286;
```

```
m = 100;
for i = 1:m
   a(i) = 0;
   b(i) = 0;
end;

for i = 1:m;
   for j = 1:m;
      for k=1:7;
         Csave(i,j,k) = 0;
      end;
   end;
end;



da = .001/m;
a(1) = 0;
ka(1) = 0.009 + a(1); % initial ka value

db = 4/m;
b(1) = 0.000001;

for k = 1:m-1;
k
   b(k+1) = b(k) + db;
   for j = 1:m-1;

      a(j+1) = a(j) + da;
      for i = 1:n-1; % Calculation of Aa (amount at absorption site) and A (amount in body)
         t(i+1) = t(i) + dt;
         ka(i+1) = 0.009 + 0.042*(exp(-a(j)*t(i)^b(k)));
         Aa(i+1) = Aa(i) - ka(i+1)*Aa(i)*dt;
         Ac(i+1) = Ac(i) + (ka(i+1)*Aa(i) - (ke + k12)*Ac(i) + k21*At(i))*dt;
         C(i+1) = Ac(i+1)/Vc; % In micrograms/mL
         At(i+1) = At(i) + (k12*Ac(i) - k21*At(i))*dt;
      end;

      for i = 1:n;
         if t(i) == t(101);
            Csave(k,j,1) = C(i);
         elseif t(i) == t(201);
            Csave(k,j,2) = C(i);
         elseif t(i) == t(301);
```

```
            Csave(k,j,3) = C(i);
         elseif t(i) == t(601);
            Csave(k,j,4) = C(i);
         elseif t(i) == t(1201);
            Csave(k,j,5) = C(i);
         elseif t(i) == t(1801);
            Csave(k,j,6) = C(i);
         elseif t(i) == t(3001);
            Csave(k,j,7) = C(i);
         end;
      end;

   end;

end;




for i = 1:m;
   for j = 1:m;
      er(i,j) = (Csave(i,j,1) - Ce(1))^2 + (Csave(i,j,2) - Ce(2))^2 + (Csave(i,j,3) - Ce(3))^2 +
(Csave(i,j,4) - Ce(4))^2 + (Csave(i,j,5) - Ce(5))^2 + (Csave(i,j,6) - Ce(6))^2 + (Csave(i,j,7) -
Ce(7))^2;
   end;
end;

ERR = 1000;

for i = 1:m;
   for j = 1:m;
      if er(i,j) < ERR;
         ERR = er(i,j);
         aopt = a(j);
         bopt = b(i);
         iopt = i;
         jopt = j;
         ermin = er(i,j);
      end;
   end;
end;

ermin
aopt
```

```
iopt

for i = 1:7;
   Copt(i) = Csave(iopt,jopt,i);
end;

semilogy(tt,Copt, tt, Ce); % Plot Copt vs t and Ce vs t;
axis([0,300,.1,10]);
grid;
xlabel('Time(min)');
ylabel('C ug/mL');
```

Appendix O

Matlab program used to optimize Ka for phenol red when co-administered with 1.5% SDS using an exponential function

```
clear; % SDS4b.m for 1.5% SDS
TIC
n = 3100; % Number of integration steps
ke = 0.0245; % ke in min-1
k12 = 0.0138; % k12 in min-1
k21 = 0.01; % k21 in min-1
Dose = 6000; %Dose in micrograms
Vc = 25; % V of the central compartment in mL
dt = 310/n; % Let experiment run for 300 min and calculate dt from 300 min.
F = 0.048; % Bioavailability after oral dose with 1% SDS

for i = 1:n % Initialize arrays;
   t(i) = 0;
   ka(i) = 0;
   Aa(i) = 0;
   Ac(i) = 0;
   C(i) = 0;
   At(i) = 0;
end;

Aa(1) = F*Dose; % Initial amount at absorption site.
Ac(1) = 0; % Initial amount in central compartment = 0 mcg.
At(1) = 0; % Intial amount in tissue compartment = 0 mcg.

tt(1) = 10;
tt(2) = 20;
tt(3) = 30;
tt(4) = 60;
tt(5) = 120;
tt(6) = 180;
tt(7) = 300;

Ce(1) = 4.698;
Ce(2) = 4.354;
Ce(3) = 3.675;
Ce(4) = 2.577;
Ce(5) = 1.154;
Ce(6) = 0.722;
Ce(7) = 0.356;
```

```
m = 100;
for i = 1:m
   a(i) = 0;
   b(i) = 0;
end;

for i = 1:m;
   for j = 1:m;
      for k=1:7;
         Csave(i,j,k) = 0;
      end;
   end;
end;



da = .001/m;
a(1) = 0;
ka(1) = 0.068; % initial ka value

db = 4/m;
b(1) = 0.000001;

for k = 1:m-1;
k
   b(k+1) = b(k) + db;
   for j = 1:m-1;

      a(j+1) = a(j) + da;
      for i = 1:n-1; % Calculation of Aa (amount at absorption site) and A (amount in body)
         t(i+1) = t(i) + dt;
         ka(i+1) = 0.009 + 0.059*(exp(-a(j)*t(i)^b(k)));
         Aa(i+1) = Aa(i) - ka(i+1)*Aa(i)*dt;
         Ac(i+1) = Ac(i) + (ka(i+1)*Aa(i) - (ke + k12)*Ac(i) + k21*At(i))*dt;
         C(i+1) = Ac(i+1)/Vc; % In micrograms/mL
         At(i+1) = At(i) + (k12*Ac(i) - k21*At(i))*dt;
      end;

      for i = 1:n;
         if t(i) == t(101);
            Csave(k,j,1) = C(i);
         elseif t(i) == t(201);
            Csave(k,j,2) = C(i);
         elseif t(i) == t(301);
```

```
            Csave(k,j,3) = C(i);
         elseif t(i) == t(601);
            Csave(k,j,4) = C(i);
         elseif t(i) == t(1201);
            Csave(k,j,5) = C(i);
         elseif t(i) == t(1801);
            Csave(k,j,6) = C(i);
         elseif t(i) == t(3001);
            Csave(k,j,7) = C(i);
         end;
      end;

   end;

end;




for i = 1:m;
   for j = 1:m;
      er(i,j) = (Csave(i,j,1) - Ce(1))^2 + (Csave(i,j,2) - Ce(2))^2 + (Csave(i,j,3) - Ce(3))^2 +
(Csave(i,j,4) - Ce(4))^2 + (Csave(i,j,5) - Ce(5))^2 + (Csave(i,j,6) - Ce(6))^2 + (Csave(i,j,7) -
Ce(7))^2;
   end;
end;

ERR = 1000;

for i = 1:m;
   for j = 1:m;
      if er(i,j) < ERR;
         ERR = er(i,j);
         aopt = a(j);
         bopt = b(i);
         iopt = i;
         jopt = j;
         ermin = er(i,j);
      end;
   end;
end;

ermin
aopt
```

```
iopt

for i = 1:7;
   Copt(i) = Csave(iopt,jopt,i);
end;

semilogy(tt,Copt, tt, Ce); % Plot Copt vs t and Ce vs t;
axis([0,300,.1,10]);
grid;
xlabel('Time(min)');
ylabel('C ug/mL');

TOC
```

Appendix P

Matlab program used to optimize Ka for phenol red when co-administered with 2% SDS using an exponential function

```
clear; % SDS5b.m for 2% SDS
TIC
n = 3100; % Number of integration steps
ke = 0.0245; % ke in min-1
k12 = 0.0138; % k12 in min-1
k21 = 0.01; % k21 in min-1
Dose = 6000; %Dose in micrograms
Vc = 25; % V of the central compartment in mL
dt = 310/n; % Let experiment run for 300 min and calculate dt from 300 min.
F = 0.072; % Bioavailability after oral dose with 1% SDS

for i = 1:n % Initialize arrays;
   t(i) = 0;
   ka(i) = 0;
   Aa(i) = 0;
   Ac(i) = 0;
   C(i) = 0;
   At(i) = 0;
end;

Aa(1) = F*Dose; % Initial amount at absorption site.
Ac(1) = 0; % Initial amount in central compartment = 0 mcg.
At(1) = 0; % Intial amount in tissue compartment = 0 mcg.

tt(1) = 10;
tt(2) = 20;
tt(3) = 30;
tt(4) = 60;
tt(5) = 120;
tt(6) = 180;
tt(7) = 300;

Ce(1) = 7.857;
Ce(2) = 7.444;
Ce(3) = 6.347;
Ce(4) = 4.305;
Ce(5) = 1.534;
Ce(6) = 0.839;
```

```
Ce(7) = 0.401;

m = 100;
for i = 1:m
   a(i) = 0;
   b(i) = 0;
end;

for i = 1:m;
   for j = 1:m;
      for k=1:7;
         Csave(i,j,k) = 0;
      end;
   end;
end;


da = 8/m;
a(1) = 0;
ka(1) = 0.009 + a(1); % initial ka value

db = 2/m;
b(1) = 0.000001;

for k = 1:m-1;
k
   b(k+1) = b(k) + db;
   for j = 1:m-1;

      a(j+1) = a(j) + da;
      for i = 1:n-1; % Calculation of Aa (amount at absorption site) and A (amount in body)
         t(i+1) = t(i) + dt;
         ka(i+1) = 0.009 + 0.073*(exp(-a(j)*t(i)^b(k)));
         Aa(i+1) = Aa(i) - ka(i+1)*Aa(i)*dt;
         Ac(i+1) = Ac(i) + (ka(i+1)*Aa(i) - (ke + k12)*Ac(i) + k21*At(i))*dt;
         C(i+1) = Ac(i+1)/Vc; % In micrograms/mL
         At(i+1) = At(i) + (k12*Ac(i) - k21*At(i))*dt;
      end;

      for i = 1:n;
         if t(i) == t(101);
            Csave(k,j,1) = C(i);
         elseif t(i) == t(201);
            Csave(k,j,2) = C(i);
         elseif t(i) == t(301);
```

```
            Csave(k,j,3) = C(i);
         elseif t(i) == t(601);
            Csave(k,j,4) = C(i);
         elseif t(i) == t(1201);
            Csave(k,j,5) = C(i);
         elseif t(i) == t(1801);
            Csave(k,j,6) = C(i);
         elseif t(i) == t(3001);
            Csave(k,j,7) = C(i);
         end;
      end;

   end;

end;


for i = 1:m;
   for j = 1:m;
      er(i,j) = (Csave(i,j,1) - Ce(1))^2 + (Csave(i,j,2) - Ce(2))^2 + (Csave(i,j,3) - Ce(3))^2 +
(Csave(i,j,4) - Ce(4))^2 + (Csave(i,j,5) - Ce(5))^2 + (Csave(i,j,6) - Ce(6))^2 + (Csave(i,j,7) -
Ce(7))^2;
   end;
end;

ERR = 1000;

for i = 1:m;
   for j = 1:m;
      if er(i,j) < ERR;
         ERR = er(i,j);
         aopt = a(j);
         bopt = b(i);
         iopt = i;
         jopt = j;
         ermin = er(i,j);
      end;
   end;
end;

ermin
aopt
iopt

for i = 1:7;
```

```
   Copt(i) = Csave(iopt,jopt,i);
end;

semilogy(tt,Copt, tt, Ce); % Plot Copt vs t and Ce vs t;
axis([0,300,.1,10]);
grid;
xlabel('Time(min)');
ylabel('C ug/mL');
TOC
```

Appendix Q

Dose calculations by Allometry [174, 175]:

$$\frac{\text{Dose (Rat)}}{\text{Dose (Human)}} = \frac{(\text{Rat body weight})^{0.67}}{(\text{Human body weight})^{0.67}}$$

References

[1] Lennernas H and Abrahamsson B. The use of biopharmaceutic classification of drugs in drug discovery and development: current status and future extension. *J.Pharm.Pharmacol.* 57: 3: 273-285, 2005.

[2] Robert Carola, John P. Harley and Charles R. Noback. The Digestive System. In: *Human Anatomy*, edited by Kathi M. Prancan and Holly Gordon. NY: McGraw-Hill Inc., 1992, chapt. Chapter 23, p. 582-620.

[3] Summers R. In: *Gastroenterology and Hepatology: Small Intestine*, edited by Mark Feldman (series editor), Lawrence R. Schiller. Current Medicine Inc.1997.

[4] Kent M. Van De Graaff and Stuart Ira Fox. Digestive System. In: *Concepts of Human Anatomy and Physiology*, edited by Collin H. Wheatley. Dubuque, IA: Wm. C. Brown Communications Inc., 1995, chapt. Chapter 26, p. 764-810.

[5] Elaine N. Marieb. The Digestive System. In: *Human Anatomy and Physiology*, edited by Mary Ann Murray. San Fransisco, CA: Pearson Education Inc., 2004, chapt. Chapter 23, p. 881-940.

[6] Carr K.E. and Toner P.G. Morphology of the Intestinal Mucosa. In: *Pharmacology of Intestinal Permeation*, edited by Csaky T.Z. Berline: Springer-Verlag Inc., 1984, p. 1-50.

[7] Muranishi S and Yamamoto A. Mechanisms of Absorption Enhancement Through Gastrointestinal Epithelium. In: *Drug Absorption Enhancement: Concepts, Possibilities, Limitations and Trends*, edited by deBoer AG. Switzerland: Harwood Academic Publishers, 1994, p. 67-99.

[8] David T. Lindsay. Digestive System. In: *Functional Human Anatomy*, edited by James M. Smith. St. Louis, MO: Mosby-Year Book Inc., 1996, chapt. Chapter 21, p. 691-729.

[9] Baumgart DC and Dignass AU. Intestinal barrier function. *Curr.Opin.Clin.Nutr.Metab.Care,* 5: 6: 685-694, 2002.

[10] Clarke RM. Progress in measuring epithelial turnover in the villus of the small intestine. *Digestion* 8: 2: 161-175, 1973.

[11] Creamer B. The turnover of the epithelium of the small intestine. *Br.Med.Bull.* 23: 3: 226-230, 1967.

[12] Eastwood GL. Gastrointestinal epithelial renewal. *Gastroenterology* 72: 5 Pt 1: 962-975, 1977.

[13] Lipkin M. Proliferation and differentiation of gastrointestinal cells. *Physiol.Rev.* 53: 4: 891-915, 1973.

[14] Potten CS. Cell cycles in cell hierarchies. *Int.J.Radiat.Biol.Relat.Stud.Phys.Chem.Med.* 49: 2: 257-278, 1986.

[15] Weinstein WM. Epithelial cell renewal of the small intestinal mucosa. *Med.Clin.North Am.* 58: 6: 1375-1386, 1974.

[16] Wong WM and Wright NA. Cell proliferation in gastrointestinal mucosa. *J.Clin.Pathol.* 52: 5: 321-333, 1999.

[17] Powell DW. Barrier function of epithelia. *Am.J.Physiol.* 241: 4: G275-88, 1981.

[18] Daugherty AL and Mrsny RJ. Regulation of the intestinal epithelial paracellular barrier. *Pharm.Sci.Technol.Today* 2: 7: 281-287, 1999.

[19] Mitic LL and Anderson JM. Molecular architecture of tight junctions. *Annu.Rev.Physiol.* 60: 121-142, 1998.

[20] Lutz KL and Siahaan TJ. Molecular structure of the apical junction complex and its contribution to the paracellular barrier. *J.Pharm.Sci.* 86: 9: 977-984, 1997.

[21] Mackay M, Williamson I and Hastewell J. Cell Biology of Epithelia. *Adv.Drug Deliv.Rev.* 7: 3: 313-338, 1991.

[22] Salama NN, Eddington ND and Fasano A. Tight junction modulation and its relationship to drug delivery. *Adv.Drug Deliv.Rev.* 58: 1: 15-28, 2006.

[23] Fordtran JS, Rector FC,Jr and Carter NW. The mechanisms of sodium absorption in the human small intestine. *J.Clin.Invest.* 47: 4: 884-900, 1968.

[24] Hudspeth AJ. Establishment of tight junctions between epithelial cells. *Proc.Natl.Acad.Sci.U.S.A.* 72: 7: 2711-2713, 1975.

[25] Parkin J and Cohen B. An overview of the immune system. *Lancet* 357: 9270: 1777-1789, 2001.

[26] Kraehenbuhl JP, Pringault E and Neutra MR. Intestinal epithelia and barrier functions. *Aliment.Pharmacol.Ther.* 11: 3-8, 1997.

[27] Csaky T.Z. Intestinal Permeation and Permeability: an Overview. In: *Pharmacology of Intestinal Permeation*, edited by Csaky T.Z. Berline: Springer-Verlag Inc., 1984, p. 51-59.

[28] Allen A, Flemstrom G, Garner A and Kivilaakso E. Gastroduodenal mucosal protection. *Physiol.Rev.* 73: 4: 823-857, 1993.

[29] Engel E, Guth PH, Nishizaki Y and Kaunitz JD. Barrier function of the gastric mucus gel. *Am.J.Physiol.* 269: 6 Pt 1: G994-9, 1995.

[30] Goke M and Podolsky DK. Regulation of the mucosal epithelial barrier. *Baillieres Clin.Gastroenterol.* 10: 3: 393-405, 1996.

[31] Trier J.S. The surface coat of the gastrointestinal epithelial cells. *Gastroenterology* 56: 618-624, 1969.

[32] Meyer-Kirchrath J and Schror K. Cyclooxygenase-2 inhibition and side-effects of non-steroidal anti-inflammatory drugs in the gastrointestinal tract. *Curr.Med.Chem.* 7: 11: 1121-1129, 2000.

[33] Russell RI. Protective effects of the prostaglandins on the gastric mucosa. *Am.J.Med.* 81: 2A: 2-4, 1986.

[34] Kokoska ER, Wolff AB, Smith GS and Miller TA. Epidermal growth factor-induced cytoprotection in human intestinal cells involves intracellular calcium signaling. *J.Surg.Res.* 88: 2: 97-103, 2000.

[35] Rao R and Porreca F. Epidermal growth factor protects mouse ileal mucosa from Triton X-100-induced injury. *Eur.J.Pharmacol.* 303: 3: 209-212, 1996.

[36] Montaner B, Asbert M and Perez-Tomas R. Immunolocalization of transforming growth factor-alpha and epidermal growth factor receptor in the rat gastroduodenal area. *Dig.Dis.Sci.* 44: 7: 1408-1416, 1999.

[37] Egger B, Carey HV, Procaccino F, Chai NN, Sandgren EP, Lakshmanan J, Buslon VS, French SW, Buchler MW and Eysselein VE. Reduced susceptibility of mice overexpressing transforming growth factor alpha to dextran sodium sulphate induced colitis. *Gut* 43: 1: 64-70, 1998.

[38] Steiling H and Werner S. Fibroblast growth factors: key players in epithelial morphogenesis, repair and cytoprotection. *Curr.Opin.Biotechnol.* 14: 5: 533-537, 2003.

[39] Choda Y, Morimoto Y, Miyaso H, Shinoura S, Saito S, Yagi T, Iwagaki H and Tanaka N. Failure of the gut barrier system enhances liver injury in rats: protection of hepatocytes by gut-derived hepatocyte growth factor. *Eur.J.Gastroenterol.Hepatol.* 16: 10: 1017-1025, 2004.

[40] Thim L. Trefoil peptides: from structure to function. *Cell Mol.Life Sci.* 53: 11-12: 888-903, 1997.

[41] Andoh A, Kinoshita K, Rosenberg I and Podolsky DK. Intestinal trefoil factor induces decay-accelerating factor expression and enhances the protective activities

against complement activation in intestinal epithelial cells. *J.Immunol.* 167: 7: 3887-3893, 2001.

[42] Wilson AJ and Gibson PR. Epithelial migration in the colon: filling in the gaps. *Clin.Sci.(Lond)* 93: 2: 97-108, 1997.

[43] Beck PL, Wong JF, Li Y, Swaminathan S, Xavier RJ, Devaney KL and Podolsky DK. Chemotherapy- and radiotherapy-induced intestinal damage is regulated by intestinal trefoil factor. *Gastroenterology* 126: 3: 796-808, 2004.

[44] Ayabe T, Satchell DP, Wilson CL, Parks WC, Selsted ME and Ouellette AJ. Secretion of microbicidal alpha-defensins by intestinal Paneth cells in response to bacteria. *Nat.Immunol.* 1: 2: 113-118, 2000.

[45] Ganz T. Paneth cells--guardians of the gut cell hatchery. *Nat.Immunol.* 1: 2: 99-100, 2000.

[46] Fagarasan S and Honjo T. Regulation of IgA synthesis at mucosal surfaces. *Curr.Opin.Immunol.* 16: 3: 277-283, 2004.

[47] Golby SJ and Spencer J. Where do IgA plasma cells in the gut come from? *Gut* 51: 2: 150-151, 2002.

[48] Thompson JS. The intestinal response to critical illness. *Am.J.Gastroenterol.* 90: 2: 190-200, 1995.

[49] Gayle JM, Blikslager AT and Jones SL. Role of neutrophils in intestinal mucosal injury. *J.Am.Vet.Med.Assoc.* 217: 4: 498-500, 2000.

[50] Okamoto R and Watanabe M. Cellular and molecular mechanisms of the epithelial repair in IBD. *Dig.Dis.Sci.* 50 Suppl 1: S34-8, 2005.

[51] Gibson Peter R. Apoptosis or necrosis - colonic epithelial cell survival. *Novartis Foundation symposium* 263: 133-150, 2004.

[52] Banan A, Fields JZ, Decker H, Zhang Y and Keshavarzian A. Nitric oxide and its metabolites mediate ethanol-induced microtubule disruption and intestinal barrier dysfunction. *J.Pharmacol.Exp.Ther.* 294: 3: 997-1008, 2000.

[53] Alverdy J, Zaborina O and Wu L. The impact of stress and nutrition on bacterial-host interactions at the intestinal epithelial surface. *Curr.Opin.Clin.Nutr.Metab.Care* 8: 2: 205-209, 2005.

[54] Soderholm JD and Perdue MH. Stress and gastrointestinal tract. II. Stress and intestinal barrier function. *Am.J.Physiol.Gastrointest.Liver Physiol.* 280: 1: G7-G13, 2001.

[55] Myers BM, Smith JL and Graham DY. Effect of red pepper and black pepper on the stomach. *Am.J.Gastroenterol.* 82: 3: 211-214, 1987.

[56] Jensen-Jarolim E, Gajdzik L, Haberl I, Kraft D, Scheiner O and Graf J. Hot spices influence permeability of human intestinal epithelial monolayers. *J.Nutr.* 128: 3: 577-581, 1998.

[57] Hoshino T, Kashimoto N and Kasuga S. Effects of garlic preparations on the gastrointestinal mucosa. *J.Nutr.* 131: 3s: 1109S-13S, 2001.

[58] Amagase H, Petesch BL, Matsuura H, Kasuga S and Itakura Y. Intake of garlic and its bioactive components. *J.Nutr.* 131: 3s: 955S-62S, 2001.

[59] Kvietys PR, Specian RD, Grisham MB and Tso P. Jejunal mucosal injury and restitution: role of hydrolytic products of food digestion. *Am.J.Physiol.* 261: 3 Pt 1: G384-91, 1991.

[60] Bird RP and Bruce WR. Effect of dietary calcium on the toxicity of bile acid and orally administered fat to colonic epithelium. *Prog.Clin.Biol.Res.* 222: 487-494, 1986.

[61] Bretagne JF, Vidon N, L'Hirondel C and Bernier JJ. Increased cell loss in the human jejunum induced by laxatives (ricinoleic acid, dioctyl sodium sulphosuccinate, magnesium sulphate, bile salts). *Gut* 22: 4: 264-269, 1981.

[62] Moriarty KJ, Kelly MJ, Beetham R and Clark ML. Studies on the mechanism of action of dioctyl sodium sulphosuccinate in the human jejunum. *Gut* 26: 10: 1008-1013, 1985.

[63] Saunders DR, Sillery J and Rachmilewitz D. Effect of dioctyl sodium sulfosuccinate on structure and function of rodent and human intestine. *Gastroenterology* 69: 2: 380-386, 1975.

[64] Murakami T, Sasaki Y, Yamajo R and Yata N. Effect of bile salts on the rectal absorption of sodium ampicillin in rats. *Chem.Pharm.Bull.(Tokyo)* 32: 5: 1948-1955, 1984.

[65] Fasano A, Budillon G, Guandalini S, Cuomo R, Parrilli G, Cangiotti AM, Morroni M and Rubino A. Bile acids reversible effects on small intestinal permeability. An in vitro study in the rabbit. *Dig.Dis.Sci.* 35: 7: 801-808, 1990.

[66] Chadwick VS, Gaginella TS, Carlson GL, Debongnie JC, Phillips SF and Hofmann AF. Effect of molecular structure on bile acid-induced alterations in absorptive function, permeability, and morphology in the perfused rabbit colon. *J.Lab.Clin.Med.* 94: 5: 661-674, 1979.

[67] *Martindale, The Extra Pharmacopoeia*, edited by James E.F. Reynolds. London: The Royal Pharmaceutical Society of Great Britain, 1989, p. 1555-1556.

[68] Millan MS, Morris GP, Beck IT and Henson JT. Villous damage induced by suction biopsy and by acute ethanol intake in normal human small intestine. *Dig.Dis.Sci.* 25: 7: 513-525, 1980.

[69] Lacy ER, Morris GP and Cohen MM. Rapid repair of the surface epithelium in human gastric mucosa after acute superficial injury. *J.Clin.Gastroenterol.* 17 Suppl 1: S125-35, 1993.

[70] Masuda K, Ikeda H, Kasai K, Fukuzawa Y, Nishimaki H, Takeo T and Itoh G. Diversity of restitution after deoxycholic acid-induced small intestinal mucosal injury in the rat. *Dig.Dis.Sci.* 48: 10: 2108-2115, 2003.

[71] Ivanov AI, Hunt D, Utech M, Nusrat A and Parkos CA. Differential roles for actin polymerization and a myosin II motor in assembly of the epithelial apical junctional complex. *Mol.Biol.Cell* 16: 6: 2636-2650, 2005.

[72] Danjo Y and Gipson IK. Actin 'purse string' filaments are anchored by E-cadherin-mediated adherens junctions at the leading edge of the epithelial wound, providing coordinated cell movement. *J.Cell.Sci.* 111: 3323-3332, 1998.

[73] Florian P, Schoneberg T, Schulzke JD, Fromm M and Gitter AH. Single-cell epithelial defects close rapidly by an actinomyosin purse string mechanism with functional tight junctions. *J.Physiol.* 545: Pt 2: 485-499, 2002.

[74] Martin P and Lewis J. Actin cables and epidermal movement in embryonic wound healing. *Nature* 360: 6400: 179-183, 1992.

[75] Moore R, Carlson S and Madara JL. Villus contraction aids repair of intestinal epithelium after injury. *Am.J.Physiol.* 257: 2 Pt 1: G274-83, 1989.

[76] Jacinto A, Martinez-Arias A and Martin P. Mechanisms of epithelial fusion and repair. *Nat.Cell Biol.* 3: 5: E117-23, 2001.

[77] Murphy MS. Growth factors and the gastrointestinal tract. *Nutrition* 14: 10: 771-774, 1998.

[78] Dignass AU. Mechanisms and modulation of intestinal epithelial repair. *Inflamm.Bowel Dis.* 7: 1: 68-77, 2001.

[79] Goodlad RA and Wright NA. Epidermal Growth-Factor and Transforming Growth-Factor-Alpha Actions on the Gut. *Eur.J.Gastroenterol.Hepatol.* 7: 10: 928-932, 1995.

[80] Mashimo H, Wu DC, Podolsky DK and Fishman MC. Impaired defense of intestinal mucosa in mice lacking intestinal trefoil factor. *Science* 274: 5285: 262-265, 1996.

[81] Yonemura S, Itoh M, Nagafuchi A and Tsukita S. Cell-To-Cell Adherens Junction Formation and Actin Filament Organization - Similarities and Differences between

Non-Polarized Fibroblasts and Polarized Epithelial-Cells. *J.Cell.Sci.* 108: 127-142, 1995.

[82] Dieckgraefe BK, Stenson WF and Alpers DH. Gastrointestinal epithelial response to injury. *Curr.Opin.Gastroenterol.* 12: 2: 109-114, 1996.

[83] Albers TM, Lomakina I and Moore RP. Structural and functional roles of cytoskeletal proteins during repair of native guinea pig intestinal epithelium. *Cell Biol.Int.* 20: 12: 821-830, 1996.

[84] Wang JY and Johnson LR. Luminal polyamines substitute for tissue polyamines in duodenal mucosal repair after stress in rats. *Gastroenterology* 102: 4 Pt 1: 1109-1117, 1992.

[85] McCormack SA, Wang JY, Viar MJ, Tague L, Davies PJ and Johnson LR. Polyamines influence transglutaminase activity and cell migration in two cell lines. *Am.J.Physiol.* 267: 3 Pt 1: C706-14, 1994.

[86] Blikslager AT and Roberts MC. Mechanisms of intestinal mucosal repair. *J.Am.Vet.Med.Assoc.* 211: 11: 1437-1441, 1997.

[87] Mammen JM and Matthews JB. Mucosal repair in the gastrointestinal tract. *Crit.Care Med.* 31: 8 Suppl: S532-7, 2003.

[88] Navia MA and Chaturvedi PR. Design principles for orally bioavailable drugs. *Drug Discov.Today* 1: 5: 179-189, 1996.

[89] Kararli TT. Gastrointestinal absorption of drugs. *Crit.Rev.Ther.Drug Carrier Syst.* 6: 1: 39-86, 1989.

[90] Kramer SD. Absorption prediction from physicochemical parameters. *Pharm.Sci.Technol.Today* 2: 9: 373-380, 1999.

[91] Lennernas H. Human intestinal permeability. *J.Pharm.Sci.* 87: 4: 403-410, 1998.

[92] Martinez MN and Amidon GL. A mechanistic approach to understanding the factors affecting drug absorption: a review of fundamentals. *J.Clin.Pharmacol.* 42: 6: 620-643, 2002.

[93] Borchardt RT. Optimizing oral absorption of peptides using prodrug strategies. *J.Control.Release* 62: 1-2: 231-238, 1999.

[94] Gomez-Orellana I. Strategies to improve oral drug bioavailability. *Expert Opin.Drug Deliv.* 2: 3: 419-433, 2005.

[95] Ramanathan S, Qiu B, Pooyan S, Zhang G, Stein S, Leibowitz MJ and Sinko PJ. Targeted PEG-based bioconjugates enhance the cellular uptake and transport of a HIV-1 TAT nonapeptide. *J.Control.Release* 77: 3: 199-212, 2001.

[96] Florence AT. Issues in oral nanoparticle drug carrier uptake and targeting. *J.Drug Target.* 12: 2: 65-70, 2004.

[97] Florence AT and Hussain N. Transcytosis of nanoparticle and dendrimer delivery systems: evolving vistas. *Adv.Drug Deliv.Rev.* 50 Suppl 1: S69-89, 2001.

[98] Bummer PM. Physical chemical considerations of lipid-based oral drug delivery--solid lipid nanoparticles. *Crit.Rev.Ther.Drug Carrier Syst.* 21: 1: 1-20, 2004.

[99] Porter CJ and Charman WN. Lipid-based formulations for oral administration: opportunities for bioavailability enhancement and lipoprotein targeting of lipophilic drugs. *J.Recept.Signal Transduct.Res.* 21: 2-3: 215-257, 2001.

[100] GanemQuintanar A, Kalia YN, FalsonRieg F and Buri P. Mechanisms of oral permeation enhancement. *Int.J.Pharm.* 156: 2: 127-142, 1997.

[101] Aungst BJ. Intestinal permeation enhancers. *J.Pharm.Sci.* 89: 4: 429-442, 2000.

[102] Nellans HN. Mechanisms of Peptide and Protein-Absorption .1. Paracellular Intestinal Transport - Modulation of Absorption. *Adv.Drug Deliv.Rev.* 7: 3: 339-364, 1991.

[103] Muranishi S. Absorption Enhancers. *Crit.Rev.Ther.Drug Carrier Syst.* 7: 1: 1-33, 1990.

[104] Aungst BJ, Saitoh H, Burcham DL, Huang SM, Mousa SA and Hussain MA. Enhancement of the intestinal absorption of peptides and nonpeptides. *J.Controlled Release* 41: 1-2: 19-31, 1996.

[105] LeCluyse EL and Sutton SC. In vitro models for selection of development candidates. Permeability studies to define mechanisms of absorption enhancement. *Adv.Drug Deliv.Rev.* 23: 1-3: 163-183, 1997.

[106] Swenson ES and Curatolo WJ. Intestinal Permeability Enhancement for Proteins, Peptides and Other Polar Drugs - Mechanisms and Potential Toxicity .2. *Adv.Drug Deliv.Rev.* 8: 1: 39-92, 1992.

[107] van Hoogdalem EJ, de Boer AG and Breimer DD. Intestinal drug absorption enhancement: an overview. *Pharmacol.Ther.* 44: 3: 407-443, 1989.

[108] Hosoya K, Kubo H, Natsume H, Sugibayashi K and Morimoto Y. Evaluation of enhancers to increase nasal absorption using Ussing chamber technique. *Biol.Pharm.Bull.* 17: 2: 316-322, 1994.

[109] Marttin E, Verhoef JC, Romeijn SG and Merkus FW. Effects of absorption enhancers on rat nasal epithelium in vivo: release of marker compounds in the nasal cavity. *Pharm.Res.* 12: 8: 1151-1157, 1995.

[110] Swenson ES, Milisen WB and Curatolo W. Intestinal permeability enhancement: efficacy, acute local toxicity, and reversibility. *Pharm.Res.* 11: 8: 1132-1142, 1994.

[111] Shao Z and Mitra AK. Nasal membrane and intracellular protein and enzyme release by bile salts and bile salt-fatty acid mixed micelles: correlation with facilitated drug transport. *Pharm.Res.* 9: 9: 1184-1189, 1992.

[112] Nakanishi K, Nadai T, Masada M and Miyajima K. Effect of cyclodextrins on biological membrane. II. Mechanism of enhancement on the intestinal absorption of non-absorbable drug by cyclodextrins. *Chem.Pharm.Bull.(Tokyo)* 40: 5: 1252-1256, 1992.

[113] Muranushi N, Takagi N, Muranishi S and Sezaki H. Effect of fatty acids and monoglycerides on permeability of lipid bilayer. *Chem.Phys.Lipids* 28: 3: 269-279, 1981.

[114] Turunen TM, Urtti A, Paronen P, Audus KL and Rytting JH. Effect of some penetration enhancers on epithelial membrane lipid domains: evidence from fluorescence spectroscopy studies. *Pharm.Res.* 11: 2: 288-294, 1994.

[115] Tomita M, Hayashi M, Horie T, Ishizawa T and Awazu S. Enhancement of colonic drug absorption by the transcellular permeation route. *Pharm.Res.* 5: 12: 786-789, 1988.

[116] Anderson JM, Balda MS and Fanning AS. The structure and regulation of tight junctions. *Curr.Opin.Cell Biol.* 5: 5: 772-778, 1993.

[117] Tomita M, Hayashi M and Awazu S. Absorption-enhancing mechanism of EDTA, caprate, and decanoylcarnitine in Caco-2 cells. *J.Pharm.Sci.* 85: 6: 608-611, 1996.

[118] Tomita M, Shiga M, Hayashi M and Awazu S. Enhancement of colonic drug absorption by the paracellular permeation route. *Pharm.Res.* 5: 6: 341-346, 1988.

[119] Schipper NG, Olsson S, Hoogstraate JA, deBoer AG, Varum KM and Artursson P. Chitosans as absorption enhancers for poorly absorbable drugs 2: mechanism of absorption enhancement. *Pharm.Res.* 14: 7: 923-929, 1997.

[120] Thanou M, Verhoef JC and Junginger HE. Oral drug absorption enhancement by chitosan and its derivatives. *Adv.Drug Deliv.Rev.* 52: 2: 117-126, 2001.

[121] Balimane PV, Chong S and Morrison RA. Current methodologies used for evaluation of intestinal permeability and absorption. *J.Pharmacol.Toxicol.Methods* 44: 1: 301-312, 2000.

[122] Levine RR, McNary WF, Kornguth PJ and LeBlanc R. Histological reevaluation of everted gut technique for studying intestinal absorption. *Eur.J.Pharmacol.* 9: 2: 211-219, 1970.

[123] Wilson TH and Wiseman G. The use of sacs of everted small intestine for the study of the transference of substances from the mucosal to the serosal surface. *J.Physiol.* 123: 1: 116-125, 1954.

[124] Ussing HH and Zerahn K. Active transport of sodium as the source of electric current in the short-circuited isolated frog skin. Reprinted from Acta. Physiol. Scand. 23: 110-127, 1951. *J.Am.Soc.Nephrol.* 10: 9: 2056-2065, 1999.

[125] Grass GM and Sweetana SA. In vitro measurement of gastrointestinal tissue permeability using a new diffusion cell. *Pharm.Res.* 5: 6: 372-376, 1988.

[126] Acra SA and Ghishan FK. Methods of investigating intestinal transport. *JPEN J.Parenter.Enteral Nutr.* 15: 3: 93S-98S, 1991.

[127] Bohets H, Annaert P, Mannens G, Van Beijsterveldt L, Anciaux K, Verboven P, Meuldermans W and Lavrijsen K. Strategies for absorption screening in drug discovery and development. *Curr.Top.Med.Chem.* 1: 5: 367-383, 2001.

[128] Hillgren KM, Kato A and Borchardt RT. In vitro systems for studying intestinal drug absorption. *Med.Res.Rev.* 15: 2: 83-109, 1995.

[129] Balimane PV and Chong S. Cell culture-based models for intestinal permeability: a critique. *Drug Discov.Today* 10: 5: 335-343, 2005.

[130] Sambuy Y, De Angelis I, Ranaldi G, Scarino ML, Stammati A and Zucco F. The Caco-2 cell line as a model of the intestinal barrier: influence of cell and culture-related factors on Caco-2 cell functional characteristics. *Cell Biol.Toxicol.* 21: 1: 1-26, 2005.

[131] Artursson P, Palm K and Luthman K. Caco-2 monolayers in experimental and theoretical predictions of drug transport. *Adv.Drug Deliv.Rev.* 46: 1-3: 27-43, 2001.

[132] Doluisio JT, Billups NF, Dittert LW, Sugita ET and Swintosky JV. Drug absorption. I. An in situ rat gut technique yielding realistic absorption rates. *J.Pharm.Sci.* 58: 10: 1196-1200, 1969.

[133] Griffiths R, Lewis A and Jeffrey P. Models of drug absorption in situ and in conscious animals. *Pharm.Biotechnol.* 8: 67-84, 1996.

[134] Amidon GE, Ho NF, French AB and Higuchi WI. Predicted absorption rates with simultaneous bulk fluid flow in the intestinal tract. *J.Theor.Biol.* 89: 2: 195-210, 1981.

[135] Lewis LD and Fordtran JS. Effect of perfusion rate on absorption, surface area, unstirred water layer thickness, permeability, and intraluminal pressure in the rat ileum in vivo. *Gastroenterology* 68: 6: 1509-1516, 1975.

[136] Jennifer Dressman and Kenji Yamada. Animal Models for Oral Drug Absorption. In: *Pharmceutical Bioequivalence*, edited by Peter Welling, Francis Tse and Shrikant Dighe. NY: Marcel Dekker, Inc., 1991, chapt. Chapter 9, p. 235-266.

[137] Kararli TT. Comparison of the gastrointestinal anatomy, physiology, and biochemistry of humans and commonly used laboratory animals. *Biopharm.Drug Dispos.* 16: 5: 351-380, 1995.

[138] Miller ER and Ullrey DE. The pig as a model for human nutrition. *Annu.Rev.Nutr.* 7: 361-382, 1987.

[139] Gruber P, Longer MA and Robinson JR. Some biological issues in oral, controlled drug delivery. 1: 1: 1-18, 1987/5.

[140] Barbara Haeberlin and David Friend. Anatomy and Physiology of the Gastrointestinal Tract: Implications for Colonic Drug Delivery. In: *Oral Colon-specific Drug Delivery*, edited by David Friend. Boca Raton, FL: CRC Press, 1992, chapt. Chapter 1, p. 1-43.

[141] DeSesso JM and Jacobson CF. Anatomical and physiological parameters affecting gastrointestinal absorption in humans and rats. *Food Chem.Toxicol.* 39: 3: 209-228, 2001.

[142] Sakai M, Imai T, Ohtake H and Otagiri M. Cytotoxicity of absorption enhancers in Caco-2 cell monolayers. *J.Pharm.Pharmacol.* 50: 10: 1101-1108, 1998.

[143] Babich H and Borenfreund E. Applications of the Neutral Red Cytotoxicity Assay to Invitro Toxicology. 18: 129-144, 1990.

[144] Borenfreund E and Puerner JA. Toxicity determined in vitro by morphological alterations and neutral red absorption. *Toxicol.Lett.* 24: 2-3: 119-124, 1985.

[145] Krishan A. Rapid flow cytofluorometric analysis of mammalian cell cycle by propidium iodide staining. *J.Cell Biol.* 66: 1: 188-193, 1975.

[146] Wrobel K, Claudio E, Segade F, Ramos S and Lazo PS. Measurement of cytotoxicity by propidium iodide staining of target cell DNA. Application to the quantification of murine TNF-alpha. *J.Immunol.Methods* 189: 2: 243-249, 1996.

[147] Nagahama S, Korenaga D, Honda M, Inutsuka S and Sugimachi K. Assessment of the intestinal permeability after a gastrectomy and the oral administration of anticancer drugs in rats: nitric oxide release in response to gut injury. *Surgery* 131: 1 Suppl: S92-7, 2002.

[148] Nakamaru M, Masubuchi Y, Narimatsu S, Awazu S and Horie T. Evaluation of damaged small intestine of mouse following methotrexate administration. *Cancer Chemother.Pharmacol.* 41: 2: 98-102, 1998.

[149] Yamamoto A, Uchiyama T, Nishikawa R, Fujita T and Muranishi S. Effectiveness and toxicity screening of various absorption enhancers in the rat small intestine: effects of absorption enhancers on the intestinal absorption of phenol red and the release of protein and phospholipids from the intestinal membrane. *J.Pharm.Pharmacol.* 48: 12: 1285-1289, 1996.

[150] Higaki K, Yata T, Sone M, Ogawara K and Kimura T. Estimation of absorption enhancement by medium-chain fatty acids in rat large intestine. *Res.Commun.Mol.Pathol.Pharmacol.* 109: 3-4: 231-240, 2001.

[151] Anderberg EK and Artursson P. Epithelial transport of drugs in cell culture. VIII: Effects of sodium dodecyl sulfate on cell membrane and tight junction permeability in human intestinal epithelial (Caco-2) cells. *J.Pharm.Sci.* 82: 4: 392-398, 1993.

[152] Walker AI, Brown VK, Ferrigan LW, Pickering RG and Williams DA. Toxicity os sodium lauryl sulphate, sodium lauryl ethoxysulphate and corresponding surfactants derived from synthetic alcohols. *Food Cosmet.Toxicol.* 5: 6: 763-769, 1967.

[153] Fitzhugh O.G. and Nelson A.A. Chronic oral toxicities of surface-active agents. *J Am Pharmacol Assoc* 37: 29-32, 1948.

[154] Yasuhara M, Katayama H, Fujiwara J, Okumura K and Hori R. Influence of acute renal failure on pharmacokinetics of phenolsulfonphthalein in rats: a comparative study in vivo and in the simultaneous perfusion system of liver and kidney. *J.Pharmacobiodyn* 8: 5: 377-384, 1985.

[155] Mehvar R and Shepard TL. Molecular-weight-dependent pharmacokinetics of fluorescein-labeled dextrans in rats. *J.Pharm.Sci.* 81: 9: 908-912, 1992.

[156] Nishida K, Sato N, Sasaki H and Nakamura J. Absorption characteristics of dextrans with different molecular weights from the liver surface membrane in rats: implications for targeting to the liver. *J.Drug Target.* 4: 3: 141-150, 1996.

[157] Higaki K, Takechi N, Kato M, Hashida M and Sezaki H. Effect of medium-chain glycerides on the intestinal absorption of phenol red: studies on mechanisms of the promoting effect. *J.Pharm.Sci.* 79: 4: 334-338, 1990.

[158] Watkins JB,3rd and Dykstra TP. Alterations in biliary excretory function by streptozotocin-induced diabetes. *Drug Metab.Dispos.* 15: 2: 177-183, 1987.

[159] *Martindale, the Extra Pharmacopoeia*, edited by James E.F. Reynolds. London: The Royal Pharmaceutical Society of Great Britain, 1989, p. 1088.

[160] Wheeler PG, Menzies IS and Creamer B. Effect of hyperosmolar stimuli and coeliac disease on the permeability of the human gastrointestinal tract. *Clin.Sci.Mol.Med.* 54: 5: 495-501, 1978.

[161] Toh Y, Korenaga D, Maekawa S, Matsumata T, Muto Y, Ikeda T and Sugimachi K. Assessing the permeability of the gastrointestinal mucosa after oral administration of phenolsulfonphthalein. *Hepatogastroenterology* 44: 16: 1147-1151, 1997.

[162] Yoshida S, Matsui M, Shirouzu Y, Fujita H, Yamana H and Shirouzu K. Effects of glutamine supplements and radiochemotherapy on systemic immune and gut barrier function in patients with advanced esophageal cancer. *Ann.Surg.* 227: 4: 485-491, 1998.

[163] Yamaoka K, Nakagawa T and Uno T. Statistical moments in pharmacokinetics. *J.Pharmacokinet.Biopharm.* 6: 6: 547-558, 1978.

[164] Goldberg M and Gomez-Orellana I. Challenges for the oral delivery of macromolecules. *Nat.Rev.Drug Discov.* 2: 4: 289-295, 2003.

[165] O'Boyle CJ, MacFie J, Mitchell CJ, Johnstone D, Sagar PM and Sedman PC. Microbiology of bacterial translocation in humans. *Gut* 42: 1: 29-35, 1998.

[166] Ansell J, Widrich W, Johnson W and Fine J. Endotoxin and bacteria in portal blood. *Gastroenterology* 73: 5: 1190, 1977.

[167] Jacob AI, Goldberg PK, Bloom N, Degenshein GA and Kozinn PJ. Endotoxin and bacteria in portal blood. *Gastroenterology* 72: 6: 1268-1270, 1977.

[168] Fox ES, Thomas P and Broitman SA. Clearance of gut-derived endotoxins by the liver. Release and modification of 3H, 14C-lipopolysaccharide by isolated rat Kupffer cells. *Gastroenterology* 96: 2 Pt 1: 456-461, 1989.

[169] Klein A, Zhadkewich M, Margolick J, Winkelstein J and Bulkley G. Quantitative discrimination of hepatic reticuloendothelial clearance and phagocytic killing. *J.Leukoc.Biol.* 55: 2: 248-252, 1994.

[170] Moore R, Carlson S and Madara JL. Rapid barrier restitution in an in vitro model of intestinal epithelial injury. *Lab.Invest.* 60: 2: 237-244, 1989.

[171] Waller DA, Thomas NW and Self TJ. Epithelial restitution in the large intestine of the rat following insult with bile salts. *Virchows Arch.A Pathol.Anat.Histopathol.* 414: 1: 77-81, 1988.

[172] Aalykke C and Lauritsen K. Epidemiology of NSAID-related gastroduodenal mucosal injury. *Best Pract.Res.Clin.Gastroenterol.* 15: 5: 705-722, 2001.

[173] Wallace JL. Pathogenesis of NSAID-induced gastroduodenal mucosal injury. *Best Pract.Res.Clin.Gastroenterol.* 15: 5: 691-703, 2001.

[174] Mahmood I. Allometric issues in drug development. *J.Pharm.Sci.* 88: 11: 1101-1106, 1999.

[175] Riviere JE, Martin-Jimenez T, Sundlof SF and Craigmill AL. Interspecies allometric analysis of the comparative pharmacokinetics of 44 drugs across veterinary and laboratory animal species. *J.Vet.Pharmacol.Ther.* 20: 6: 453-463, 1997.

[176] Tamai H, Kato S, Horie Y, Ohki E, Yokoyama H, Ishii H: Effect of acute ethanol administration on the intestinal absorption of endotoxin in rats Alcoholism. *Clinical and Experimental research* 24: 3: 390-394, 2000.